SPACE RESEARCH IN SLOVAKIA

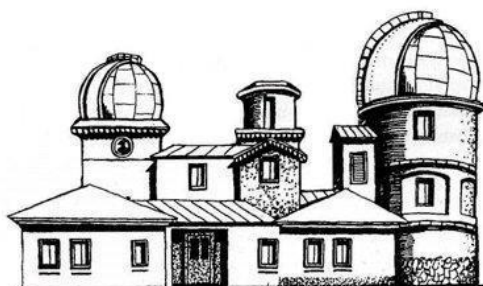## 2018 – 2019

SLOVAK ACADEMY OF SCIENCES

COSPAR

SLOVAK NATIONAL COMMITTEE

Slovak Central Observatory Hurbanovo

MAY 2020

CONTENTS

1. EXPERIMENTS FOR MEASUREMENTS IN SPACE

J. Baláž, P. Bobík, M. Musilová

Experiment MEP-2 on board of Spektr-R (Radioastron)

The data acquisition from the experiment MEP-2 was terminated on 10th January 2019 as a result of failure of communication with the Spektr-R spacecraft due to the spacecraft command receiver malfunction. The mission was anyway very successful as it was operative on orbit for 7.5 years instead of planned 3 years. The programmable energetic particle spectrometer MEP-2, developed and constructed at the Department of Space Physics IEP-SAS was operative over entire mission lifetime and delivered large amount of valuable science data.

Figure 1.1. *Energetic particle spectrometer MEP-2. The configuration on delivery and after installation on board of the space observatory Spektr-R (Radioastron).*

The description and on-orbit operation of the PLAZMA-F suite is described in [1], the MEP-2 experiment is described in [2]. Amid significant results of the MEP-2 experiment, e.g., a new type of oscillations of energetic ions flux near the Earth's bow shock was revealed [3]. This kind of particle flux variability could be ever observed due to high time resolution and wide energy range of MEP-2 spectrometer.

Experiment SERENA/PICAM for mission ESA-BepiColombo

IEP SAS contributed to ESA-BepiColombo mission to planet Mercury in the frame of scientific-technical cooperation with Space Technology Ireland (STIL) and Institute for Space Research of Austrian Academy of Sciences (IWF-ÖAW). The delivery involved the mechanical structures of the PICAM (Planetary Ion Camera) instrument that were manufactured in Slovakia (mechanical stress simulations and mechanical components manufacture on 5-axis centre of Q-Products, Bratislava, space-qualified processing and integration and testing at IEP-SAS, Košice).
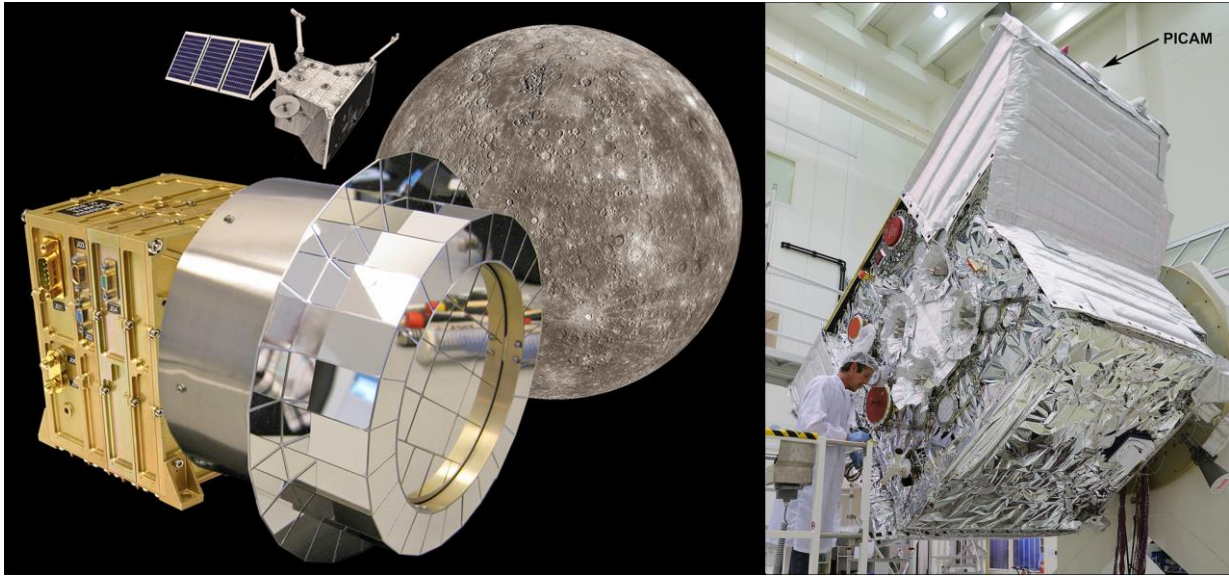
Figure 1.2. SERENA / PICAM and Mercury planetary orbiter (MPO) of BepiColombo mission.

PICAM is a part of a complex space science suite SERENA for particle detection at planet Mercury, the launch of the mission was on 20th October 2018, the science payload is operating nominally. The first flyby of planet Earth is scheduled on March 2020 followed be flyby of planet Venus in October 2020. The arrival to Mercury is scheduled in 2025. The detailed description of the PICAM device is provided in [4].

Experiment PEP/JDC for mission ESA-JUICE

Experiment PEP (Particle Environment Package) will provide comprehensive detection and analysis of the plasma and particle environment in the system of planet Jupiter and its Galilean moons Europa, Calisto and Ganymede. PEP will measure density and flux of positive and negative ions, electrons, exospheric neutral gas, thermal plasma and energetic neutral atoms in the energy range from <0.001 eV to >1 MeV with full angular coverage. The PEP suite includes six sensors (JDC, JEI, JoEE, NIM, JNA and JENI) that are under development at

several EU and US institutions led by Swedish Institute for Space Physics (IRF, P.I. prof. S. Barabash). Based on invitation from IRF, the IEP-SAS contributes to development and construction of anti-coincidence particle detection system for JDC sensor (Jovian plasma Dynamics and Composition) of the PEP suite. The anti-coincidence system will improve the plasma particles detection efficiency on the background of penetrating electron radiation from Jovian radiation belts. The system consists from silicon solid state detector (SSD) and dedicated processing electronic unit (ANU).
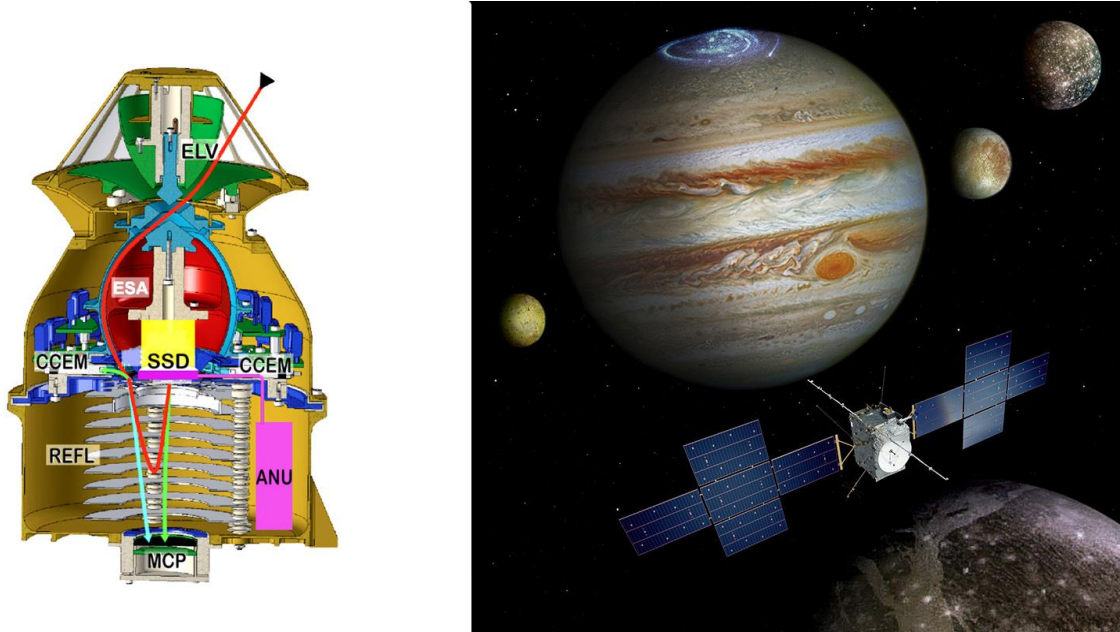
Figure 1.3. *JDC sensor of the PEP science suite and JUICE spacecraft orbiting in the system of Jupiter and its Galilean moons.*

The JUICE mission including the PEP science suite description is described in [5], the JDC sensor is in details described in [6].

The participation of IEP SAS to JUICE mission is supported by Slovak PECS (Plan for European Cooperating States) project named: *"Slovak contribution to ESA-JUICE mission: Development of Anti-Coincidence Module ACM for Particle Environment Package PEP"*.

The development, manufacture, testing and calibration of the ACM/EM (engineering model) were finished in December 2018. The EM unit was then delivered to IRF Kiruna, Sweden, where it was successfully integrated to the JDC/EM sensor system.

The flight model (ACM/FM) was built from the space-qualified components during 2019, the final assembly, testing and calibration was performed in October-November 2019 at IEP SAS Kosice and the unit was finally delivered to IRF Kiruna for integration to JDC/FM system.
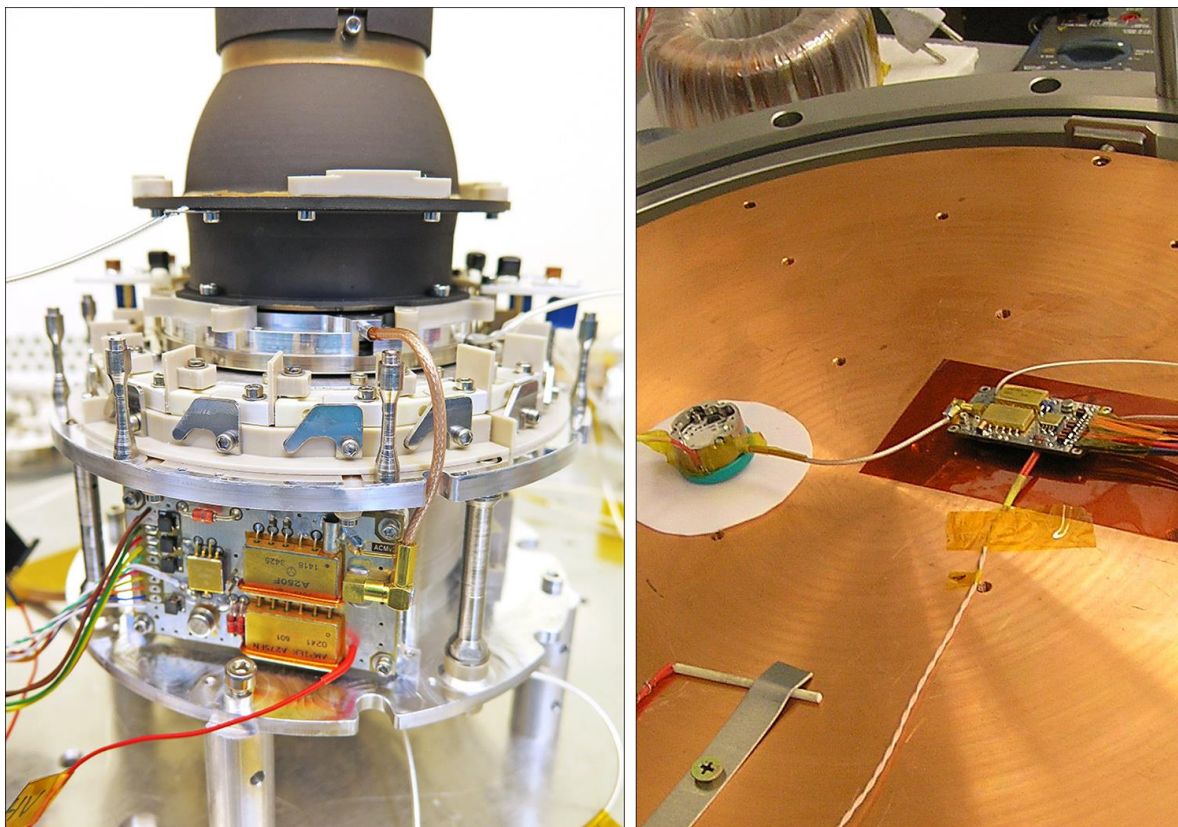
Figure 1.4. *(Left) ACM/EM subsystem after integration to JDC/EM at IRF Kiruna. (Right) ACM/FM under thermal-vacuum test in SPACEVAC space simulator at IEP-SAS Kosice.*

Experiment ASPECT-L for project LUNA-26

The experiment ASPECT-L is currently under development at IEP-SAS in cooperation with Institute for Space Research (IKI-RAN), Moscow, for lunar mission LUNA-26.
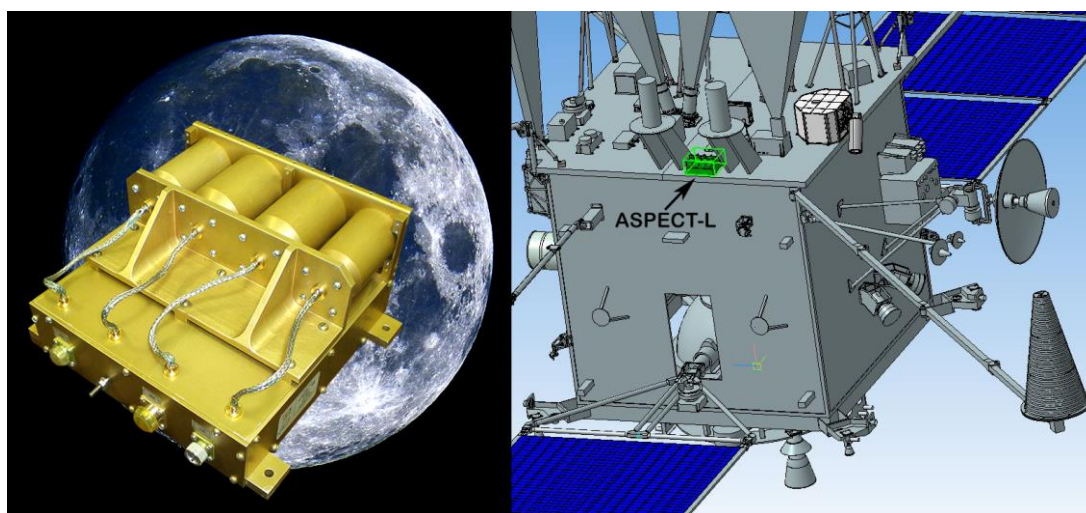
Figure 1.5. *Energetic particle spectrometer ASPECT-L for LUNA-26 mission and its position onboard of the Orbiter spacecraft.*

The Structural Thermal Model (ASPECT-L/STM) was delivered to IKI-RAN in 2015, the engineering model of the instrument (ASPECT-L/EM) was delivered to IKI-RAN in October 2019.

Figure 1.6. *ASPECT-L/EM (Engineering Model) as delivered to IKI-RAN, Moscow, Russia, in October 2019.*

Participation of Slovakia in the project JEM-EUSO

JEM-EUSO (Japanese Experiment Module – Extreme Universe Space Observatory) experiment will search for ultra-high energy cosmic rays (UHECR, with energy above 10^19 eV) by monitoring UV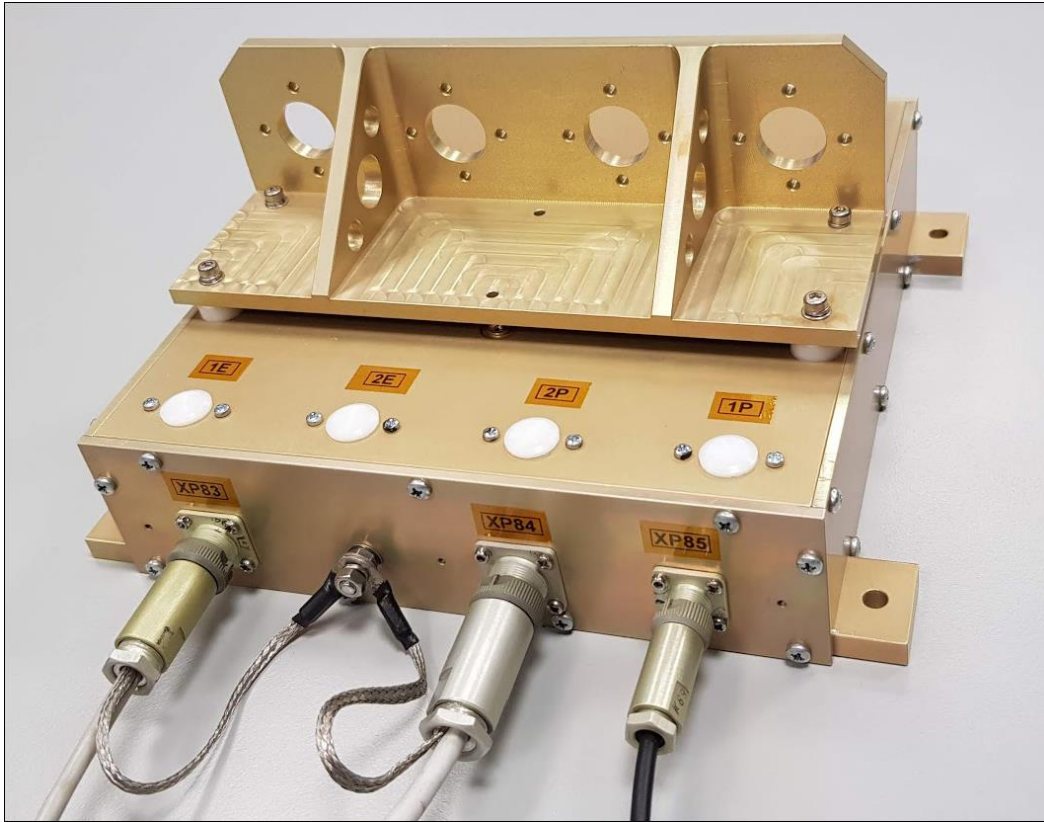 light produced in their interaction with atmosphere from International Space Station. Department of Space Physics IEP-SAS works in project frame mainly on UV background model at the Earth night side. Pattern recognition methods for showers detection in EUSO experiments measurements are developed at Technical University in Kosice.

In the UV background model, we focus specifically on identification and quantification of in the upper atmosphere produced airglow light intensity variations. The analysis shows the main variations that should be searched in measurements of the Mini-EUSO experiment operating at ISS since August 2019.

As an important outcome, we present the article Ultra-violet Imaging of the Night-Time Earth by EUSO-Balloon towards space-based ultra-high energy cosmic ray observations [7]. This is an article with the analysis of measurements

of the EUSO balloon experiment, which took its flight in August 2014. The article is devoted to the first measurement by a EUSO class detector looking for ultra-high energy cosmic ray showers from above. The probability of capturing the shower signal during this flight was not high, the flight served as a technology test detector and for background measurement, which is a limiting factor in the observation of showers.

The activities of the IEP SAS group were oriented also on preparing and building a global network of UV detectors. The UV detector network named AMON-net is designed for long-term monitoring of the global dynamics of airglow radiation generation. At present, the network has been in operation and its main stations have been continuously measuring for more than two years (the stations in Mexico at the Astronomico Nacional de San Pedro Martir Observatory and the Canary Islands, Los Muchachos Observatory, La Palma). Other stations in Germany and the Kolonica Observatory have been measuring continuously for over a year. Test measurements and control measurements of weeks to months were carried out in Sweden, the USA, and the Lomnicky Stit. Publication [8] describing the AMON detector, which is the measuring station for the AMON-net network. The development of the flight version of the AMON detector is an ongoing activity. Two test flights were realized at the stratospheric platform HiDron (www.stratodynamics.ca) in August 2019. First to altitude 30 km, second to altitude 34 km. A flight version of the detector, AMON (2 pieces) and EMON (3 pieces) are prepared for NASA EUSO-SPB2 flight, to perform UV background and light conditions measurements in the main EUSO mission detector.

The evaluation of EUSO-SPB measurements by machine learning methods is presented in [9]. Analysis of the first measurements from TA-EUSO presents the ground experiment [10]. Results of calibration measurements of UV light sources during EUSO flight balloon shows [11].

Figure 1.7. *HiDron with AMON on CNES balloon before the flight from Timmins, 31. August 2019.*

Information regarding the first Slovak satellite skCUBE

The first Slovak satellite skCUBE was designed, developed and successfully launched into orbit on the 23rd June 2017. The skCUBE project was run by the Slovak Organisation for Space Activities (SOSA), in collaboration with the Slovak University of Technology in Bratislava, Technical University in Košice and the University of Žilina and dozens of companies. In total, over 60 people volunteered on this project. It was partially funded by the Ministry of Education, Science, Research and Sport, the Ministry of Transport and the Prime Minister of the Slovak Republic. In July 2017 the nanosatellite suffered a problem in orbit. Despite this issue, it continued to transmit data, which were collected by multiple ground stations all around Slovakia on a daily basis. The satellite functioned without a restart for 569 days. On the 15th of January 2019, the nanosatellite stopped transmitting data. A few days prior to this, some parts of the satellite seemed to be overheating. Members of SOSA attempted to reconnect to the satellite for several days without success. The project was therefore terminated on the 1st of February 2019.

Data from the satellite are freely available. They are still being processed by SOSA members and by students from all over Slovakia, Czechia and elsewhere in the world, who have included them in their bachelors and masters theses. SOSA also prepared a course open to the public, providing basic information about receiving and processing satellite data. There was a lot of interest for this course, which may continue to be provided to students and the public in the future.

Furthermore, the success of the skCUBE project inspired several members of SOSA and collaborators abroad from Hungary, Japan and the Czech Republic to prepare a scientific mission called Cubesats Applied for MEasuring and LOcalising Transients (CAMELOT). Members of SOSA and the skCUBE team are taking part in the preparation of the CAMELOT nanosatellite fleet hardware.

References:

[1] ZELENYI, L.M. - ZASTENKER, G.N. - PETRUCHOVICH, A.A. - CHESALIN, L.S. - NAZAROV, V.N. - BALÁŽ, J. - KUDELA, K. - STRHÁRSKÝ, I. - SLIVKA, M. PLASMA-F Experiment: Three Years of On-Orbit Operation. In Solar System Research, 2015, vol. 49, no. 7, p. 580-603, ISSN 0038-0946.

[2] BALÁŽ, J. - GLADYSHEV, V.A. - KUDELA, K. - PETRUKOVICH, A.A. - SARRIS, E. - SARRIS, T. - SLIVKA, M. - STRHÁRSKÝ, I. Energetic Particle Measurements Onboard Spectr-R with MEP-2. Kosmicheskie Issledovaniya 2013, Vol. 51, No. 2, pp. 100–106.

[3] PETRUKOVICH, A.A. - INAMORI, T. - BALAZ, J. - KUDELA, K. - SLIVKA, M. - STRHARSKY, I. - GLADYSHEV, V.A. - SARRIS, T. -SARRIS, E. (2015). Oscillations of energetic ions flux near the Earth's bow shock, J. Geophys. Res. Space Physics, 120, doi:10.1002/2015JA021077.

[4] ORSINI, S. - LIVI, S. ,..., BALAZ, J. - KUDELA, K., et al. SERENA: A suite of four instruments (ELENA, STROFIO, PICAM and MIPA) on board BepiColombo-MPO for particle detection in the Hermean environment. Planetary and Space Science 58 (2010), pp 166-181, doi:10.1016/j.pss.2008.09.012

[5] http://sci.esa.int/juice/54993-juice-definition-study-report-red-book/

[6] STUDE, J. Advanced Plasma Analyzer for Measurements in the Magnetosphere of Jupiter. Doctoral Thesis. Swedish Institute of Space Physics and Umeå University, 2016.
https://www.diva-portal.org/smash/get/diva2:926416/FULLTEXT01.pdf

[7] The JEM-EUSO Collaboration (corresponding authors: MACKOVJAK, Š. - SHINOYAKI, K.), Astroparticle Physics, 111, 54, 2019

[8] MACKOVJAK, Š. - BOBÍK, P. - BALÁŽ, J. – STRHÁRSKY, I. – PUTIŠ, M. – GORODETZKY, P., Nuclear Instruments and Methods in Physics Research Section A: Accelerators, Spectrometers, Detectors, and Associated Equipment, 992,150, 2019

[9] VRABEL, M. - GENCI, J. - BOBÍK, P. - BISCONTI, F., 36th ICRC, July 24th-August 1st, 2019 in Madison, WI, U.S.A. Online at https://pos.sissa.it/cgi-bin/reader/conf.cgi?confid=358, id.456

[10] The JEM-EUSO Collaboration, Astroparticle Physics, Volume 102, p. 98-111, 2018

[11] The JEM-EUSO Collaboration, Journal of Instrumentation, Volume 13, Issue 05, pp. P05023, 2018

[12] SZABÓ, P. - GOMBÍKOVÁ, K. - FERENCOVÁ, M. - KOŠUDA, M., "Keplerian Orbit and Satellite skCUBE," 2019 New Trends in Aviation Development (NTAD), Chlumec nad Cidlinou, Czech Republic, 2019, pp. 174-179.

[13] VERTAT, I. - LINHART, R. - Pokorny, M. - MASOPUST, J. - FIALA, P. - MRAZ, J., "Small satellite ground station in Pilsen — experiences with VZLUSAT-1 commanding and future modifications toward open reference ground station solution," 2018 28th International Conference Radioelektronika (RADIOELEKTRONIKA), Prague, 2018, pp. 1-6.

[14] OJUR, B.A., 2019. Low cost and portable software defined radio ground station (Doctoral dissertation, Engineering and the Built Environment).

[15] BURGER, E. – BORDACCHINI, G., 2019. Chronology of Space Activities in 2017. In Yearbook on Space Policy 2017 (pp. 313-357). Springer, Cham. Zimmer, P., McGraw, J.T. and Ackermann, M.R., 2019. Optical measurements of faint LEO RSOs: Cubesats and Fengyun 1C Debris.

[16] SPODNIAK, M. - Semrád, K. - AS AL-RABEEI, S. - MAJCHEROVÁ, N. - KORBA, P. - HOVANEC, M., "MKP analýza vlastných frekvencií lopatiek plynovej turbíny motora iSTC-21v." (2019).

[17] BULANOV, D., 2018. Thesis for Doctor's Degree (Doctoral dissertation, Chongqing University of Posts and Telecommunications).

[18] ONDREJÁK, M., 2019. Česko a Slovensko v kozmickej ekonomike (Doctoral dissertation, Masarykova univerzita, Ekonomicko-správní fakulta).

[19] SWARTWOUT, M., 2018. Reliving 24 Years in the Next 12 Minutes: A Statistical and Personal History of University-Class Satellites.

2. SPACE PHYSICS, GEOPHYSICS AND ASTRONOMY

J. Baláž, P. Bobík, I. Dorotovič, L. Kornoš, R. Langer, Š. Mackovjak,
M. Revallo, J. Rybák, J. Šilha, J. Tóth

The Department of Space Physics, ***Institute of Experimental Physics, SAS, Košice*** (http://space.saske.sk) in collaboration with the laboratories in abroad continued studies of the dynamics of low energy cosmic rays (CR) and of suprathermal cosmic particles, as well as high energy cosmic rays based on measurements in space and on the ground.

Analysis of long term continual measurements by Neutron Monitor at High Altitude Laboratory of IEP SAS Lomnický štít (LŠ, data in real time available at http://neutronmonitor.ta3.sk) along with other neutron monitors were used to confirm correlation between radiation exposures of aircrew members from selected airline operators registered in the Czech Republic from 1998 up to 2018. Results of this radiation protection study are presented in [1].

Thunderstorm ground enhancements (TGEs) of secondary cosmic ray fluxes, recorded by the SEVAN detector system, are compared with simultaneous measurements of electric field at the LŠ mountain top and on its slope at the observatory of Skalnaté Pleso from May to September in 2017 and from May to October in 2018

Observation of the processes in Earth's magnetosphere by means of energetic neutral atoms (ENA) continues by analysis of data obtained by Neutral atom imaging detector NUADU [2]. The device was constructed at the Institute of Experimental Physics in collaboration with Space Technology Ireland, Swedish Institute of Space Physics, Chinese National Space Science Center and operated on board of the Double Star TC2 spacecraft [3]. Although the TC2 spacecraft was injected to high apogee orbit, its perigee in range 500 - 800 km also allowed close up observations at low altitudes in polar region where energetic ion precipitation take place. The novel analyses has concentrated to emissions of low-altitude ENA during magnetospheric substorms and showed that the best way to observe dynamics of magnetospheric ring current variations is from a low orbit spacecraft. It was shown that the closer the imaging device is to the ENA emission source, the higher temporal and spatial resolution data can be obtained. In the substorm expansion phase, magnetic field stretching tailward causes the ion deposition due to the pitch angle diffusion of RC ions. During the substorm recovery phase, magnetic field di-polarization with the energetic ion injection at night accompanied by precipitating ions caused by the pitch angle diffusion at dusk. This was demonstrated for the first time at a temporal resolution of one minute.

Within the studies of Sun-Earth relations, we have concentrated on the research of a faint light in the altitudes 80 - 300 km, called airglow. The airglow is not a well-explored phenomenon. To determine the response of airglow production to disturbances of the magnetosphere for ground measurements. The result is a

publication [4] with an estimation of the decrease in airglow intensity depending on the degree of magnetosphere disturbances described by the Dst index for selected positions on the Earth's surface. These are observatories with suitable meteorological conditions and a series of positions along the auroral boundary for a highly disturbed magnetosphere (Kp = 8). The second area was the evaluation of UV background measurements from the EUSO balloon flight in 2014. This activity was a continuation of the work of previous years published in the article [5] in 2018 with the conclusions of the analysis. Characterization of its influence on the detection of extensive air showers, where it acts as a background, is just in the beginning. Therefore, we have started our own program of airglow monitoring with one-pixel detectors [6]. This program is supported by the government of Slovakia through an ESA (European Space Agency) contract under the PECS (Plan for European Cooperating States).

References:

[1] KUBANČÁK, J. - KYSELOVÁ, D. - KOVÁŘ, I. - HLAVÁČOVÁ, M. - LANGER, R. - STRHÁRSKY, I. - KUDELA, K. - DAVÍDKOVÁ, M. - PLOC, O. Radiation Protection Dosimetry, Volume 186, Issue 2-3, December 2019, Pages 211–214, https://doi.org/10.1093/rpd/ncz204

[2] LU, L. - McKENNA-LAWLOR, S. - BALÁŽ, J. Close up observation and inversion of low-altitude ENA emissions during a substorm event. Sci. China Earth Sci. 62, 1024-1032 (2019). https://doi.org/10.1007/s11430-018-9307-x

[3] McKENNA-LAWLOR, S. - BALÁŽ, J. - STRHÁRSKÝ, I. - BARABASH, S. - BRINKFELDT, K. - LI, L. - SHEN, C. - SHI, J. - ZONG, Q. - KUDELA, K. - FU, S. - ROELOF, E. C. - son BRANDT, P. C. - DANDOURAS, I. The energetic NeUtral Atom Detector Unit (NUADU) for China's Double Star Mission and its calibration. Nucl Inst Method Phys Res Sect A, 2004, 530: 311-322. https://doi.org/10.1016/j.nima.2004.04.244

[4] PUTIŠ, M. - BOBÍK, P., - MACKOVJAK, Š.: 2018, Method for analysis of the effect of geomagnetic disturbances on Ultraviolet airglow intensity. Earth and Space Science, 5, 790–800. https://doi.org/10.1029/2017EA000358

[5] The JEM-EUSO Collaboration (corresponding authors: Mackovjak, Š. & Shinozaki, K.): 2019, Ultra-violet imaging of the night-time earth by EUSO-Balloon towards space-based ultra-high energy cosmic ray observations, Astroparticle Physics, 111, 54. https://doi.org/10.1016/j.astropartphys.2018.10.008

[6] MACKOVJAK, Š. - BOBÍK, P. - BALÁŽ, J. - STRHÁRSKÝ, I., PUTIŠ, M. - GORODETZKY, P.: 2019, Airglow monitoring by one-pixel detector, Nuclear Instruments and Methods in Physics Research Section A: Accelerators, Spectrometers, Detectors, and Associated Equipment, 992, 150. https://doi.org/10.1016/j.nima.2018.12.073

The *Faculty of Mathematics, Physics and Informatics, Comenius University, Bratislava* was involved in the following eight directions of research as listed below.

Photometric observations and research of asteroids at Astronomical and Geophysical Observatory Modra, Faculty of Mathematics, Physics and Informatics, Comenius University in Bratislava

The photometric program of asteroid observations continued at Astronomical and Geophysical Observatory in Modra, Comenius University in Bratislava, some of the projects also in collaboration with the Astronomical Institute of the Czech Academy of Sciences, Ondřejov, Czech Republic.

In [1] we studied the membership, size ratio and rotational properties of 13 asteroid clusters consisting of between 3 and 19 known members that are on similar heliocentric orbits. By backward integrations, we confirmed their cluster membership and estimated times elapsed since separation of the secondaries from the primary that are between 10^5 and a few 10^6 years. By using photometric observations we derived the accurate absolute magnitudes of primaries and rotation periods for all the clusters. We found that 11 of the 13 clusters follow the same trend of primary rotation period vs. mass ratio as revealed by Pravec et al. (2010).

The spin states of Non-Principal Axis (NPA) rotators offer significant clue to the evolutionary processes of these asteroids because their excited spin states are thought to be caused by internal and/or external forces in the past. Incorporating the photometric datasets obtained from the three apparitions, 2006, 2016 and 2017, we constructed its spin state and shape model of Krylov [2]. We found that the asteroid is rotating in Short Axis Mode (SAM) with rotation and precession periods of 68.15 h and 396.30 h, respectively. The largest and intermediate principal inertia moments are nearly the same: Ib/Ic = 0.98. However, the smallest principal inertia moments is less than the half of the others: Ia/Ic = 0.23. We outlined the possible evolutionary processes which led to the observed spin state.

We conducted a photometric, spectroscopic, and dynamical study of V-type asteroids outside the Vesta family in the inner main belt [3]. The aim was to find traces of once existing differentiated planetesimals other than Vesta, to provide the missing observational evidence for theories predicting an abundance of such planetesimals in the early solar system.

In [4] we presented the study of a sample of 93 asteroid pairs that are on highly similar heliocentric orbits. We estimated times elapsed since separation of pair members that are between $7{\times}10^3$ yr and a few 10^6 yr. With photometric observations, we derived the rotation periods P1 for all the primaries and a sample of secondaries. For a part of the studied pairs, we refined their WISE geometric albedos and collected or estimated their taxonomic classifications. For 17 asteroid pairs, we also determined their pole positions. Moreover, we found that the

primaries of 13 asteroid pairs in our sample are actually binary or triple systems, i.e., they have one or two bound, orbiting secondaries. We compared the obtained asteroid pair data with theoretical predictions and discussed their implications. We found that 86 of the 93 studied asteroid pairs follow the trend of primary rotation period vs mass ratio that was found by Pravec et al. (2010). Of the 7 outliers, 4 are high mass ratio pairs that were unpredicted by the theory of asteroid pair formation by rotational fission. The 13 asteroid pairs with binary primaries are particularly interesting systems that place important constraints on formation and evolution of asteroid pairs.

**Meteor observations and analyses by AMOS network**

In 2018-2019 continued the monitoring of meteor activity above the Central Europe, Canary Islands, Atacama desert in Chile and Hawaii by All-sky Meteor Orbit System (AMOS), autonomous video observatory for detection of transient events on the sky. Hardware and software of AMOS have been developed and constructed at the Astronomical and Geophysical observatory of Comenius University in Modra.

We introduced and demonstrate the capability of the updated All-Sky Meteor Orbit System (AMOS) (called AMOS-Spec) [5] to measure the emission lines intensites of meteoric element abundances of meteors. The AMOS-Spec program has been created with the intention of carrying out regular systematic spectroscopic observations. At the same time, the meteoroid trajectory and pre-atmospheric orbit are independently measured from data collected by the AMOS camera network. This, together with spectral information, allows us to find the link between the meteoroid and its parent body, from both dynamical and physical consideration. Here we report results for 202 selected cases.
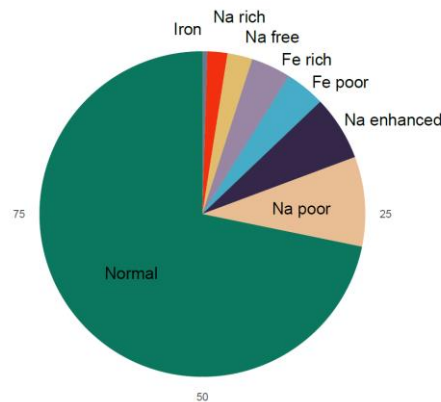
Figure 2.1. Distribution of spectral classes identified within the sample of 202 meteoroids in the mm to dm size range.
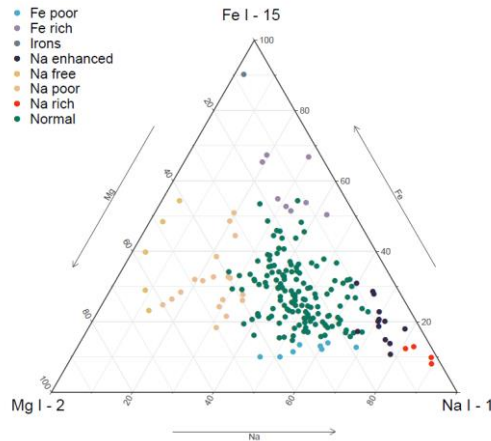
Figure 2.2. *Ternary diagram displaying the spectral classification of 202 meteors of -1 to -14 abs. mag. (corresponding to meteoroids of mm to dm sizes) observed by the AMOS-Spec system during 2013–2017 from AGO Modra Slovakia.*

Development of Slovakian optical sensor for space debris objects cataloguing and research

The Department of Astronomy which is part of the Faculty of Mathematics, Physics and Informatics of Comenius University in Bratislava, Slovakia (FMPI CU) won an ESA PECS Slovakia activity with a main goal to transform a 0.7-m Newton telescope (AGO70) dedicated to amateur astronomical observations to a professional optical system for regular support of the space debris tracking and research [6]. The development started with the telescope installation at the FMPI's Astronomical and Geophysical Observatory in Modra, Slovakia (AGO) in September 2016. It was necessary to adapt the low-level telescope control to the needs of space debris tracking. For the image processing software we have chosen a modular design. It contains several individual elements performing tasks such as objects search on the frames, centroiding, astrometric reduction and tracklet building. The observation planning has been developed focusing on Low Earth Orbits (LEO) up to Geosynchronous Earth Orbits (GEO). The output products delivered by the system are astrometric positions in international formats (CCSDS TDM and MPC), light curves and relative color indices obtained by using Johnson-Cousins BVRI filters.

Fully operational AGO70 system will support cataloguing efforts of the European partners, which are maintaining their own space debris catalogues for research and space surveillance and tracking purposes. AGO70 shall support the tracking of LEO debris by the Satellite Laser Ranging (SLR) stations. In case of contingencies during ESA satellite missions, e.g., when the spacecraft is not responsive, a dedicated observation campaign can be performed with AGO70 to exam the integrity status of the affected spacecraft, to monitor its attitude motion state and to improve the object's orbital information.
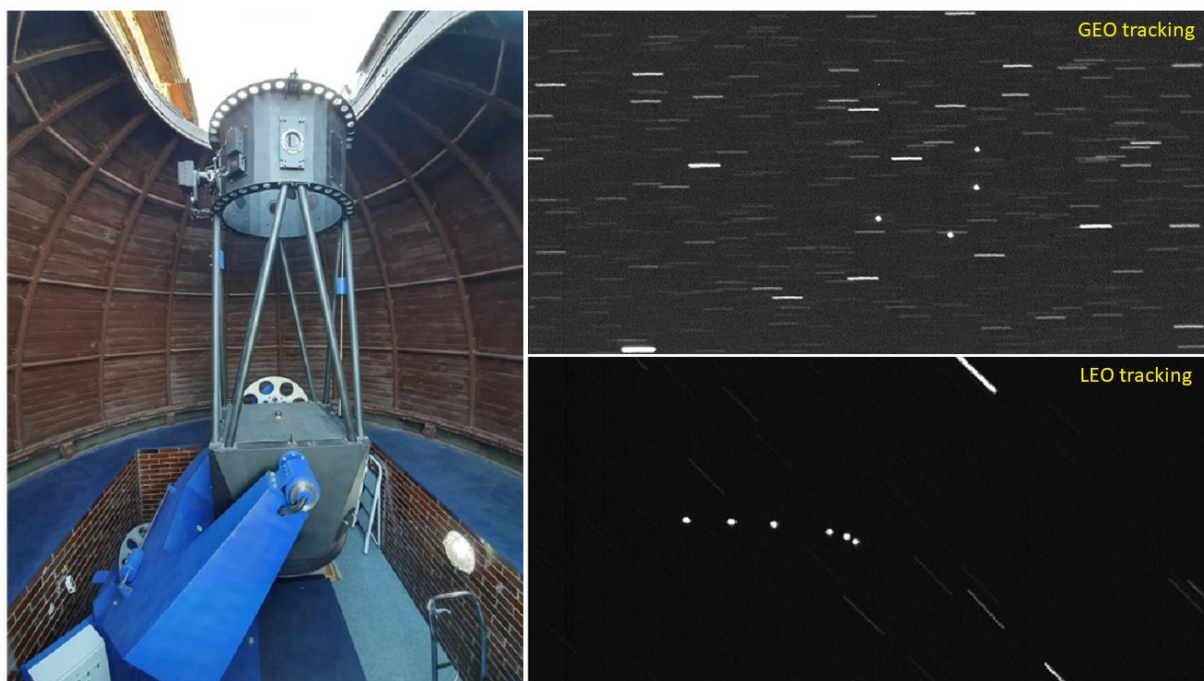
Figure 2.3. *AGO70 telescope installed at the Astronomical and Geophysical Observatory in Modra, Slovakia (left) and light frames acquired with GEO (top right) and LEO tracking (top bottom).*

References:

[1] PRAVEC, P. - FATKA, P. - VOKROUHLICKÝ, D - SCHEERES, D. J. - KUŠNIRÁK, P. - HORNOCH, K. - GALÁD, A. - VRAŠTIL, J. - PRAY, D. P. - KRUGLY, YU. N. - GAFTONYUK, N. M. - INASARIDZE, R. YA. - AYVAZIAN, V. R. - KVARATSKHELIA, O. I. - ZHUZHUNADZE, V. T. - HUSÁRIK, M. - COONEY, W. R. - GROSS, J. - TERRELL, D. - VILÁGI, J. - KORNOŠ, L. - GAJDOŠ, Š. - BURKHONOV, O. - EHGAMBERDIEV, SH. A. - DONCHEV, Z. - BORISOV, G. - BONEV, T. - RUMYANTSEV, V. V. - MOLOTOV, I. E.: Asteroid clusters similar to asteroid pairs. Icarus, 2018, Volume 304, p. 110-126.

[2] LEE, H.-J. - DURECH, J. - KIM, M.-J. - MOON, H.-K. - KIM, CH.-H. - CHOI, Y.-J. - GALAD, A. - PRAY, D. - MARCINIAK, A. - KAPLAN, M. - ERECE, O. - DUFFARD, R. - KORNOS, L. - GAJDOŠ, Š. - VILAGI, J.: Spin State of (5247) Krylov. American Astronomical Society, DPS meeting #50, 2018, id.414.10

[3] MARCINIAK, A. - OSZKIEWICZ, D. - TROIANSKYI, V. - FOHRING, D. - KWIATKOWSKI, T. - SKIFF, B. - GEIER, S. - BORCZYK, W. - MOSKOWITZ, N. - GALAD, A. - KANKIEWICZ, P. - KLUWAK, T. - GAJDOŠ, Š. - VILAGI, J. - POLČIC, Ľ. - WILAWER, E.: Investigating V-type

asteroids outside Vesta family. EPSC-DPS Joint Meeting 2019, held 15-20 September 2019 in Geneva, Switzerland, id. EPSC-DPS2019-1379

[4] PRAVEC, P. - FATKA, P. - VOKROUHLICKÝ, D. - SCHEIRICH, P. - ĎURECH, J. - SCHEERES, D. J. - KUŠNIRÁK, P. - HORNOCH, K. - GALÁD, A. - PRAY, D. P. - KRUGLY, YU. N. - BURKHONOV, O. - EHGAMBERDIEV, SH. A. - POLLOCK, J. - MOSKOVITZ, N. - THIROUIN, A. - ORTIZ, J. L. - MORALES, N. - HUSÁRIK, M. - INASARIDZE, R. YA. - OEY, J. - POLISHOOK, D. - HANUŠ, J. - KUČÁKOVÁ, H. - VRAŠTIL, J. - VILÁGI, J. - GAJDOŠ, Š. - KORNOŠ, L. - VEREŠ, P. - GAFTONYUK, N. M. - HROMAKINA, T. - SERGEYEV, A. V. - SLYUSAREV, I. G. - AYVAZIAN, V. R. - COONEY, W. R. - GROSS, J. - TERRELL, D. - COLAS, F. - VACHIER, F. - SLIVAN, S. - SKIFF, B. - MARCHIS, F. - ERGASHEV, K. E. - KIM, D.-H. - AZNAR, A. - SERRA-RICART, M. - BEHREND, R. - ROY, R. - MANZINI, F. - MOLOTOV, I. E.: Asteroid pairs: A complex picture. Icarus, 2019, Volume 333, p. 429-463.

[5] MATLOVIČ, P. – TÓTH, J. – RUDAWSKA, R. – KORNOŠ, L. - PISARČÍKOVÁ A.: Spectral and orbital survey of medium-sized meteoroids, A&A 629, A71 (2019)

[6] ŠILHA, J. - KRAJČOVIČ, S. - ZIGO, M. - ŽILKOVÁ, D. - ZIGO, P. - ŠIMON, J. - TÓTH, J. - KORNOŠ, L. - SETTY, S. - FLOHRER, T. - JILETE, B.: Development of the Slovak 70-cm Optical Passive System Dedicated to Space Debris Tracking on LEO to GEO orbits, Proceedings of the Advanced Maui Optical and Space Surveillance Technologies Conference, held in Wailea, Maui, Hawaii, September 17-20, 2019, Ed.: S. Ryan, The Maui Economic Development Board, id.85

In the ***Earth Science Institute of the Slovak Academy of Sciences, Bratislava and Hurbanovo***, a number of issues concerning space weather were investigated and ground magnetic field measurements were performed.

Theoretical studies were devoted in particular to the mechanisms of severe magnetic stoms with the use of historical magnetograms recorded long time before the space age. Owing to geomagnetically induced currents, extreme mid-latitude geomagnetic disturbances might cause serious damages to some vulnerable technological systems. A part of the space weather research has therefore to be focused on deeper understanding of the origins and mechanisms of these phenomena. In [1], three cases of mid-latitude geomagnetic variations are presented. One of them is a typical mid-latitude magnetic storm. The other two cases then represent a phenomenon, which is well known in polar and sub-polar regions; however, it is less common in mid-latitudes. As this phenomenon can sometimes be very intensive also at mid-latitudes and it can exhibit rapid temporal changes of the geomagnetic field, it must not be underestimated. In [2], the extreme magnetic storms are discussed to possibly caused be auroral ionospheric currents or electric currents parallel to magnetic induction lines. The study relies on magnetic observations storms from the modern digital era and also uses the historical magnetograms.

Recently, a new insight into the mechanism of the Carrington magnetic storm was published, which identified the field aligned currents as the main cause of this well-known event. The new idea seems to be a promising alternative to the generally accepted theory, in which the ring current is the main cause of the low- and mid-latitude magnetic storms. In [5], some records of rapid mid-latitude magnetic storms are shown. Most of them were recorded by historical magnetic observatories (years 1837, 1848, 1872, 1918). The profiles of the horizontal component show that, instead ofthe ring current, the substorm-related current system probably played an important role in the development of these interesting geomagnetic variations.

Historical magnetograms recorded in Clementinum (Prague) and reported previously in yearbooks were collected and prepared for future applications [3]. Daily magnetic observations at the Prague Astronomical Observatory started 180 years ago, on 1st July 1839. The observatory was equipped with standardized instruments developed by Gauss and Weber at Observatory of Goettingen. The observations were carried out manually, at the beginning the measurements were performed more than ten times per day but later the number of the daily observations decreased to five. Having been a part of Goettingen Magnetic Union, however, the sampling interval of readings from magnetometers was shortened to 5 minutes during appointed days. Even more dense measurements were carried out during periods of strong magnetic disturbances. As the results were printed in yearbooks Magnetische und meteorologische Beobachtungen zu Prag, no measured data were lost. Absolute measurements reported in the yearbooks are

sufficient for reliable reduction of declination. The Prague series of annual means of declination is the longest continuous series in the 19th century. The data are thus fully reliable for the study of geomagnetic activity and space weather applications, which will be demonstrated for a remarkable geomagnetic event recorded in Prague on 17th November 1848.
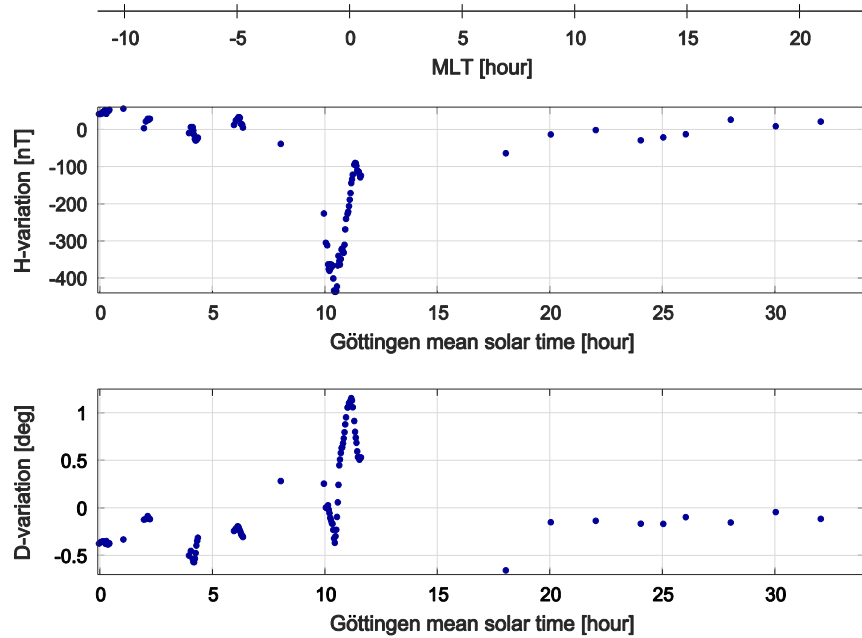
Figure 2.4. The variations of the horizontal intensity and declination that were recorded at the Clementinum observatory on 17 November 1848. The additional time axis at the top of the figure shows the magnetic local time (MLT).

Some recent studies point out that currents related to the auroral oval, electrojets and field aligned currents (FACs), are serious candidates for the mechanism of the intense mid-latitude magnetic storms. It is interesting to re-analyse historical data under the light of this modern knowledge. In this aim, two intense magnetic storms are analysed in [4] that were recorded by observatories Clementinum (Prague) and Greenwich on 17 November 1848 and 4 February 1872, respectively. The latter has been marked as an extraordinary event by several authors, in particular in connection with auroras. The former (Fig.2.4.), however, has been little known in the space weather community. Both these events possessed swift and extensive variations of the horizontal (H) component (>400 nT and >500 nT, respectively) and were accompanied by auroras sighted at very low magnetic latitudes. This implies that the auroral oval on the north hemisphere was vastly extended southward. The variations of the magnetic declination also indicate that during these events the auroral oval was situated at magnetic latitudes lower than those of the observatories. The storms studied in this paper occurred at different magnetic local times (MLTs), ~23 MLT (Fig 2.5.) and ~19 MLT. Therefore, they might represent mid-latitude events related to different parts of the auroral oval. In this paper, the H-variation recorded at

21

Clementinum in 1848 is interpreted to be a substorm due to the ionospheric substorm electrojet. The Greenwich event registered in 1872 then seems to be a combination of the ring-current storm with a positive variation of the H-component caused by the eastward electrojet. Both the events of 1848 and 1872 appear to exemplify phenomena that are common in high magnetic latitudes but which may occasionally happen also at mid-latitudes.
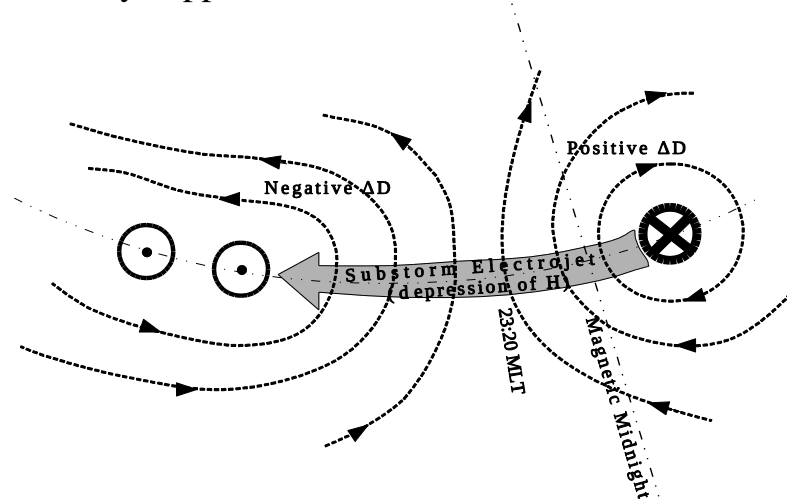
Figure 2.5. The schematic sketch of the conditions of the Clementinum observatory during the magnetic storm on 17 November 1848. The circles with dots in their centres indicate the location of the upward FAC, the circle with a cross mark the position of the downward FAC. The intensity of the electric currents is expressed by means of the boldness of the markers. The dashed lines represent the lines of force of the magnetic field generated by the FACs. The ΔD sign stands for the deviation of the magnetic declination. It is supposed that the substorm electrojet then flowed at a magnetic latitude which was lower than the magnetic latitude of Clementinum.

Hurbanovo Geomagnetic Observatory of the Earth Science Institute of the SAS, is located at geographical latitude 47.87° and geographical longitude 18.18°. It performs continuous monitoring and registration of the geomagnetic field components. The one-minute mean values of all components of the geomagnetic field as well as the records acquired with the one-second sampling interval are available. K-indexes characterising the geomagnetic activity in the middle latitudes are computed regularly. Main equipment of the observatory includes the digital variometer station TPM made in Poland (1996) and magnetoregistration device DI-fluxgate Magson gained on the co-operation bases withGeo Forshung Zentrum Potsdam and VW Stiftung. For absolute geomagnetic measurements, the DI-fluxgate magnetometer and proton precession magnetometer ELSEC are employed. The magnetovariational data in the one-minute step are supplied via the internet to the INTERMAGNET centre. The data are sent to World Data Centers in Edinburgh and Paris, from where they are available for the whole geomagnetic and space weather community. The data are published also on the CD-ROMs prepared in the frame of INTERMAGNET. That is beacuse the Hurbanovo Geomagnetic Observatory of the Earth Science Institute of the SAS is

a member of INTERMAGNET, the international network of world first order magnetic observatories. Information about the geomagnetic activity is also published on the web site of the observatory, www.geomag.sk. The level of the geomagnetic activity si reported to public media (TV), too.

The members of the Hurbanovo Geomagnetic Observatory staff regularly perform field measurements at the observation points of the national magnetic repeat station network, which is a part of the European repeat station network. The measurements are coordinated by the MagNetE Group. Measurements of the magnetic declination are performed regularly at selected Slovak airports.

The knowledge of the distribution of the geomagnetic field elements over a country is important for many practical as well as scientific reasons. Such distributions result from magnetic surveys. The surveys need to be repeated periodically: two-year period has been agreed for repeat stations by the MagNetE Group. This periodicity enables to find out information about the magnetic secular variations. The last repeat station survey was carried out in Slovakia in 2018.

References:

[1] VALACH, F. - VÁCZYOVÁ, M. Extrémne magnetické poruchy v pozorovaniach Hurbanovského observatória. In Zborník. X. medzinárodnej vedeckej konferencie Univerzity J. Selyeho. Webové aplikácie vo vzdelávaní. Komárno: Univerzita J. Selyeho, 2018, s. 78-85. ISBN 978-80-8122-251-1.

[2] VALACH, F. - HEJDA, P. - REVALLO, M. - BOCHNÍČEK, J. Aký je mechanizmus extrémnych magnetických porúch v stredných šírkach. In DOROTOVIČ, Ivan. Zborník referátov z 24. celoštátneho slnečného seminára, Kežmarok 2018. - Hurbanovo: Slovenská ústredná hvezdáreň Hurbanovo, 2018, ISBN 978-80-89998-01-2.

[3] HEJDA, P. - VALACH, F. - REVALLO, M. What can be learned from geomagnetic observations at Prague Observarory (1839-1917): abstract: IUGG19-0281. In 27th IUGG General Assembly-Assemblée Générale de L´UGGI: abstracts. - Montreal: IUGG General Assembly, 2019.

[4] VALACH, F. - HEJDA, P. - REVALLO, M. - BOCHNÍČEK, J. Possible role of auroral oval-related currents in two intense magnetic storms recorded by old mid-latitude observatories Clementinum and Greenwich. In Journal of Space Weather and Space Climate, 2019, vol. 9, p. A11.

[5] VALACH, F. - HEJDA, P. - BOCHNÍČEK, J. - REVALLO, M. - VÁCZYOVÁ, M. Rapid mid-latitude magnetic storms recorded by old observatories. In Conrad Observatory Journal: IAGA Workshop 2018, 2019, special issue no. 5, p. 38.

In the ***Slovak Central Observatory* (SCO)** in Hurbanovo (http://www.suh.sk), a number of activities related to space research were performed. We observed sunspots (the Wolf number data were submitted to the SILSO in Brussels, Belgium and to the SONNE Netz in Germany) and prominences (images are published at the website of the Observatory). We performed also spectrographic observations of the solar spectrum (variations of selected spectral lines during a solar activity cycle) using a horizontal solar telescope with spectrograph, we registered solar radio bursts using a solar radio spectrometer CALLISTO and impact of solar flares on the Earth's ionosphere using a SID monitor. The research activities comprise study of the:

- differential rotation of the solar corona, automatic detection and tracking of the sunspots and the coronal bright points,
- automatic detection of the chromospheric plages,
- asymmetry of the north and south hemispheric solar activity.

One researcher from the SCO is the national ISWI (International Space Weather Initiative, http://iswi-secretariat.org) coordinator for the Slovak Republic and since September 2014 he is also as a Scientific Discipline Representative of the SCOSTEP for the field of solar physics. He is member of the National Committee of the SCOSTEP and chair and representative to the COSPAR.

We continued to publish at the website of the SCO data on the modified coronal index (MCI) and the modified homogeneous data set (MHDS) of coronal intensities based on satellite EUV measurements as a replacement of ground-based coronagraphic observations at Lomnický Štít. Both the MCI and the MHDS data sets can be used further for studies of the coronal solar activity and its cycle. These data are available at http://www.suh.sk/online-data/modifikovany-koronalny-index and http://www.suh.sk/online-data/modifikovany-homogenny-rad, respectively.

In the Computer Intelligence Group (CA3) of the CTS/UNINOVA (Caparica, Portugal) has been developed in previous years a software tool for automatic tracking of solar activity features (sunspots and coronal bright points - CBPs) using a hybrid algorithm combining PSO (Particle Swarm Optimization) and Snake algorithms and recently an image segmentation algorithm, respectively, for detecting and tracking of a feature, and determining the differential rotation of the Sun. In [1] we applied a segmentation algorithm called Gradient Path Labelling (GPL), used originally to identify drusens in medical retinal images, to detect and track the coronal bright points (CBPs) using images from the AIA instrument onboard the SDO satellite. Individual measurements of rotational velocity in respect to latitude are depicted in Fig. 2.6. The CBPs have a tendency to change shape and size along time, to disappear and reappear at a corresponding heliographic position, therefore, decision trees were also included in the tracking solution. Since our CBP detection algorithm uses an active region mask to filter

out the CBPs, whose centroid is inside the active regions, the number of identifications clearly depends on the level of solar activity. Our approach uses the commonly applied fitting relation to the latitudinal dependence of the rotational velocity, which resulted in calculation of the optimum fit parameters as well as the Gegenbauer orthogonal polynomial.

Another segmentation algorithm for automatic detection of CBPs developed using SunPy and OpenCV in Python is described in [2] (Fig. 2.7). An automatic tool to detect coronal holes (CHs) and to determine solar differential rotation using CBPs inside and outside the CHs, respectively, is being developed in the CTS/UNINOVA-CA3 group.

In the SCO we developed also an alternative software tool to estimate the solar rotational profile based on cross-correlation (CC) method [3]. Rotational velocity was calculated for each day in the years 2011 – 2018 from CC maxima of two consecutive SDO/AIA images with a cadence of 30 minutes taken through the 21.1 nm filter, in a window of 6° in heliographic longitude and 69° in heliographic latitude (241 x 2761 pxs). It was performed only in the rows where the CC maximum was higher than 0.5 (Fig. 2.8). The calculation of ω was repeated separately for rows that intersect a CBP and for rows without the contribution of a CBP, respectively. We call these background rows BCGs (Fig. 2.9).

In collaboration with the Observatório Geofísico e Astronómico da Universidade de Coimbra (OGAUC, Coimbra, Portugal) we developed new algorithms to detect and track solar activity features, chromospheric plages as test features. The Ca II K3 spectroheliograms registered in the OGAUC were used to investigate the evolution of the chromospheric plages activity during the 24th solar cycle. Research team of the OGAUC created a special tool based on the segmentation by watershed method combined with other mathematic morphological operators to detect automatically and analyse the plages and/or other solar features. Several procedures are applied to achieve the automatic detection (top-hat transform, hole filling, tresholding, watershed operation, gradient operation which allows to obtain contours of plage regions). One of the great potentialities of using mathematical morphology is its power to deal with the geometry of complex and irregular shapes. More, north-south asymmetry of the solar activity can be studied using this tool. The results were published in [4] (Fig. 2.10).
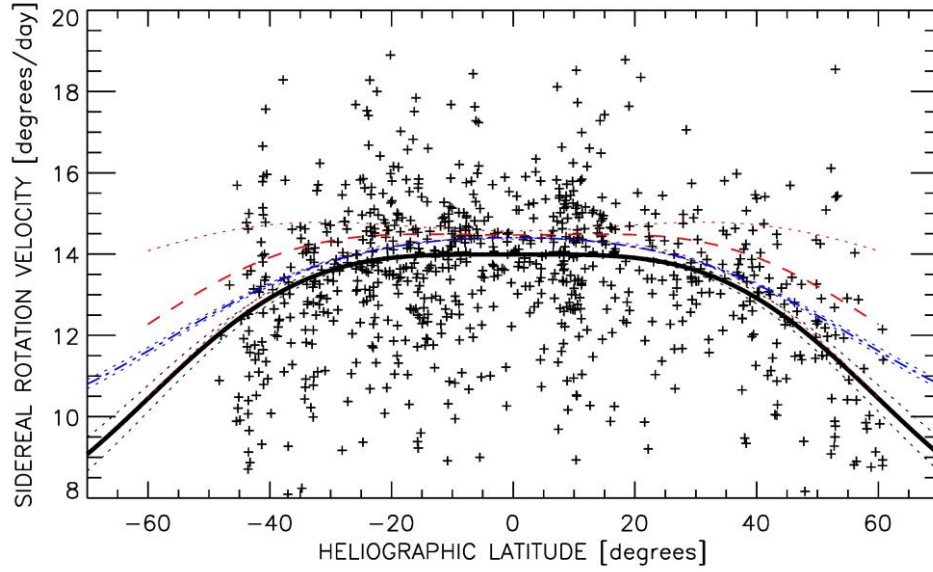
Figure 2.6. *Individual measurements of rotational velocity in respect to latitude. Thick solid black line indicates the best fit to these values using the relation $\omega(b) = A + B \sin^2(b) + C \sin^4(b)$, where ω is the rotational velocity and the b is the latitude. Thin dotted black lines mark the fit uncertainty using the 1-sigma of the A, B, C parameters. The equatorial rotational velocity is 14°/day. Rotational profiles derived by other authors are showed for comparison.*
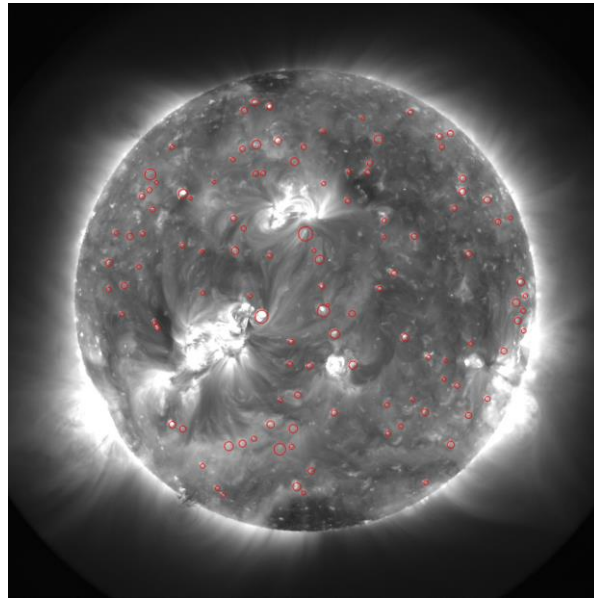
Figure 2.7. *Illustrative result of the segmentation process using the Python tool for detection of CBPs in the 19.3 nm SDO/AIA image.*
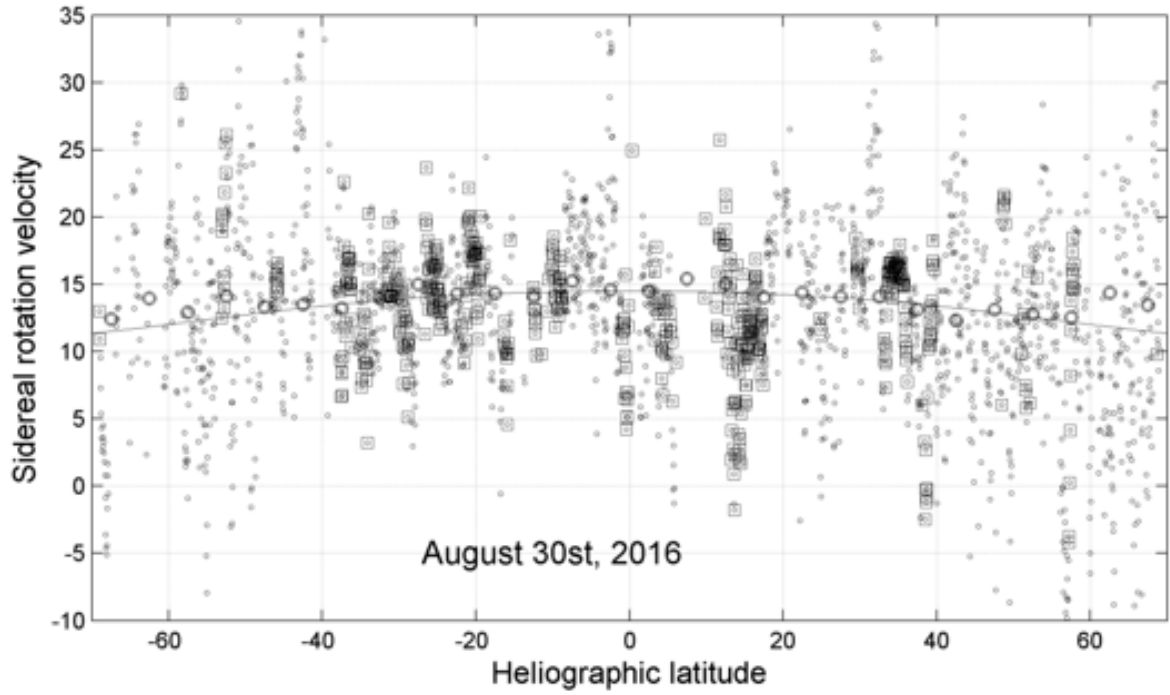
Figure 2.8. *Rotational profile as derived using the CC method, where squares mark the mean values in 5° sectors and the solid line is the best fit of these values.*
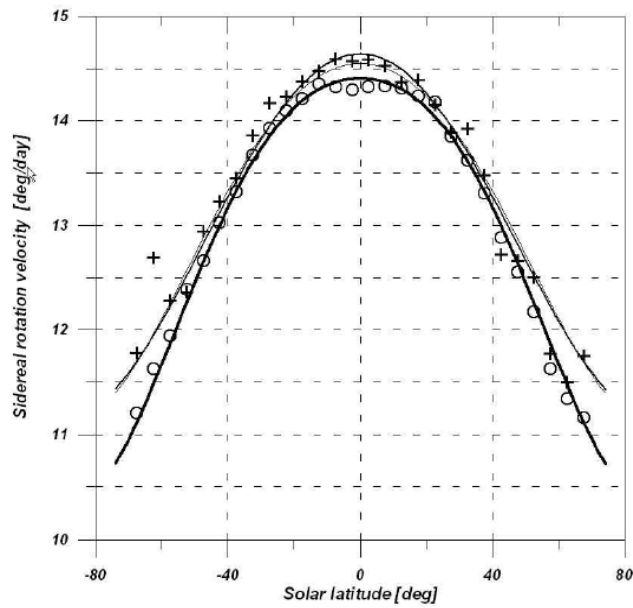
Figure 2.9. *Profile of sidereal rotation velocity showing BCG data (circles) and CBP data (crosses). Solid lines show approximations, for o:* $\omega = 12.183 - \sin^2 b - 1.955 \sin^4 b$ *and for +:* $\omega = 14.642 - 3.185 \sin^2 b - 0{:}304 \sin^4 b.$

27
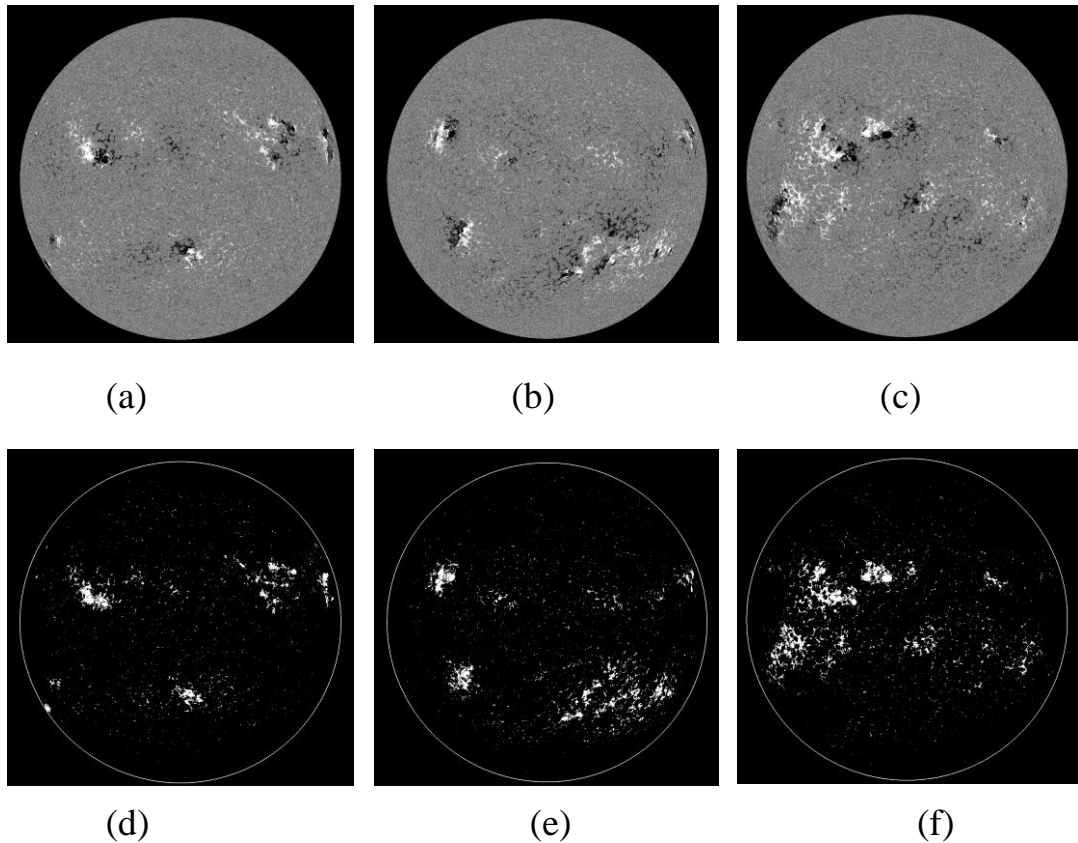
Figure 2.10. HMI SDO images showing the polarity of magnetic field: a) original image acquired on 3 September 2011; b) original image acquired on 10 August 2012; c) original image acquired on 10 May 2014; d) facular regions of the image of Figure (a); e) facular regions of image of the Figure (b) and f) facular regions of the image of Figure (c).

The SCO organised in the year 2018 the 24th National Solar Physics Meeting with participation from abroad. The goal of the Meeting was to present new results of solar physics and from the field of the space weather (Sun-Earth connections), to provide overview of present status in selected fields of solar physics, geophysics, meteorology, and climatology. A separate space was devoted to the presentation of research results of undergraduate and PhD students of university and academic departments and also to results of scientific and popularisation activities of Astronomical Observatories in the Slovak Republic and the Czech Republic. Invited talks, short contributions and posters covered the following fields: physical phenomena in the solar atmosphere, solar activity, total solar eclipses, space weather, geoactivity, meteorological events with solar forcing.

References:

[1] DOROTOVIČ I. - COELHO A. - RYBÁK J. - MORA A. - RIBEIRO R.A. (2018). Gradient Path Labelling Method and Tracking Method for Calculation of Solar Differential Rotation using Coronal Bright Points, Astronomy and Computing, Vol. 25, pp.168-175. doi: 10.1016/j.ascom.2018.09.008

[2] DOROTOVIČ I. - COELHO A. - RYBÁK J. - MORA A. - RIBEIRO R.A. - KUSA W. (2018). Solar Differential Rotation Profile Estimation using Coronal Bright Points Data Derived from the SDO/AIA Images, Sun and Geosphere, Vol.13, no.2, p.129-133. doi: 10.31401/SunGeo.2018.02.02

[3] DOROTOVIČ I. - RYBANSKÝ M. (2019). Rotation of Some Solar Coronal Bright Features as Derived from the Solar Dynamics Observatory/Atmospheric Imaging Array (SDO/AIA) 21.1 nm Images (for the Years 2011 - 2018), Solar Physics, Vol. 294, Issue 8, article id. 109, 9 pp. doi: 10.1007/s11207-019-1501-z.

[4] BARATA T. - CARVALHO S. - DOROTOVIČ I. - PINHEIRO F.J.G. - GARCIA A. - FERNANDES J. - LOURENÇO A.M. (2018). Software tool for automatic detection of solar plages in the Coimbra Observatory spectroheliograms, Astronomy and Computing, Vol. 24, s. 70-83. doi: 10.1016/j.ascom.2018.06.003.

The activities of ***the Astronomical Institute of the Slovak Academy of Sciences (AISAS)***, Tatranská Lomnica (http://www.astro.sk), related to COSPAR, were devoted to research in stellar, solar, and interplanetary physics using different satellite observations, mainly in the UV, XUV and X-ray spectral regions. Stellar data of the XMM-Newton, MOST, and Kepler satellites, including the HST were used for research of various variable stars and start hosting exoplanets [2-8]. Data of the current SDO, IRIS, STEREO, ACE, and other satellites were used for solar research mostly focused on solar prominences and flares. In common, these data were used with the simultaneously acquired data by the ground-based solar telescopes [9-15]. Topic of the interstellar particles has been also addressed [1]. Hereby we present some examples of the results obtained by the AISAS staff.

Observations carried out with the space observatories, the European Space Agency's (ESA) X-ray Multi-Mirror Mission (XMM-Newton) and the Hubble Space Telescope (HST), were used to model the spectral energy distribution (SED) of the classical nova V339 Delphini, which exploded on August 14, 2013 (= nova age 0) [8]. Using our original method of multiwavelength modeling the nova spectrum, we revealed new striking results: (i) At the nova age of 35 days, the WD photosphere was oblate in poles and a slow equatorially concentrated mass-outflow contained dust grains. (ii) From day 35 to 72, the nova significantly stopped-down the mass-outflow. (iii) On day 100, the co-existence of the strong dust emission and the luminous high-temperature WD confirmed the disk-like formation around the WD, where the dust can spend a long time. (iv) Our modeling revealed highly super-Eddington luminosity of the burning WD lasting, at least, for the first 100 days of the nova life. Fig. 2.11. shows a sketch for the nova ejecta as can be inferred from our SED models on days 35 and 100. This finding represents a new challenge for theoretical modeling of the nova phenomenon.

The X8.2-class solar flare SOL2017-09-10T16:06 ranks as the second most energetic flare in the solar cycle 24. This major eruptive event happened at the western solar limb and triggered a very fast coronal mass ejection followed by significant space weather and heliospheric effects including a solar energetic particles event detected also as ground level enhancement. *The flare displayed an extended arcade of flare loops*, being detected in the range of temperatures from X-rays down to cool chromospheric-like plasmas. While hot flare loops with temperatures of $10^6 - 10^7$ K were observed in the EUV channels of the Atmospheric Imaging Assembly (Fig. 2.12) aboard the Solar Dynamics Observatory (SDO/AIA), cool loops with temperatures of 10^4 K were captured by two UV SDO/AIA channels and also by the ground-based Swedish Solar Telescope (SST) which made a series of spectral and spectropolarimetric images of the cool off-limb loops in the spectral line of single ionized calcium Ca II 8542 Å and the hydrogen Balmer line Hβ at 4861 Å (Fig. 2.12.). The article by Kuridze et al. (2019) [12] reports on inferring the magnetic field strengths of the cool flare

loops using the weak-field approximation applied to the Stokes I and V profiles of the Ca II 8542 Å line. The analysis reveals coronal magnetic field strengths as high as 350 G at heights up to 25 Mm above the solar limb. These measurements
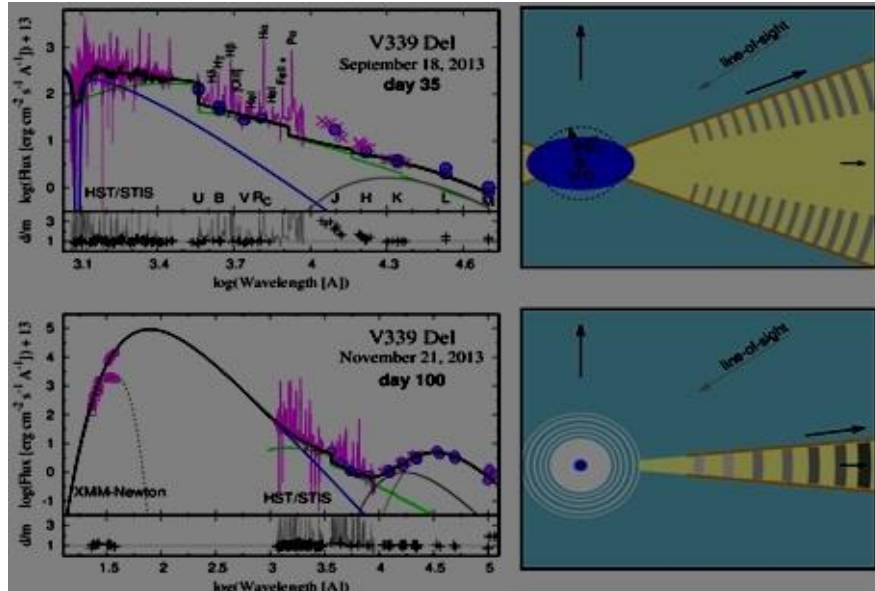
Figure 2.11. *Left: Observed spectrum of the nova V339 Del (in magenta) and its model (black line). The model consists of the radiation from the WD (blue line), nebula (green) and dust (gray). Right: Sketch for nova ejecta. The WD pseudophotosphere is in dark-blue, stellar wind in light-blue, equatorially concentrated outflow with dust in yellow with gray strips and bow shocks as orange lines. The white array represents stopping-down the wind from the WD indicated on day 100 of the nova age.*
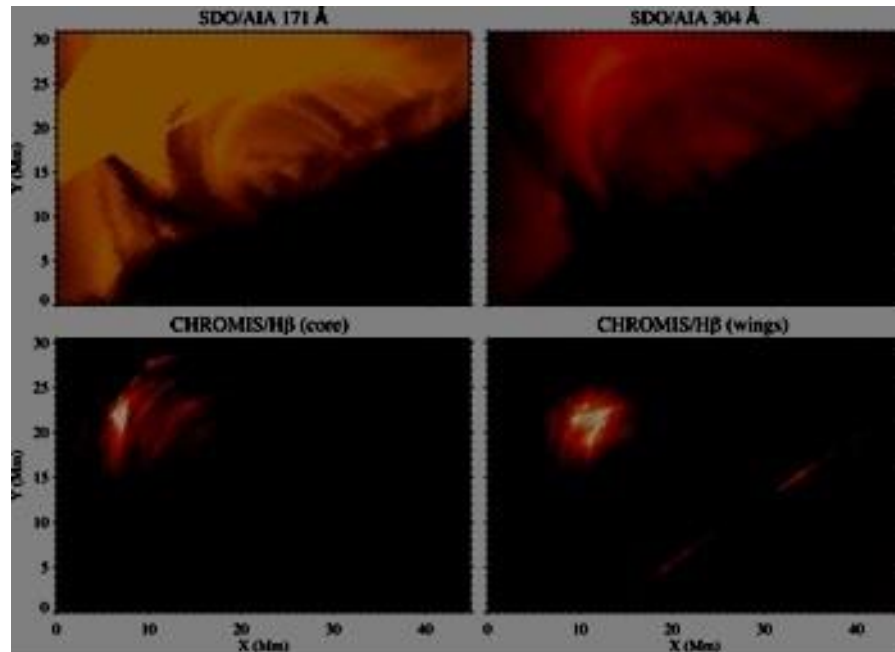
Figure 2.12. *SDO/AIA 171 Å and 304 Å images (*top panels*) of the X8.2 class solar flare loops on 2017 September 10, 16:29 UT co-aligned with SST/CHROMIS Hβ line core (*bottom left panel*) and the composite of Hβ wing images at ± 0.735 Å (*bottom right panel*).*

are substantially higher than a number of previous estimates and may have considerable implications for our current understanding of the extended solar atmosphere.

How much of the dust population originates locally in the solar system and how much comes from beyond? How big is the probability that an interstellar meteoroid passing through the solar system will hit the Earth? How are the speed measurements by which interstellar meteoroids are identified affected by the uncertainties of the statistical treatment or measurement errors? These problems and the presence of a large number of meteoroid orbits determined as hyperbolic in meteor databases has led to meteor astronomers who deal with particles registered in the Earth's atmosphere from AISAS and scientists who work with the dust measured on detectors on board of the space probes working together. The results, summarized in the chapter „Interstellar Meteoroids", in a book published by Cambridge University Press in 2019 [1], showed that, except for two macroscopic interstellar objects, the only dependable detection of interstellar particles in our solar system to date are the measurements of interstellar dust originating from the Local Interstellar Cloud. Not a single case of a meteor claimed to be produced by an interstellar particle has proven satisfactorily convincing and not one interstellar fireball has yet been reported.

Researchers from AISAS carried out follow-up observations of targets from the K2 mission and discovered a unique object, a chemically peculiar Ap-type star showing δ Scuti pulsations that is bound in an eclipsing binary system with an orbital period shorter than 3 d [7]. HD 99458 is therefore a complex astrophysical laboratory opening doors for studying various, often contradictory, physical phenomena at the same time. It is the first Ap star ever discovered in an eclipsing binary. The orbital period of 2.722 d is the second shortest among all known chemically peculiar (CP2) binary stars. Pulsations of δ Scuti type are also extremely rare among CP2 stars and no unambiguously proven candidate has been reported. HD 99458 was formerly thought to be a star hosting an exoplanet, but we definitely reject this hypothesis using photometric observations from the K2 mission and new radial velocity measurements.

Besides of this, the AISAS staff was involved (or leading) in the last two years in 4 coordinated observing campaigns focused on observations of several aspects of the solar activity. The integral part of campaigns were also measurements performed by the space-born instruments on different satellites, e.g. IRIS, SDO. The measurements were coordinated with the ground-based instruments including the AISAS owned CoMP-S and SCD instruments at the Lomnicky Peak Observatory.

References:

[1] HAJDUKOVÁ, M., Jr. - STERKEN, V. - WIEGERT, P. Interstellar meteoroids. Meteoroids: Sources of Meteors on Earth and Beyond. Cambridge: Cambridge University Press, 2019, p. 235-252.

[2] GAJDOŠ, P. - VAŇKO, M. - PRIBULLA, T. - DUPKALA, D. - ŠUBJAK, J. - SKARKA, M. - KABÁTH, P. - HAMBÁLEK, Ľ. - PARIMUCHA, Š. Transit timing variations, radial velocities, and long-term dynamical stability of the system Kepler-410. Monthly Notices of the Royal Astronomical Society, 2019, vol. 484, no. 3, p. 4352-4359.

[3] GAJDOŠ, P. - VAŇKO, M. - JAKUBÍK, M. - EVANS, P. - BRETTON, M. - MOLINA, D. - FERRATFIAT, S. - GIRARDIN, E. - GUDMUNDSSON, S. - SCAGGIANTE, F. -PARIMUCHA, Š. WASP-92, WASP-93, and WASP-118: transit timing variations and long-term stability of the systems. Monthly Notices of the Royal Astronomical Society, 2019, vol. 485, no. 3, p. 3580-3587

[4] GAJDOŠ, P. - VAŇKO, M. - PARIMUCHA, Š. Transit timing variations and linear ephemerides of confirmed Kepler transiting exoplanets. Research in Astronomy and Astrophysics, 2019, vol. 19, no. 3, article no. 41, p. 1-6

[5] HAMBÁLEK, Ľ. - VAŇKO, M. - PAUNZEN, E. -SMALLEY, B. T Tauri stars in SuperWASP and NSVS surveys. Monthly Notices of the Royal Astronomical Society,2019, vol. 483, no. 2, p. 1642-1654.

[6] PAUNZEN, E. - HANDLER, G. - WALCZAK, P. -HUMMERICH, S. - NIEMCZURA, E. - KALLINGER, T. - WEISS,W.W. - BERNHARD, K. - FEDURCO, M. - GÜTL-WALLNER, A. - MATTHEWS, J.M. - PRIBULLA, T. - VAŇKO, M. - WALLNER, S. - RÓZANSKI, T. A revisit to the enigmatic variable star 21 Comae. Monthly Notices of the Royal Astronomical Society, 2019, vol. 485, no. 3, p. 4247-4259

[7] SKARKA, M. - KABÁTH, P. - PAUNZEN, E. - FEDURCO, M. - BUDAJ, J. - DUPKALA, D. - KRTIČKA, J. - HATZES, A. - PRIBULLA, T. - PARIMUCHA, Š. - MIKULÁŠEK, Z. - GUENTHER, E. - SABOTTA, S. - BLAŽEK, M. - DVOŘÁKOVÁ, J. - HAMBÁLEK, Ľ. - KLOCOVÁ, T. - KOLLÁR, V. - KUNDRA, E. - ŠLECHTA, M. - VAŇKO, M. HD 99458: First time ever Ap-type star as a delta Scuti pulsator in a short period eclipsing binary? Monthly Notices of the Royal Astronomical Society, 2019, vol. 487, no. 3, p. 4230-4237.

[8] SKOPAL, A. Multiwavelength modeling of the SED of Nova V339 Del: Stopping the wind and long-lasting super-Eddington luminosity with dust emission. The Astrophysical Journal, 2019, vol. 878, no. 1, article no. 28,p. 1-18.

[9] DORAN, D.J. - DALLA, S. - ZELINA, P. Temporal evolution of heavy-ion spectra in solar energetic particle events. Solar Physics, 2019, vol. 294, no. 5,

article no. 55, p. 1-26.

[10] HERNANDEZ-PEREZ, A. - SU, Y. - VERONIG, A. -THALMANN, J.K. - GÖMÖRY, P. - JOSHI, B. Pre-eruption processes: Heating, particle acceleration, and the formation of a hot channel before the 2012 October 20 M9.0 limb flare. The Astrophysical Journal, 2019, vol. 874, no. 2, article no. 122, p. 1-11.

[11] KOZA, J. - KURIDZE, D. - HEINZEL, P. - JEJČIČ, S. -MORGAN, H. - ZAPIÓR, M. Spectral diagnostics of cool flare loops observed by the SST. I. Inversion of the Ca II 8542 A and H-beta lines. The Astrophysical Journal, 2019, vol. 885, no. 2, article no. 154, p. 1-13.

[12] KURIDZE, D. - MATHIOUDAKIS, M. - MORGAN, H. - OLIVER, R. - KLEINT, L. - ZAQARASHVILI, T. V. - REID, A. - KOZA, J. - LOFDAHL, M. G. - HILLBERG, T. - KUKHIANIDZE, V. - HANSLMEIER, A. Mapping the magnetic field of flare coronal loops. The Astrophysical Journal, 2019, vol. 874, no. 2, article no. 126, p. 1-12.

[13] SCHWARTZ, P. - GUNÁR, S. - JENKINS, J. M. - LONG, D. M. - HEINZEL, P. - CHOUDHARY, D. P. 2D non-LTE modelling of a filament observed in the H alpha line with the DST/IBIS spectropolarimeter. Astronomy and Astrophysics, 2019, vol. 631, aricle no. A146, p. 1-12.

[14] VERONIG, A. - GÖMÖRY, P. -DISSAUER, K. - TEMMER, M. - VANNINATHAN, K. Spectroscopy and differential emission measure diagnostics of a coronal dimming associated with a fast halo CME. The Astrophysical Journal, 2019, vol. 879, no. 2, article no. 85, p. 1-11.

[15] ZEMANOVÁ, A. - DUDÍK, J. - AULANIER, G. - THALMANN, J.K. - GÖMÖRY, P. Observations of a footpoint drift of an erupting flux rope. The Astrophysical Journal, 2019, vol. 883, no. 1, article no. 96, p. 1-13.

3. LIFE SCIENCES

M. Musilová

Life sciences research in Slovakia, within the space sector, is primarily performed by the Slovak Organisation for Space Activities (SOSA) and at the Faculty of Electrical Engineering and Information Technology of the Slovak University of Technology in Bratislava (FEI STU), in collaboration with multiple Slovak and international partners. It is primarily focused on astrobiology and human space exploration. From an astrobiological perspective, researchers and students at SOSA and FEI STU study life in extreme environments (extremophiles) as analogue organisms for the lifeforms that we could potentially find on other celestial bodies. Part of the research projects focus on the degradation of biological molecules when exposed to the harsh conditions in the stratosphere, such as DNA and cell membranes. This is performed by taking biological samples into the stratosphere using stratospheric balloons developed by SOSA. SOSA and FEI also have various instruments that can be used to simulate the atmospheric pressure, temperatures and vacuum at different altitudes.

Extremophiles have also been studied by SOSA and FEI STU in extreme conditions, such as on the glaciers in Svalbard and within lava tubes on volcanoes in Hawaii. The former project was based on a collaboration with the University of South Bohemia (Czech Republic) and the Faculty of Natural Sciences of the Comenius University in Bratislava (Slovakia). A team from SOSA studied two different environments in Svalbard, from an ecological, geological and microbiological perspective and their relevance to extraterrestrial conditions. Biochemical and genetic analyses were performed on the samples by high school and university students in Slovakia for educational and outreach purposes. Students have been studying the survival of these extremophiles in different simulated planetary conditions and they have used them for their bachelors and masters projects.

Regarding the human space exploration research, a member of SOSA and visiting professor at FEI STU has been selected to take part as a Commander of multiple simulated missions to the Moon and Mars in Hawaii, funded by NASA and ESA. The research has been focused on both testing the scientific and technological research that needs to be performed so that humans can return to the Moon and explore Mars one day. Furthermore, the missions are also aiming to determine what the ideal types of crewmembers are to send on long duration missions into space. For these reasons, the missions try to recreate the difficulties and extreme circumstances of long duration space missions. Then, they assess the performance of each of the crewmembers individually and how they work as a team together. These particular missions take place at the Hawaii - Space Exploration Analog and Simulation (HI-SEAS) habitat, which is located at 2,500 meters in elevation

on the active volcano Mauna Loa, on the Big Island of Hawaii. As of 2018, the International Moonbase Alliance (IMA), an organization dedicated to building sustainable settlements on the Moon, has been organizing regular simulated missions to the Moon and Mars at HI-SEAS. The constraints for these missions depend on which celestial body the mission is simulating to be on. For instance, for lunar missions the time delay in communications is only of a few seconds, in comparison to the 20 minute one way delay imposed on communications with Mars. The crews are supported by a Mission Control Centre based on the Big Island of Hawaii as well.

In 2019, the EuroMoonMars IMA HI-SEAS (EMMIHS) campaign was launched at HI-SEAS, bringing together researchers from ESA, IMA, the International Lunar Exploration Working Group (ILEWG), European Space Research and Technology Centre (ESTEC), VU Amsterdam and many other international organizations. During this campaign, two crews spent two weeks each at HI-SEAS in 2019, performing research relevant to both the Moon and Mars there. The campaign aims to increase the awareness about the research and technology testing that can be performed in analogue environments, in order to help humans become multiplanetary species. Furthermore, the research and technological experiments conducted at HI-SEAS are going to be used to help build a Moon base in Hawaii, and ultimately to create an actual Moon base on the Moon, as part of IMA's major goals. An example of one of Slovak outreach experiments on the EMMIHS I mission was a biology project designed by high school students in Slovakia, as part of a nationwide competition organized by a member of SOSA and visiting professor at FEI STU. It focused on fertilizing soils to grow plants on using human hair from the crewmembers during an analogue mission. Slovak hardware has also been tested at HI-SEAS during missions, such as the RoboTech Vision rover.

Additionally, SOSA and FEI STU representatives regularly present about the life sciences research projects that they are working on at multiple international conferences, including the International Astronautical Congress (IAC) run by the International Astronautical Federation (IAF) and the Europlanet Science Congress (EPSC). A member of SOSA and visiting professor at FEI STU is also a reviewer for the NASA Planetary Protection Research Program and many other grant programs and research journals in life sciences, such as Astrobiology and the National Science Foundation. They are an Adjunct Faculty of the International Space University as well, where they lecture and organise workshops in astrobiology and the exploration of the Moon and Mars.

References:

[1] MUSILOVÁ, M. - ROGERS, H. - FOING, B. (2019) Analogue research performed at the HI-SEAS research station in Hawaii. *Geophysical Research Abstracts*, EGU General Assembly 2019, Vol. 21, EGU2019

[2] MUSILOVÁ, M. - ROGERS, H. - FOING, B. - SIRIKAN, N. - WEERT, A. - MULDER, S. - POTHIER, B. - BURSTEIN, J. (2019) EMM IMA HI-SEAS campaign February 2019. *EPSC Abstracts*, EPSC-DPS Joint Meeting 2019, Vol. 13, EPSC-DPS2019

[3] ROGERS, H. - MUSILOVÁ, M. - FOING, B. (2019) International MoonBase Alliance: Goals and Update. *EPSC Abstracts*, EPSC-DPS Joint Meeting 2019, Vol. 13, EPSC-DPS2019

[4] ROGERS, H. - MUSILOVÁ, M. (2019) How to Live Sustainably on the Moon. *Proceedings of the 70th International Astronautical Congress (IAC) by the International Astronautical Federation (IAF)*, 21-25 October 2019 in Washington DC, USA. Paper IAC-19,A3,2C,11,x52856

[5] SIRIKAN, N. - FOING, B. - MUSILOVÁ, M. - WEERT, A. - POTHIER, B. - BURSTEIN, J. - MULDER, S. - COX, A. - ROGERS, H. (2019) EuroMoonMars IMA HI-SEAS 2019 Campaign: An Engineering Perspective on a Moon Base. *Proceedings of the 70th International Astronautical Congress (IAC) by the International Astronautical Federation (IAF)*, 21-25 October 2019 in Washington DC, USA. Paper IAC-19,A3,2C,9,x54636

[6] BURSTEIN, J. - FOING, B. - MUSILOVÁ, M. - ROGERS, H. - SIRIKAN, N. - MULDER, S. - WEERT, A. - POTHIER, B. (2019) Messaging on the Human Condition as Space Residents. *Proceedings of the 70th International Astronautical Congress (IAC) by the International Astronautical Federation (IAF)*, 21-25 October 2019 in Washington DC, USA. Paper IAC-19,A3,2C,9,x54636

[7] WEERT, A. - FOING, B. - MUSILOVÁ, M. (2019). Hydrous alteration of lava flows on Mauna Loa (Hawaii) compared to Martian volcanic soils. *Proceedings of the 50th Lunar and Planetary Science Conference*, 18–22 March 2019 in The Woodlands, Texas. 10.13140/RG.2.2.18931.17448/1.

4. MATERIALS RESEARCH IN SPACE

J. Lapin

Materials research in space at the ***Institute of Materials and Machine Mechanics of the Slovak Academy of Sciences*** (IMMS SAS) has not been performed during the period of 2018 – 2019.

5. REMOTE SENSING

Ľ. Balažovič, I. Barka, T. Bucha, J. Feranec, M. Gallay, T. Goga, J. Hofierka, M. Kopecká, J. Oťaheľ, J. Pajtík, J. Papčo, P. Pastorek, M. Rusnák, I. Sačkov, M. Sviček, D. Szatmári, A. Zverková

Selected activities of five institutions are included in this report (2018-2019):

Institute of Geography, Slovak Academy of Sciences (IG SAS) in Bratislava

Project: ***Advanced Techniques for Biomass Mapping in Abandoned Agriculture Land Using Novel Combination of Optical and Radar Remote Sensing Sensors (ATBIOMAP);*** under the 2nd call European Space Agency (ESA) – the Plan for European Cooperating States (PECS) Slovakia, contract No. 4000123812/18/NL/SC (2018-2020): National Forest Centre (prime contractor), Zvolen, IG SAS (subcontractor); project link: http://atbiomap.nlcsk.org

Results of identification of agricultural abandoned land (AAL) and land cover (LC)/land use (LU) classes obtained by the computer-assisted photointerpretation (CAPI) and object-based image analysis (OBIA) methods

Agricultural land abandonment is a widespread LU change in different parts of the Earth´s land surface. This phenomenon is especially notable in countries of Eastern and Central Europe, where the formerly intensively worked farmland has been abandoned due to the deep social and political change (disintegration of the deep socialist agrarian policy, accession to the European Union, increased tele-connections and joining the global markets).
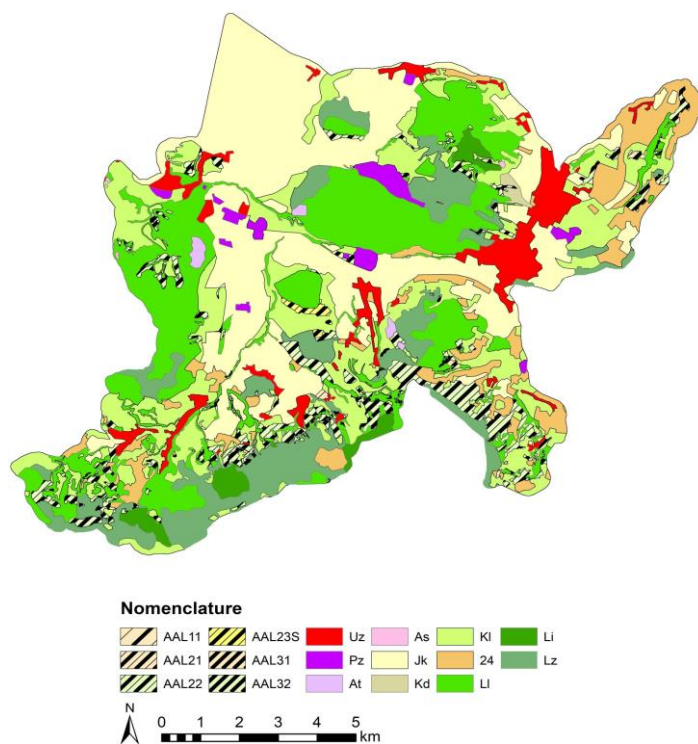
An example of such changes of agricultural land is Slovakia, where the abandonment of cultural agricultural landscape has been obvious during recent almost 30 years. It is a phenomenon perceived in this country as a new social and landscape-ecological problem. It is also a large-scale issue as the unused area amounts to approximately 435,000 ha representing 18% of total 2,423,478 ha farmland in the country.

The theme of mapping the AAL and LC/LU classes by satellite Sentinel data, biomass quantification and its management is covered by this project.
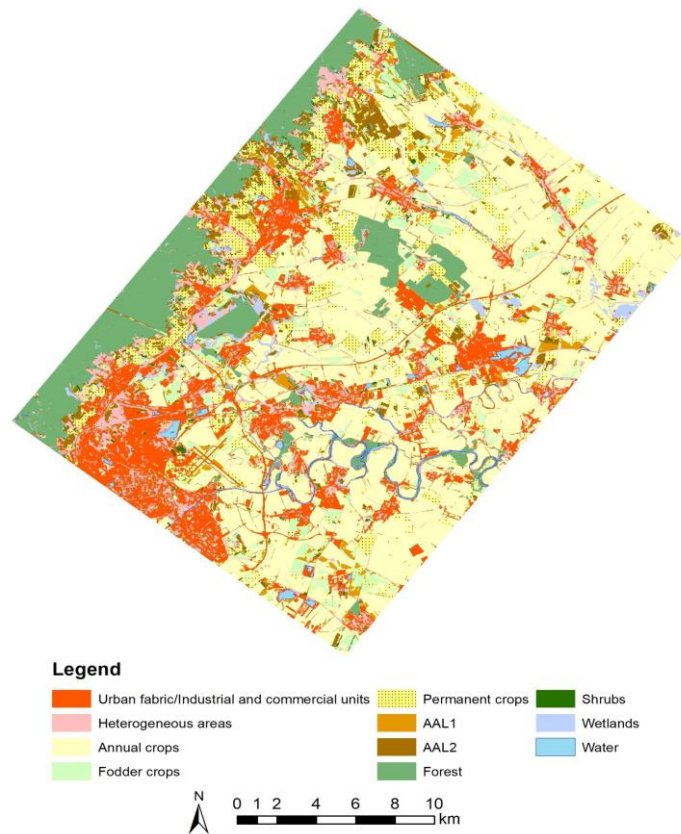
Attached results (Figs. 5.1, 5.2, 5.3 and 5.4) document the possibilities of the use of satellite Sentinel data and the CAPI methods, as well as the OBIA in the process of AAL classes identification in experimental areas of the Podunajská nížina (PN) lowland and in the Zvolenská kotlina (ZK) basin.
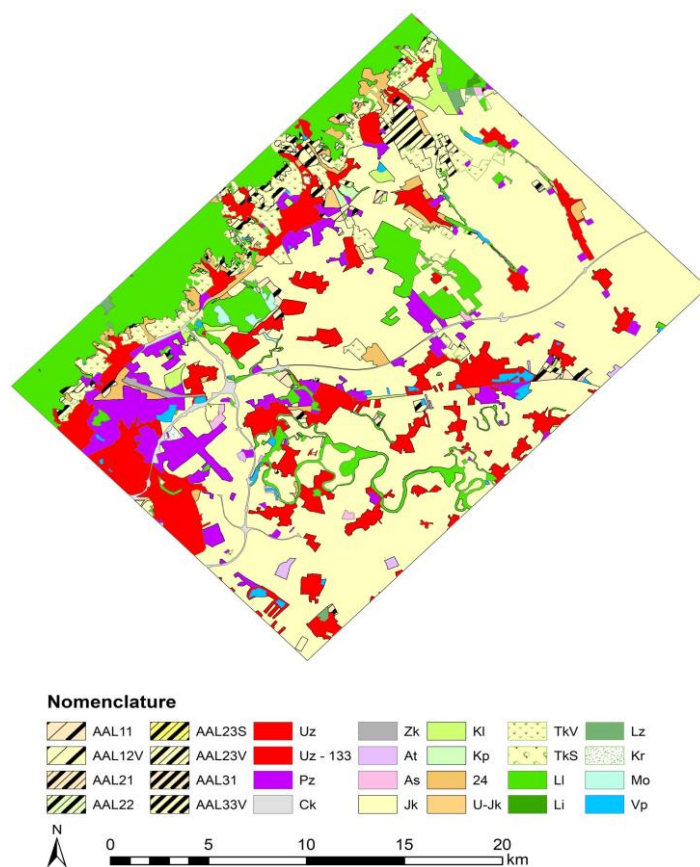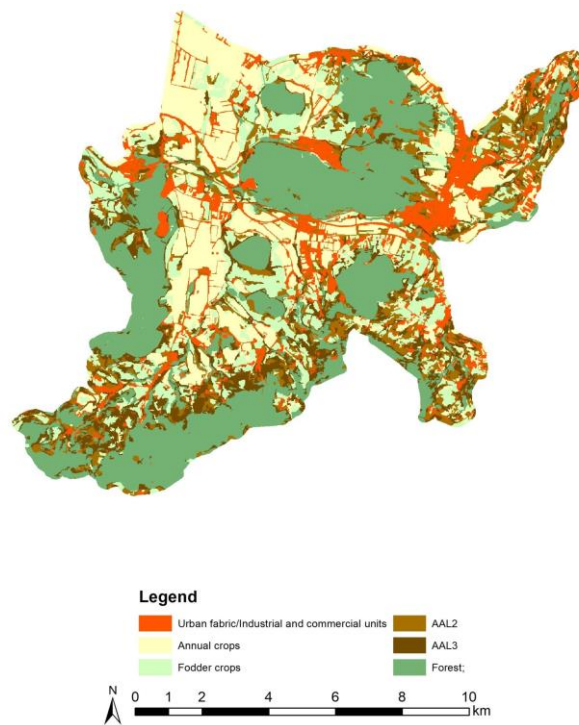
Figure 5.1. *AAL and LC/LU classes identified by CAPI method in experimental area PN.*

Figure 5.2. *AAL and LC/LU classes identified by CAPI method in experimental area ZK.*

Legend

⬛ Urban fabric/Industrial and commercial units	⬛ Permanent crops	⬛ Shrubs
⬛ Heterogeneous areas	⬛ AAL1	⬛ Wetlands
⬛ Annual crops	⬛ AAL2	⬛ Water
⬛ Fodder crops	⬛ Forest	

0 1 2 4 6 8 10 km

Figure 5.3. AAL and LC/LU classes identified by OBIA and Random Forest classifier in experimental are PN.

Legend

⬛ Urban fabric/Industrial and commercial units	⬛ AAL2
⬛ Annual crops	⬛ AAL3
⬛ Fodder crops	⬛ Forest;

0 1 2 4 6 8 10 km

Figure 5.4. AAL and LC/LU classes identified by OBIA and Random Forest classifier in experimental are ZK.

41

Project: ***Effect of impermeable soil cover on urban climate in the context of climate change*** (supported by the Slovak Research and Development Agency – APVV-15-0136); project link:
https://www.vupop.sk/projekty_apvv_15_0136.php

Land cover and its change of Bratislava, Trnava and Žilina for the years 1998, 2007, 2016 obtained by interpretation of satellite data (SPOT, Sentinel and Formosat)

One of the aims of this project is to document identification and delimitation of LC/LU classes (Fig. 5.5) and their change (Fig. 5.6) based on Urban Atlas (UA) data and satellite SPOT, Sentinel and Formosat data in three cities in Slovakia: the capital Bratislava and two regional centres Trnava and Žilina – functional urban areas (FUAs; located in different geographical conditions) in the years 1998-2007-2016 and their effect on the temperature change by application of the MUKLIMO_3 model. This model was used in the APVV-15-0136 project for the purposes of urban heat island modelling. The largest LC/Lu changes were in benefit of artificial surfaces in FUAs as demonstrated in Fig. 5.6.
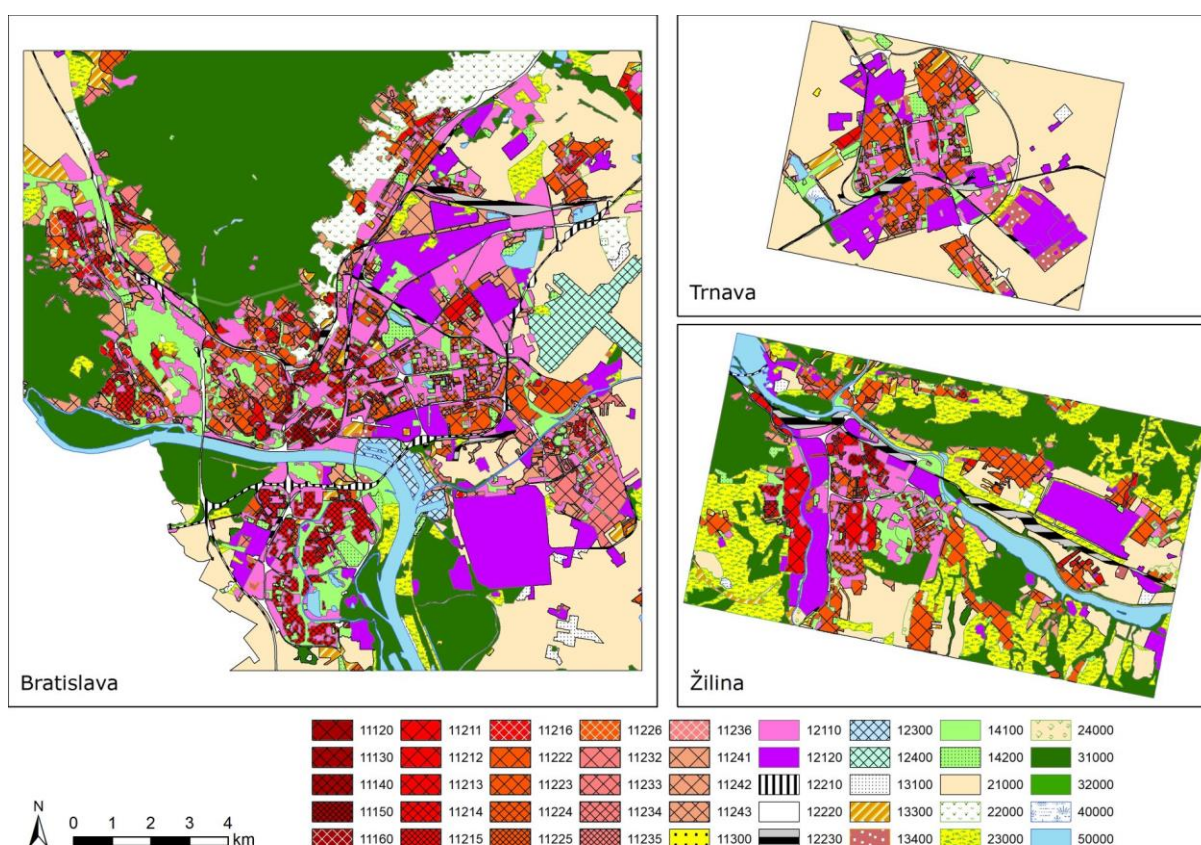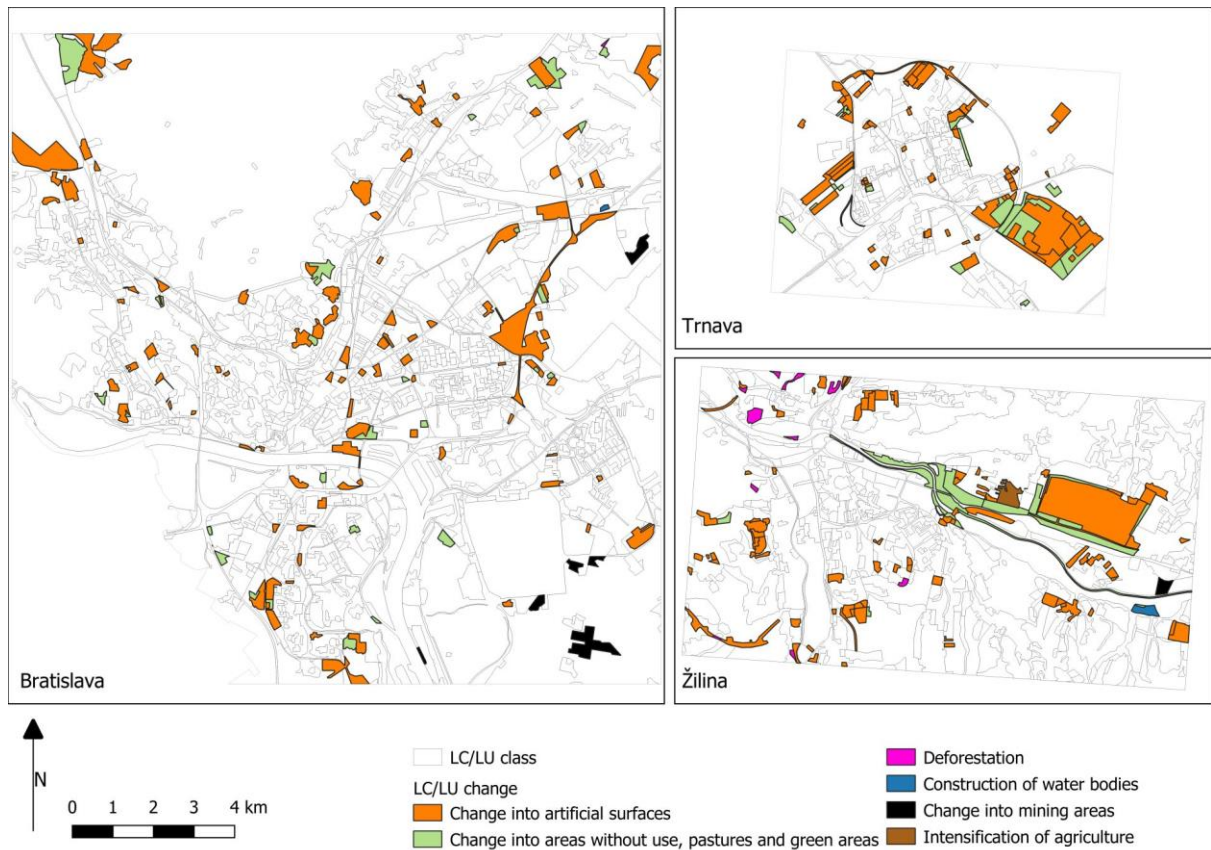

Figure 5.5. *Spatial distribution of LC/LU classes in the year 2016.*

42

Figure 5.6. LC/LU changes between 1986 and 2016.

The long-term co-operation of the Institute of Geography SAS in pan-European projects CORINE land cover (CLC) resulted in 2018 in the book publishing: *Land cover of Slovakia and its change in 1990-2012 (in Slovak), 160 p. Bratislava, Veda*.

CLC data became a valuable source of original information for those interested in knowing the landscape of European countries and its dynamism. This monograph (Feranec et al. 2018) document more than 20-year development of Slovakia's landscape. Individual parts of the monograph describe CLC projects regarding the application of satellite data. The methodology of the generation of four data layers, particularly CLC 1990, CLC 2000, CLC 2006 and CLC 2012, as well as assessments of their precision and generation of three change layers i.e. CLCC1990-2000, CLCC2000-2006 and CLCC2006-2012 are demonstrated in an easy-to-follow manner. Time-spatial characteristics about changes of LC for more than two decades indicate the increasing trend in deforestation, decreasing trend in forestation, intensification of agriculture, construction of water reservoirs, and a mixed trend of the developments in urbanisation, and other changes. Part of the monograph also brings examples of possible solutions to environmental issues in Slovakia by application of CLC data. The final part is dedicated to a brief outline of the prospects for tracking the development of LC in Slovakia in the future in accord with the European activities in this field.

Institute of Geography, Faculty of Science, Pavol Jozef Šafárik University in Košice

Project: ***SURGE: Simulating the cooling effect of urban greenery based on solar radiation modelling and a new generation of ESA sensors (feasibility study for the European Space Agency***; under the 1st call ESA PECS Slovakia, contract nr. 4000117034/16/NL/NDe, 2016-2018)

Urban greenery has a considerable effect on cooling the urban environment during heat waves. It is a dynamic component of the urban land cover which can be observed by the Sentinel 2 (S2) satellite mission in a higher spatial and temporal resolution than is enabled by other similar missions. The SURGE feasibility study aimed to explore the potential of S2 multispectral data in simulating the cooling effect of urban greenery. The main objective was to define a methodical approach for spatial modelling of land surface temperature based on modelling the solar irradiation and parameterizing the land cover properties from S2 data. While solar irradiation can be precisely calculated on a fine scale using virtual 3D city models other important parameters for land surface temperature modelling are difficult to ascertain, such as surface thermal emissivity, broad-band albedo and evapotranspiration. The approach was tested in an area comprising 4 sq. km of the central part of the Košice City in Slovakia (Fig. 5.7). Virtual 3D city model of Košice was generated from airborne lidar and photogrammetric data acquired in a single mission. A time-series of Sentinel 2 data was gathered to be compared with a reference time-series of terrestrial lidar (TLS) data of urban greenery on 4 small sites. Statistical linear relationship was defined between the vegetation metrics derived from S2 and TLS data. A geobotanical database of urban trees was generated based on field survey. Algorithmic structure of a toolbox for modelling the land surface temperature in the open-source GRASS GIS was developed based on the Stefan-Boltzmann law and Kirchhoff rule. This study demonstrated how Sentinel 2 data can be used for estimating broad-band albedo, land surface emissivity and solar transmittance of vegetation. The primary benefits are in the developed algorithm for estimating the land surface temperature in a GIS environment providing a unique platform (i) for integrating various kinds of datasets to become usable in urban planning and (ii) for exploiting the S2 data in mitigation of the urban heat island.
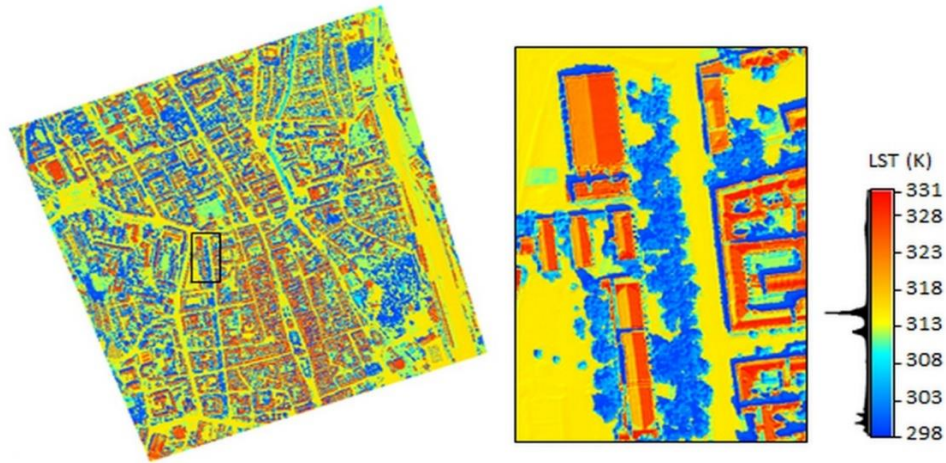
Figure 5.7. *Land surface temperature (LST) modelling for a central area of Košice using Sentinel 2, terrestrial laser scanning data and GIS tools.*

Project: ***APVV-15-0054: Physically based segmentation of georelief and its geoscience application*** (research project supported by the Slovak Research and Development Agency – APVV-15-0054)

Airborne and terrestrial laser scanning and close-range photogrammetry are frequently used for very high-resolution mapping of land surface. These techniques require a good strategy of mapping to provide full visibility of all areas otherwise the resulting data will contain areas with no data (data shadows). Especially, deglaciated rugged alpine terrain with abundant large boulders, vertical rock faces and polished roche-moutones surfaces complicated by poor accessibility for terrestrial mapping are still a challenge. In this project, we present a novel methodological approach based on a combined use of terrestrial laser scanning (TLS) and close-range photogrammetry from an unmanned aerial vehicle (UAV) for generating a high-resolution point cloud and digital elevation model (DEM) of a complex alpine terrain (Fig. 5.8). The approach is demonstrated using a small study area in the upper part of a deglaciated valley in the Tatry Mountains, Slovakia. The more accurate TLS point cloud was supplemented by the UAV point cloud in areas with insufficient TLS data coverage. The accuracy of the iterative closest point adjustment of the UAV and TLS point clouds was in the order of several centimeters but standard deviation of the mutual orientation of TLS scans was in the order of millimeters. The generated high-resolution DEM was compared to SRTM DEM, TanDEM-X and national DMR3 DEM products confirming an excellent applicability in a wide range of geomorphologic applications (Šašak et al., 2019).

45
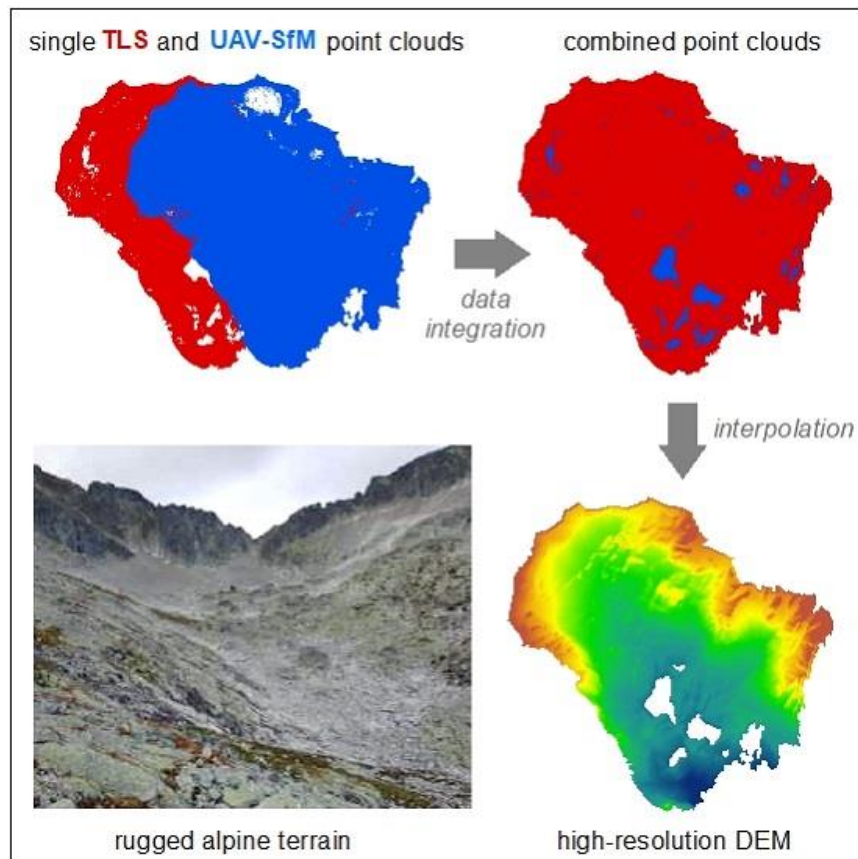
Figure 5.8. *A workflow of combining terrestrial lidar and photogrammetric point clouds for DEM production in rugged alpine topography.*

Project: ***TOKAJGIS: Development of webGIS platform based on big-geodata for the Tokaj Wine Region foster cross-border collaboration*** (co-financed by the EU within the programme INTERREG V-A Slovakia-Hungary, contract nr. SKHU/1601/4.1/052)

The Tokaj wine region may be considered as a unique area from the point of view of geography, characterized to a large extent by the wine- and viticulture, as well as the special mining assets close to the national border and a wide variety of tourist attractions.

The fundamental idea behind the creation of a joint GIS framework by Pavol Jozef Šafárik University Košice, Slovakia and Eszterházy Károly Univerity Eger, Hungary was to support the development of the wine region based on the integration of basic territorial data and the joint handling of GIS by the two European member states. Databases with different structures and nomenclature hamper the processing of the GIS data of the wine region, its integration and the preparation of mutually advantageous regional development concepts as well as the transparency of developmental efforts.

The aim of the project was to pool the professional experience of the two institutions and to facilitate joint learning processes based on specific modular frameworks in keeping with the character of the wine region. The proposed

46

system is capable of integrating the GIS databases present on both sides of the border and various remote sensing data including cutting-edge UAV and laser scanning technology (Fig. 5.9 and Fig. 5.10). Furthermore, it deepens the remote sensing skills and knowledge present at the two institutions. The thematic content of the trilingual GIS framework published on the website can be used as a validated source of information for wine producers, local government and administration, local people as well as the participants (both on the demand and supply side) of tourism. It provides an easily accessible dissemination platform on which to publish the research results of the area.
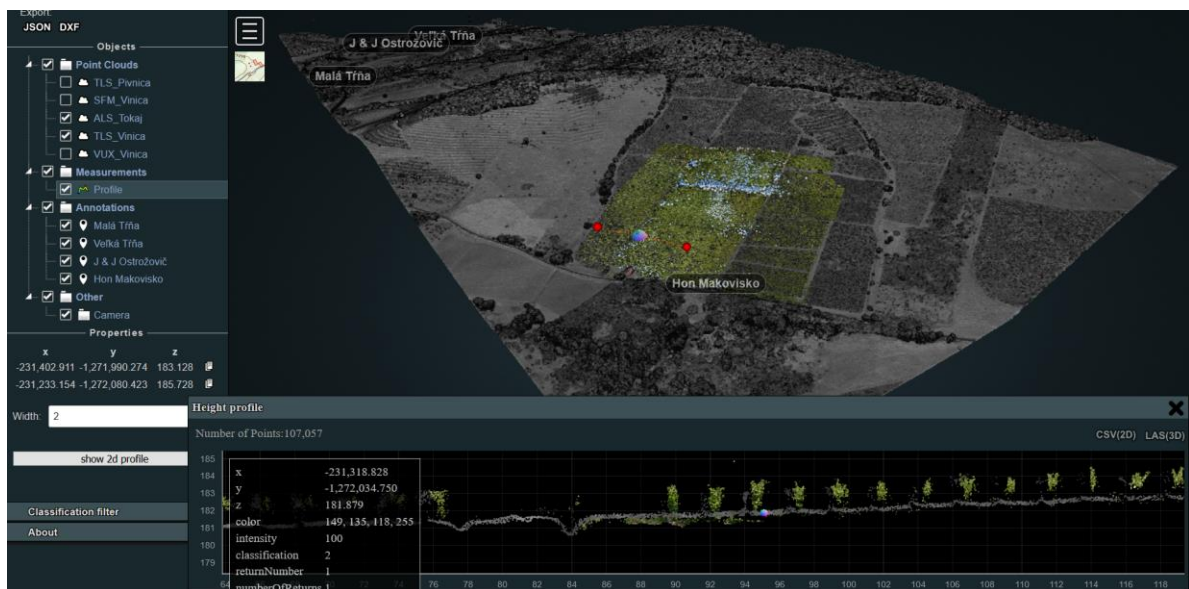
Figure 5.9. *The interactive website of the project with remote sensing data https://geografia.science.upjs.sk/webshared/Laspublish/Tokaj/Tokaj.html.*
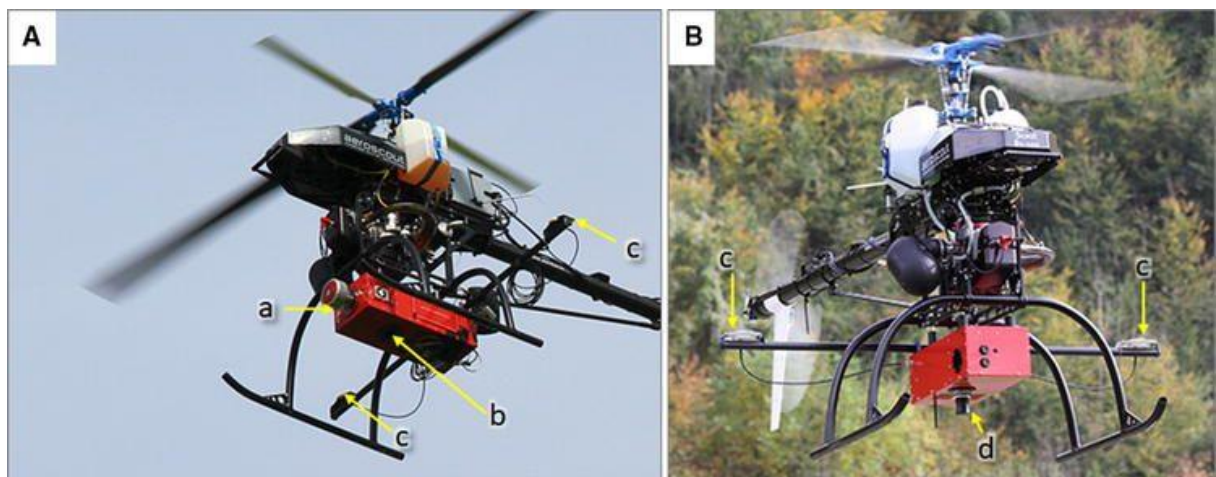
Figure 5.10. *Scout B1-100 UAV with the integrated laser scanning payload (A) and hyperspectral payload (B). A comprises the VUX-1 laser scanner (Riegl, Austria) (a) and the Sony A6000 E-Mount photo camera (b). The position and orientation of the sensors is precisely monitored by dual GNSS antennas (c) and an embedded INS unit xNAV550 (Oxford Technical Solutions Ltd., United Kingdom) for the sensor attitude and position monitoring. B comprises the AISA Kestrel 10 hyperspectral camera (Specim, Finland) (d) and the INS (c)*

47

Activities within the Copernicus Academy

Pavol Jozef Šafárik University in Košice is a member of the Copernicus Academy network of institutions as the Institute of Geography promotes use of the Copernicus Services via teaching and research. The Copernicus data are actively used on practical classes and lectures focusing on Remote Sensing and Geographic Information Science. We have organized a summer school in July 2018 within the TOKAJGIS project (see above) where the participants were discussed the benefits of Sentinel 2 and other Earth Observation data in precision viticulture and farming in general.

National Agricultural and Food Centre - Soil Science and Conservation Research Institute

Remote sensing control of area-based subsidies in agriculture (2018)

The subsidies play a key role in agriculture sector and contribute to the prosperity of agricultural subjects. The subsidies to agriculture sector represent major part of European budget and that is why there is taken an emphasis to the control.

Slovak Administration decided to have six control sites for the 2018 campaign, defined by 710 km^2 ANNA, 225 km^2 IRMA, 640 km^2 JANA, 260 km^2 NORA, 371 km^2 OLGA and 486 km^2 ZORA (Fig. 5.11). Two sites were covered by WorldView2 images. Two sites were covered by WorldView3 images and two sites by GeoEye1 images. Two HR acquisition windows were used: HR-1 and HR+1.
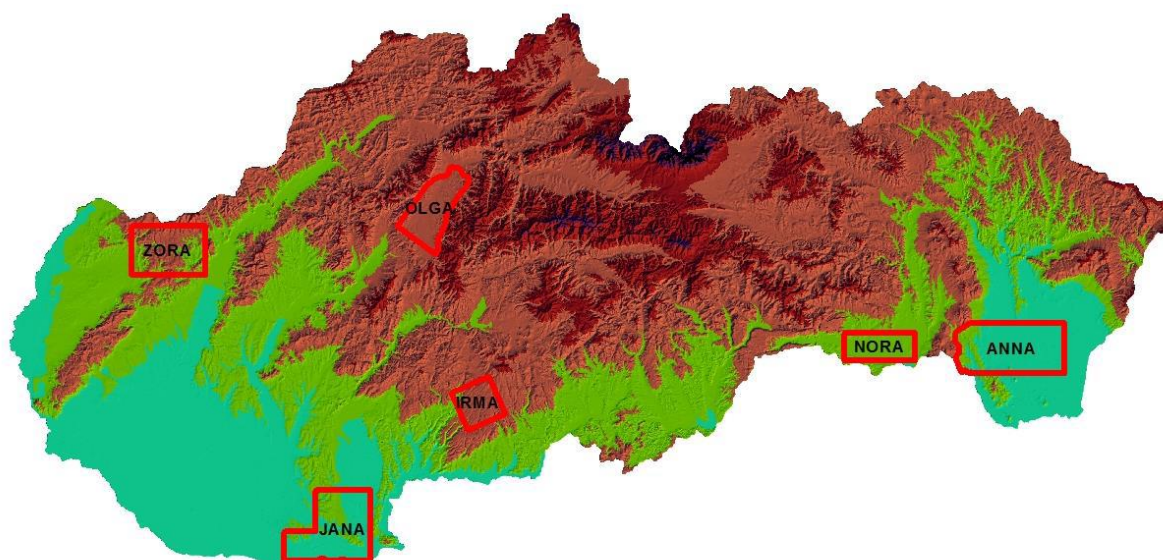

Figure 5.11. *Localization of the controlled sites in campaign 2018.*

In 2018 campaign the total number of applicants was 18 611, the number of dossiers controlled with remote sensing was 1125 (6.04% of all dossiers). The total area controlled was 123,499.78 hectares, with 6477 reference parcels. There were 28,526 agricultural parcels to control (in 11 schemes), on average 25 parcels/farmer and 109.78 hectare/ dossier.

To determine the agricultural parcel areas, the parcels were located on the screen with the help of the reference parcel vectors and its limits validated on the VHR images (WorldView 2 – 4, GeoEye1 – 2 images). The agriculture parcels boundaries were taken as vector data from IS Geospatial aid application – IS GSAA

The Fig. 5.12 shows an example of boundary and land use check. Areas, which are not subsidised like path or stables, are excluded and coded as C6 – those are well visible on the VHR image.
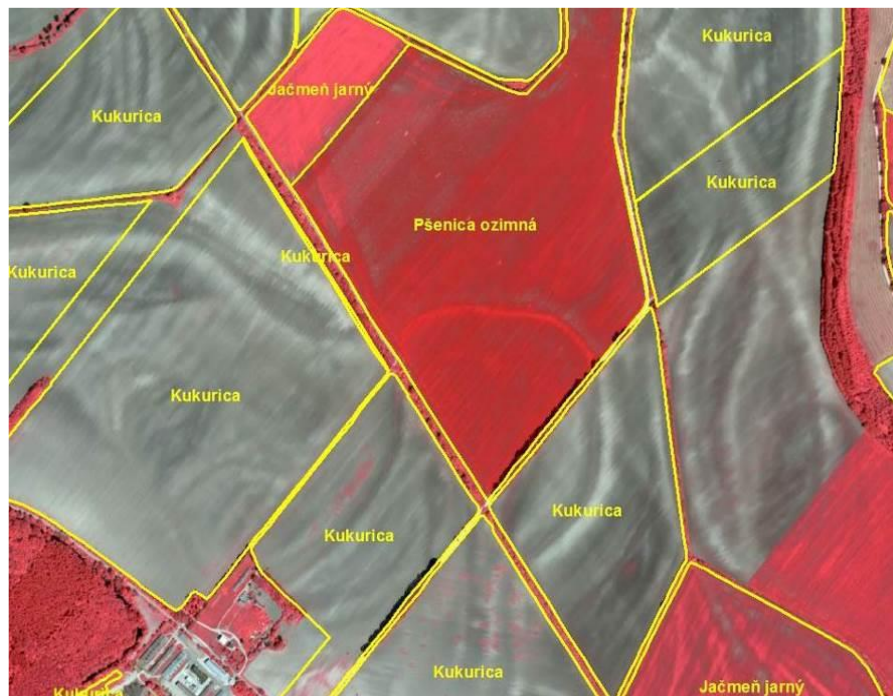
Figure 5.12. *Example of boundary check and land use on WorldView4 image.*

The land use check with multi-temporal HR images (SPOT 6 images) was made by computer-assisted photointerpretation (CAPI). The images were overlaid with the digitized vectors showing the position of the parcels which were checked. The land use check was completed by Rapid field visits RFVs. As a complement to control vegetation development, the freely available Sentinel2 satellite images (resolution 10m/ pixel) were used. The satellite images Sentinel 2 are provided by ESA.

Areas which are cultivated but the crop haven't emerged properly or were hit by some disaster like flood or drought have to be proved on more images from different acquisition windows (Fig. 5.13).
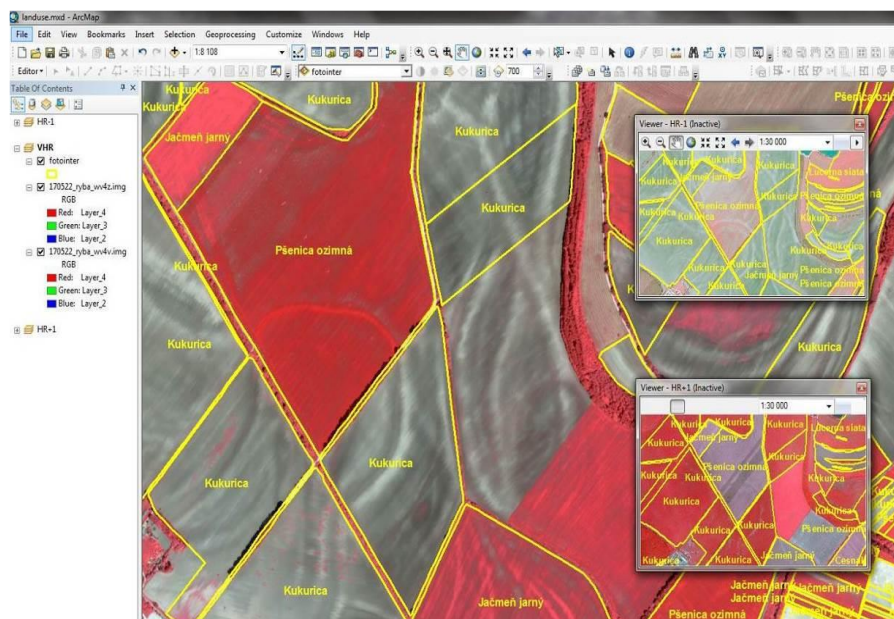
***Figure 5.13.*** *Example of land use check on HR images from different acquisition windows.*

High resolution (HR) images were corrected to a "master image" – digital orthophotomaps with a ground sample distance 0.5 m and declared 1.5 m RMSExy. Ground control points for VHR images were determined from field survey – post-processed GPS measurement with the use of Slovak spatial observation system. Ground control points were represented by well defined points in the build-up area (crossings, path edges in the cemeteries, around the houses).

The purpose of the remote-sensing control is to check the area and land use of the agricultural parcels in the dossier. The CAPI is used for checking the area claimed and generally the land use. The CAPI has been adjusted to the annual conditions of the regulations of subsidy schemes.

The 2017 campaign is based on Common Technical Specification for the 2018 Campaign of On-The-Spot-checks and area measurement according to art. 24-27, art. 30, 31 and 34-41 of Regulation (EU) No 809/2014 as amended by Regulation (EU) 2015/2333 (http://marswiki.jrc.ec.europa.eu) and also is based on agreement of delegated activities between APA SR and NAFC – SSCRI.

According to the final diagnosis, which summarizes the diagnoses of the conformity and completeness tests at dossier level, 401 (35.64%) dossiers were accepted for Single area payment scheme, 2 (0.17%) for payment for agri-environment – climate action, 89 (7.91%) for area facing natural constraints, 361 (32.08%) for Complementary National Direct Payment scheme, 3 (0.26%)no dossier for payments on organic farming, 58 (5.15 %) for payment for agricultural practices beneficial for the climate and the environment, no dossier for coupled direct payments for sugar beet and for coupled direct payments for fruit with high labour inputs, 3 (0.26%) for coupled direct payments for fruit with very high

labour inputs, no dossier for coupled direct payments for tomatoes, 1 (0.08%) for coupled direct payments for vegetables with high labour inputs, no dossier for coupled direct payments for vegetables with very high labour inputs, for coupled direct payments for hops and no dossier for Special Areas Of Conservation too. The declared and retained area on all control zones is compared on Fig. 5.14.
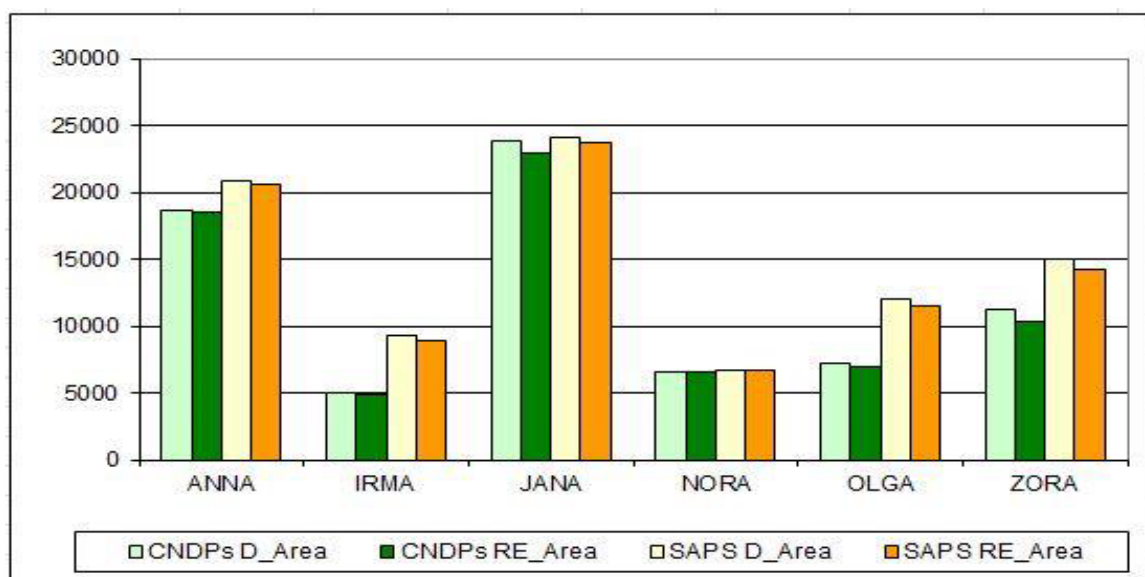
Figure 5.14. *Declared and retained area (ha) for schemes CNDPs and SAPS per site.*

Quality Assesment of Land Parcel Information System – QA LPIS (2019)

Land Parcel Identification System (LPIS) is the main component of Integrated Administration and Control System (IACS) for land based direct support. The purpose of LPIS is to implement the common agricultural policy of the European Union measures. The quality assessment framework of LPIS is an integral part of LPIS management and upkeep processes. In this framework, the LPIS of a MS/Region is regarded as a system under test, which is composed of two major components: the local application schema and the data records stored in the system. The Executable Test Suite (ETS) targets at the data component by annually assessing conformity according to Article 6 of (EU) Regulation No 640/2014.

QA implementation is based on current images taken in the year of review. Selected reference parcels by EC for QA LPIS were on SCRI vectorised on the background of current satellite images, provided by EC. Subsequently, they are compared with the valid state of the LPIS layer. The images were overlaid with the digitized vectors showing the position of the parcels which were checked. The land use check was completed by Rapid field visits RFVs.

QA LPIS is realized through 9 quality elements, grouped into two conformance classes, as defined by the Regulation. Based on the item conformance verdicts

issued for the various criteria during the item inspection, verdicts made on each conformance class. There are several reasons for errors. The two most common are operator error and outdated orthophotomaps.

The conformance class 1 means to *"assess the quality of LPIS"*, and counts non-conforming items. Furthermore, counting items offers a straightforward entry for the LPIS upkeep processes. This counting of items includes the first three types of the quality elements (QE1, QE2 and QE3) (Fig. 5.15).

QE1 assesses the maximum eligible area of the system and evaluates 2 quality elements: QE1a absence of bias (i.e. accuracy) of the land represented in the LPIS as a whole, QE1b parcel level precision of the land represented in the LPIS as a whole – overestimation areas and underestimation areas (Fig. 5.16).

QE2 assesses individual parcels with correctness issues and evaluates 3 quality elements: QE2a proportion of items with incorrectly recorded area or "contaminated" with ineligible features –error type Update – outdated orthophotomaps (Fig. 5.17).

QE2b distribution of items, according to the correctness of the eligible area recorded and QE2c number of non-conforming reference parcels in LPIS with classification error –mistake/ error of operator (Fig. 5.18).

QE3 shows number of reference parcels that have functional issues – "critical defects" (Fig. 5.16).

Conformance class 2 is assessed under the last three elements (QE4, QE5 and QE6). QE4 categorization of the non-conformities, QE5 ratio of total declared area in relation to the total area recorded for the area conforming reference parcels and QE6 rate of non-conforming reference parcels due to undetected and unaccounted land cover change, as observed in ETS, accumulated over the years.

These 3 elements aim to *"identify possible weaknesses"*, and this requires a broader system wide analysis, beyond the individual item or reference parcel. This is most obvious for QE4 which analyses the LPIS processes and design as factors for creating quality problems. For instance, a single, large parcel can be contaminated, can have critical defect (for example, multi-parcel), and can have its land wrongly classified. Although this represents a single non-conforming item, it does reflect three different system weaknesses.

Quality assessment of the Slovak LPIS was realized in three zones for campaign year 2019 (Fig. 5.15). VHR satellite imagery for each zone was delivered from JRC EC. Site 2019 QA SK – 1 cover part of Michalovce district (EK provided World View 3 satellite image from 8th April 2019), Site 2019 QA SK – 2 cover parts of Svidník and Stropkov Districts (EK provided GEO EYE 1 satellite image also from 8th April 2019, both SK –1 and SK – 2 QA zones are localised in East Slovakia). Site 2019 QA Sk – 3 cover parts of Nitra, Šaľa and Nové Zámky districts in the west part of Slovakia (EK provided World View 3 satellite image from 27th June 2019). The Satellite images were georeferenced by SSCRI staff. Measured and archive control and check points were used. For all

three zones the Quality checks of georeference were carried out and control protocol were elaborated.
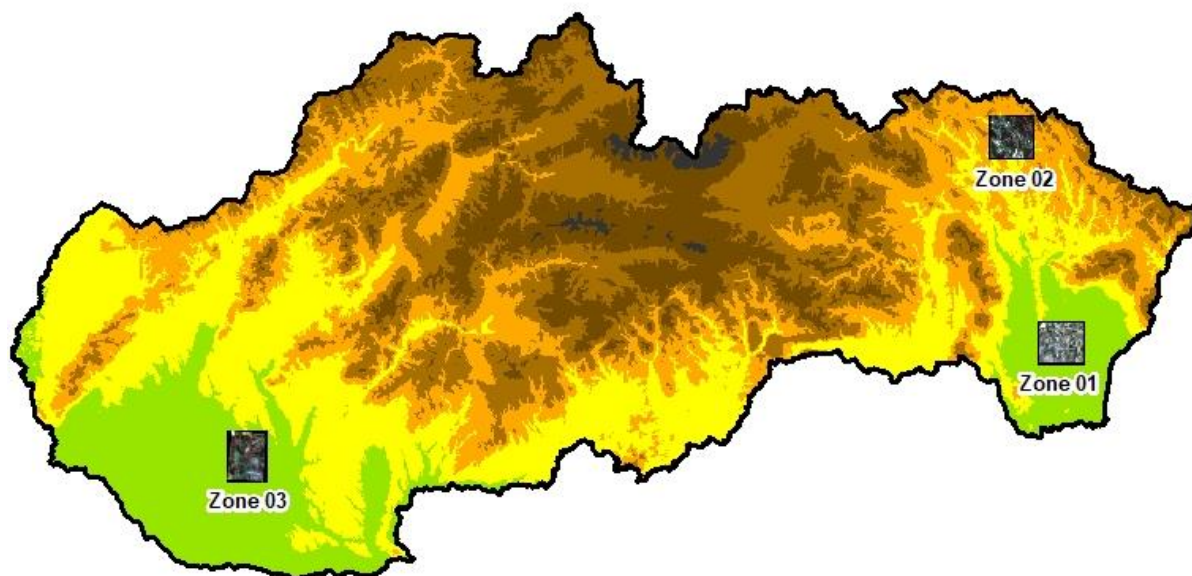
Figure 5.15. Localization of the controlled sites in QA LPIS 2019.
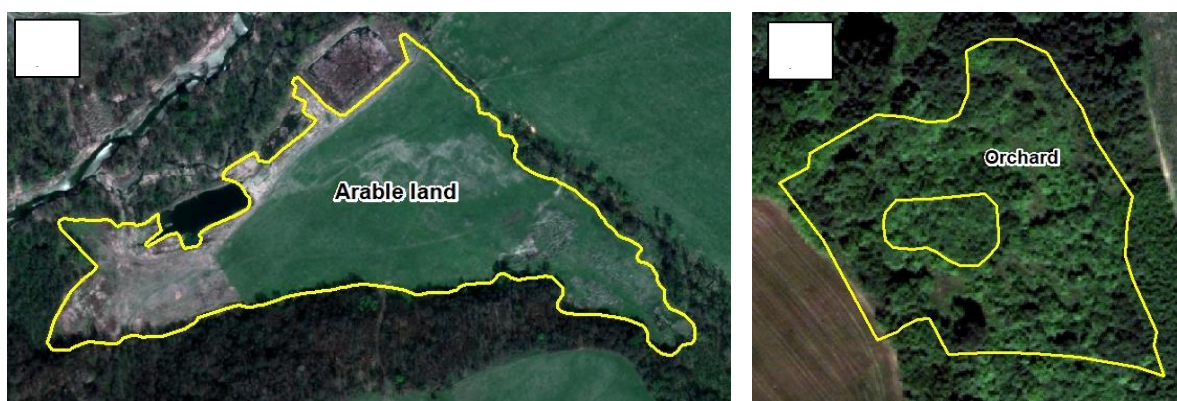
Figure 5.16. Example of case with identified critical defect: a) Invalid perimeter of reference parcel and b) Total absence of eligible features.

Figure 5.17. *Example of the occurrence of non-agricultural land cover features on the reference parcels with causes "Update" – changes of the underlying land were not applied.*

Figure 5.18. *Example of the occurrence of non-agricultural land cover features on the reference parcels with causes "Erroneous processing" – a mistake of LPIS operator.*

<u>Remote sensing within crop yield and crop production forecasting (2018-2019)</u>

Monitoring of Crop Conditions and Crop Monitoring

Regional monitoring of natural crop conditions aims to study the influence of weather (coupled with soil) on crop growth and crop development during current vegetation season.

NDVI (Normalized Difference Vegetation Index) are derived from NOAA's AVHRR sensor. The NDVI vegetation index, characterizes the total biomass state (volume and vitality), the higher the NDVI value, the more biomass is developed (characterized by a higher content of chlorophyll in plants and hence a more potent photosynthesis) (Fig. 5.19).
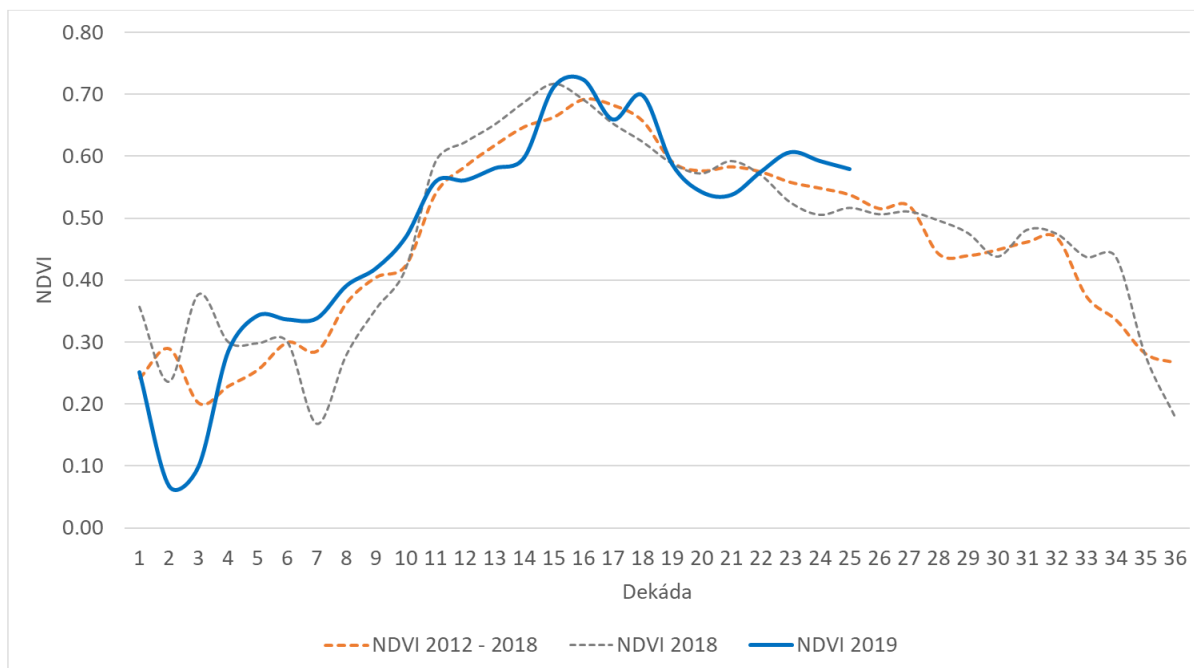
Figure 5.19. *Development of the NDVI vegetation index in 2019 and its comparison with the situation in 2018 and long-term average. Data source: NPPC-VÚPOP.*
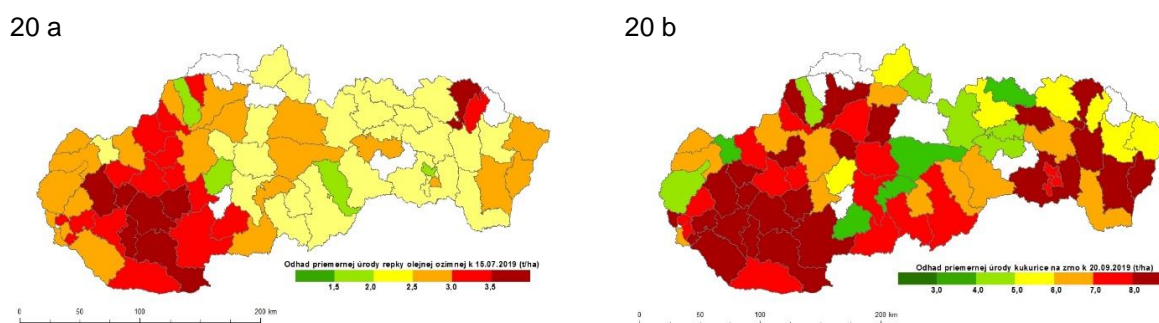
Crop yield forecasting

The aim of the crop yield and crop production forecasting is to provide the most likely, scientific, and as precise as possible independent forecast for main agricultural crop yields for Ministry of Agriculture and Rural Development of the Slovak Republic and for the public.

National Crop Yield and Crop Production Forecasting System has been created on SSCRI and is based on three different principles which are applied to specify vegetation indexes as biomass development stage and biomass development:

- Remote Sensing method – method of interpretation of vegetation indicators (as NDVI or DMP – Dry matter development) from satellite images (mainly from low resolution satellite sensors as NOAA AVHRR and SPOT Vegetation satellite system);
- Bio-physical modelling (WOFOST model) and simulation of vegetation indexes (mainly TWSO – Total Dry Weight of Storage Organs and TAGP – Total Above Ground Production). In WOFOST, weather and phenological data, soil hydro-physical data and crop physiological data are utilized as model key inputs;
- Integrated assessment method, which means the implementation of specific meteorological and vegetation indicators in the statistical analysis, assesses the impact of weather on the projected harvest. Integrated estimate summarizes a wider range of disparate indicators and indices that are

56

currently for the purposes of forecasting yields and consequently the production of crops used.

The crop yield and crop production forecasting is carried out for main agricultural crops – winter wheat, spring barley, oil seed rape, grain maize, sugar beet, sunflower and potatoes. The forecasts are reported six times per year – in the half of May, June and July for "winter and spring crops" and in the end of July, August and September for "summer crops". The forecast results are interpreted at national level as well as at NUTS3 and NUTS4 level. The example of crop yield forecasting in 2019 can be seen in the Figs. 5.20a and 5.20b.

Figure 5.20. Example of crop yield forecasting with remote sensing in first decade of July in 2019 for rape (a) and in the second decade of September for maize (b).

Verification of high resolution layer – „HRL" permanent grasslands for the reference year 2015

Verification of the High Resolution Layer (HRL) of Permanent Grassland TTP / Grassland was conducted on NPPC – VUPOP according to the current methodology. „Guidelines for verification of High Resolution Layers produced by the CLMS (Copernicus Land Monitoring Service) as part of the 2015 reference year production". Thematic accuracy assessment of the HRL Grassland layer is the goal of verification. The HRL layers are provided by EEA to NPPC through contract with Slovak Environmental Agency. The HRLs are part of the land use/land cover mapping component of the Copernicus Land Monitoring Service (CLMS), serving a broad user community from European public bodies to Member States and regional environmental authorities, as well as the value-adding sector. They provide support to various environmental policies and political decision-making, and significantly contribute to assessing Europe's current environmental status and monitoring changes over time. The Pan-European High Resolution Layers (HRL) provide information on specific land cover characteristics, and are complementary to land cover / land use mapping such as in the CORINE land cover (CLC) datasets. HRL -GRA is produced

primarily from Sentinels. The pan-European HRL 2015 Grassland Layer is available at 20 m and 100 m resolutions. To achieve the 100 m map, an aggregation process was carried out weighting grassland, non-grassland and unclassifiable pixels at 20 m level within a 100 m grid cell. The class majority determined the final assignment of the 100m grid cell to a specific class.

Verification was done by two methods: a general overview of HRL Grassland data quality and using the "Look and Feel" method (for the recommended six strata and two types of errors Commission and Omission). One type of "Omission error" – is documented on Fig. 5.21 – mostly grasslands without trees are correct classified as permanent grassland. If part of the scattered trees is also presented on agricultural land, some of them are not classified as HRL grassland TTP by automatic classification of satellite images Sentinels. Example of Commission error – is showed on Fig. 5.22 – arable land was classified as permanent grassland. Relatively frequent error, especially if arable land and permanent grassland are located side by side.

Verification was carried out visually in GIS environment interpretation and comparison HRL Grassland with orthophotos and with thematic GIS layers generated from the LPIS, biotopes of natural and semi-natural grassland and ZB GIS. Generally, we conclude that the layer HRL permanent grassland is not well classified. Time series of satellite images would help to improve the accuracy of HRLs. In particular, various vegetation phases are a problem when identifying Grasslands. In the future, data HRL Grassland are prerequisites for the use of data and outcomes in a broader context.
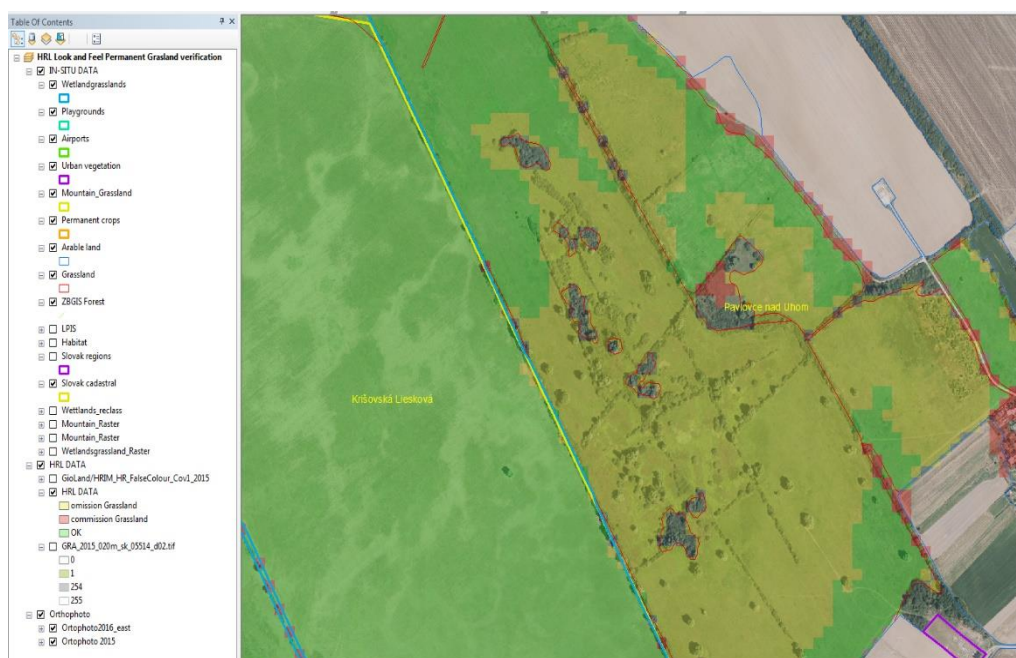
Figure 5.21. *„Omission error" – Mostly grassland without scattered trees and bushes are classified correct as HRL Grassland.*
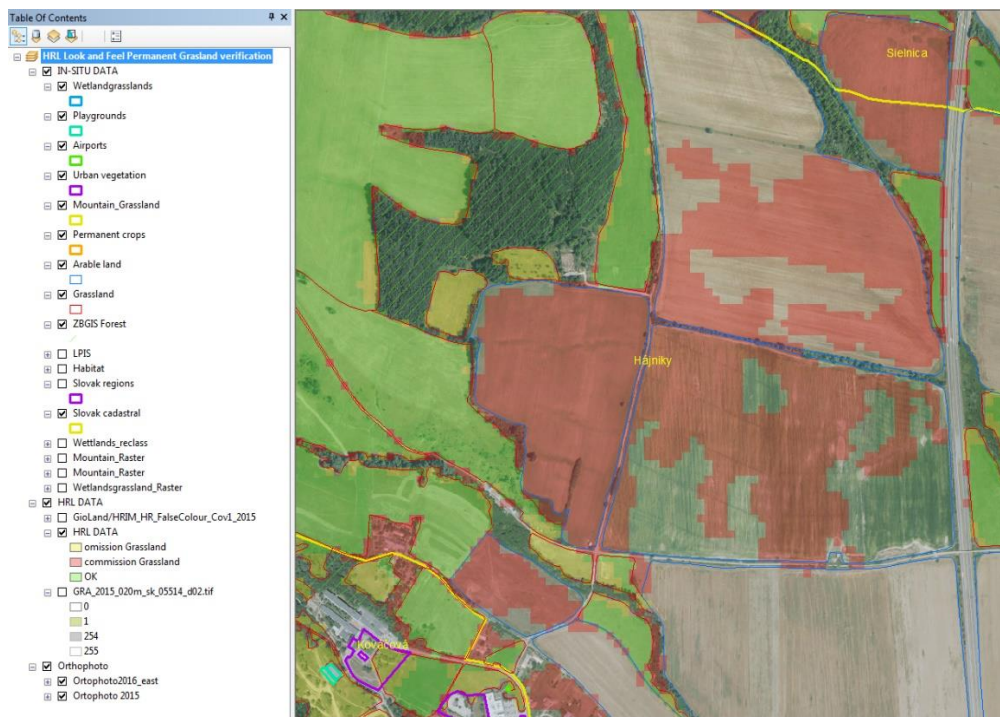
Figure 5.22. *„Commission error" – arable land has been classified as permanent grassland – TTP.*

National Forest Centre Zvolen

Remote Sensing research activities of the National Forest Centre in Zvolen were aimed at two main topics:
- Advanced Techniques for Biomass Mapping in Abandoned Agriculture Land
- Applications of airborne laser scanner technology in the forest management

**Advanced Techniques for Biomass Mapping in Abandoned Agriculture Land**

Abandonment of agricultural landscape is an all-European problem. In Slovakia, this is a problem of large-scale land use in the area of 420-450 thousand. ha, ie 17.5% – 18.6% of the area of 2,423,478 ha of agricultural land. Wood biomass outside forestland is not inventoried therefore information on the spatial distribution, increment and volume of biomass on non-forest land is not available.

ATBIOMAP, the common project of the National Forest Centre and Institute of Geography SAS supported by European Space Agency is aimed at mapping and quantification of aboveground biomass on Abandoned Agricultural Land (AAL).

Methodological framework is based on analyses and cross-validation of optical (Sentinel 2) and radar satellite data (Sentinel 1 and ALOS PALSAR-2), supported by field research and airborne laser scanning data (ALS). The project consists of two main parts. In the first one (responsibility of the IG SAS), a classification system for herbaceous, shrub and tree formations on AAL has been created and included into a land cover (LC) mapping systems to contribute to tracking the dynamics of AAL and its assessment. In the second part (responsibility of the NFC), a mathematical model of biomass stock estimation and an innovative methodology of permanent tree biomass inventory on AAL, based on satellite data, has been developed. The models were derived and verified comparing satellite biomass estimates and field data. A total of 104 plots (Fig. 5.23 and Fig. 5.24) were established to represent the full height growth range and heterogeneity of the shrub and tree species composition on:
- Study Area 1 – Podunajská nížina, 39 plots, of which 33 scrubs (70% doge rose dominated areas), 2 tree-like (Acer negundo) and 4 shrub-tree stands (plums and nuts)
- Study area 2 – Zvolenská kotlina – Víglaš: 65 plots, of which 30 scrubs (blackthorn, dog rose), 25 forest stands (beech 28%, acacia 23%, cherry 12%, spruce 10%) and 10 shrub-tree stands
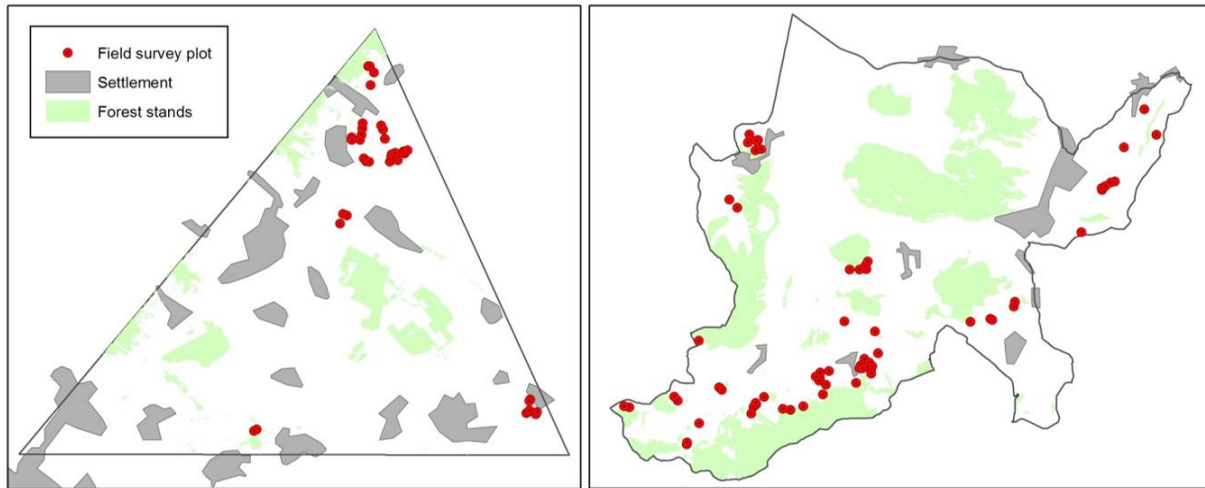
Figure 5.23. *Field survey plots localisation in study area 1 – Podunajská nížina (left) and study area 2 – Zvolenská kotlina (right).*

Figure 5.24. *Left: field survey – cut out of biomass from plot 2x2 m; Right: biomass weighing after harvest using hanging scales.*

Satellite data aquisition

- Sentinel-1 satellite data were acquired from 5th September 2017 to 30th September 2018

- Sentinel-2 satellite data were acquired to 4 time periods: 22nd June 2016 (top of vegetation season); 28th January 2017 (leaf-off vegetation season with snow); 29th March 2017 (leaf-off vegetation season without snow) and 30th September 2018 (autumn season).

- Satelite radar ALOS-2 data we acquired in Stripmap mode (SLC format). Study area 1: from 13th April 2017 (North–east part) and 27th April 2017 (South-west part). Study area 2: 22nd April 2017.

Sentinel-1 processing include derivation of average intensity from both polarisation VV and VH; Sigma0, Gamma0, Beta0 and applying Refined Lee filter from 61 images acquired from 5th September 2017 to 30th September 2018.

61

Coherence between images were calculated from leaf-off periods: 14-20January 2017; 14-26January2017; 20-26January2017.

The aim of Sentinel-1 stratification was to analyse separately:

- Leaf-on period (from 5.IX.2017 to 15.X.2017 and from 20.IV.2018 to 30.IX.2018)
- Leaf-off period: 17.X.2017 – 19.IV.2018 with sub-stratum 1: Leaf-off period without snow (from 17.X. to 14.XI.2017 and from 22.III. to 19.IV 2018) and sub-stratum 2: Leaf-off period with snow (from 14.XI.2017 to 22.III.2018)

Sentinel-2 bands in the red, near and short-wavelength infrared regions were included in the analysis, namely B4, B5, B8, B8a and B11 with a resolution of 10 and 20 m from all four periods. Topographically normalized images (L2A) were used for all dates.

ALOS-2 data processing included derivation of backscatter – sigma nought (HH,VH,VV,HV), polarimetric parameters (Span, Pedestal Height, Radar Vegetation Index, Radar Forest Degradation Index, Canopy Structure Index, Volume Scattering Index, Biomass Index, Co and Cross Pol Ratio) and polarimetric decomposition – Sinclair and Pauli colour coding (Fig. 5.25), Freeman-Durden, Sinclair, Yamaguchi and H/A/alfa decompositions (Fig. 5.26), resp. Single bounce, Double bounce and Volume scattering layers. All relevant products were also speckle filtered using Refined Lee approach.
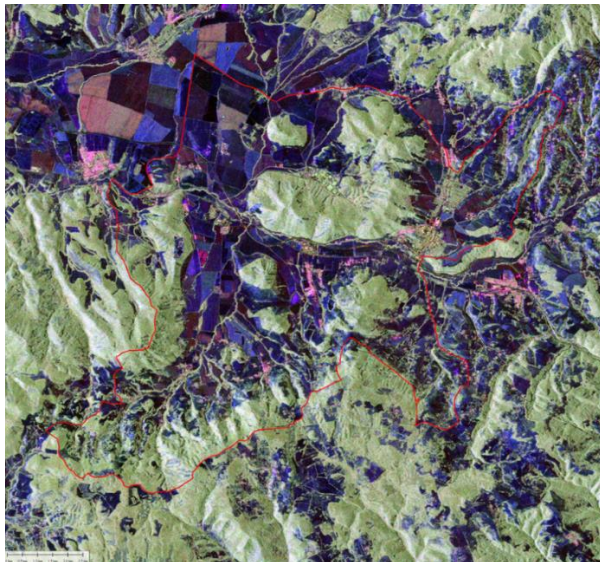
Figure 5.25. *Pauli combination of ALOS-2 satellite bands for test area Viglas, red – HH-VV green – HV, blue – HH+VV.*
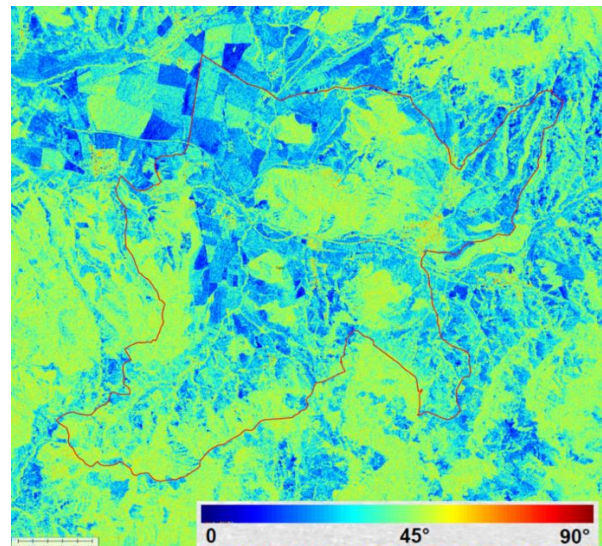
Figure 5.26. *H/A/alfa decomposition for test area Viglas – Alfa parameter.*

The extensive database allows derive many combinations of stock prediction models on AAL (Tab. 5.1). We focused our attention on:

1) estimation of biomass volume on AAL from ALOS-2 bands applying nonlinear (power) model,
2) fusion of Sentinel-1 and Sentinel-2 data and finding the most appropriate methods for biomass volume prediction on AAL in 2 variants: linear and nonlinear models of biomass estimation (Fig. 5.27),
3) Fusion of all disposable RS layers applying Random Forest Algorithm (Fig. 5.28).

Table 5.1. *Models for biomass retrieval on AAL for RS data*

Inputs (bands)	Model – backward stepwise multiple regression AGB (t.ha^{-1})=	R^2	RMSE (t.ha^{-1})	Remark
ALOS-HV, HH	$e^{(-5.75 + 5.10 * lnALOS\_HV – 3.12 * lnALOS\_HH)} * 1.51$	0.63	117.9	ALOS-2
ALOS-VH, VV, HH, HV	-106.60 + 4.71 * ALOS-VH – 3.19 * ALOS-HH	0.33	154.1	ALOS-2
Yamaguchi 1, Yama2, Yama3	-86.34 + 24.17 * yama2 - 23.45 * yama3	0.39	146.6	ALOS-2
Sinclair decomposition	-153.45 – 70.71 * sinc1 + 78.02 * sinc2	0.38	147,4	ALOS-2
Freeman decomposition	-54.45 + 21.64 * frem2 - 21.49 * frem3	0.38	147.7	ALOS-2
22.6.2016 (B4, B5,B8, B8a, B11)	730.71 - 0.79 * B5 – 1.62 * B8 + 1.47 * B8a	0.63	115.4	Sentinel-2
22.1.2017 (B4, B5,B8, B8a, B11)	295.66 + 0.43 * B8 – 0.51 * B8a + 0.17 * B11	0.36	151.2	Sentinel-2
29.3.2017 (B4, B5,B8, B8a, B11)	384.15 - 0.98 * B8 + 1.02 * B8a - 0.21 * B11	0.32	156.1	Sentinel-2
30.9.2018 (B4,B8, B11)	161.92 - 0.74 * B4 + 0.08 * B8	0.40	145.9	Sentinel-2
SNEH-VH0 VV0, VegO-VH0 VV0	-15.35 + 5.41 * SNEH-VH0 – 6.16 * VegO-VV0	0.37	148.8	Sentinel-1
SNEH-VH0-VV0, VegO-VH0-VV0, Coherence VV-VH (14-20-26.I.2017)	179.68 - 3.65 * C2026iVV – 4.37 * VegO-VV0 + 3.93 * SNEH-VH0	0.44	141.1	Sentinel-1
22.6.2016-B5, SNEH-VH, Veg-VV	544.61 - 0.54 * B5-22vi + 2.89 * S1-VHleaf-off - 3.38 * S1-VVleaf-on	0.58	100.1	Sentinel-1,2
Whole dataset	Random Forest Algorithm (in m^3.ha^{-1})	0.75	106.8	All layers
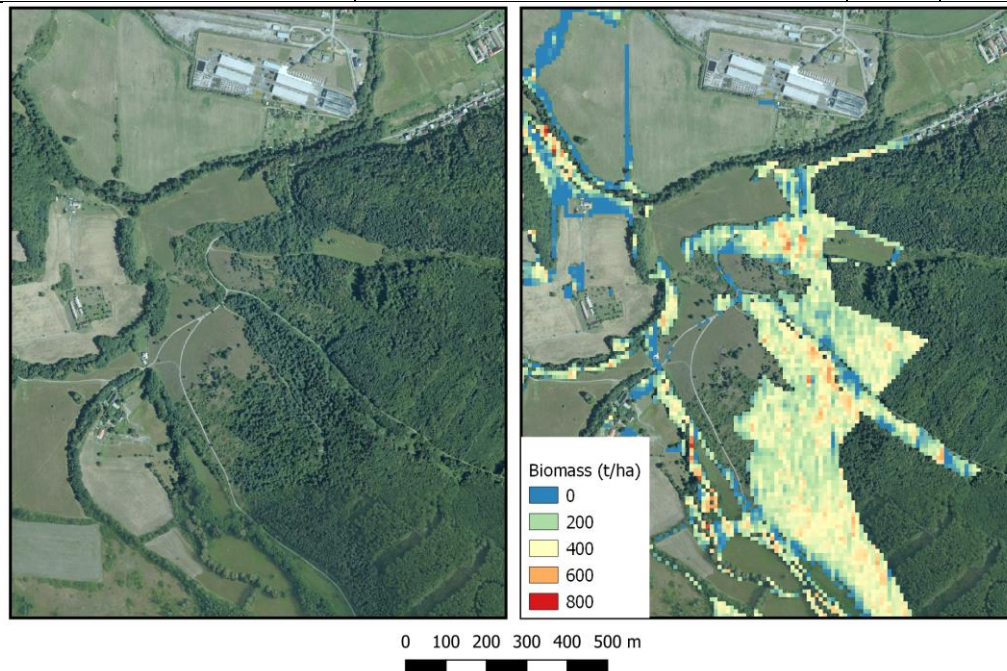
Figure 5.27. *Example of application of linear regression model (Sentinel-1,2) in the western part of study area "Viglas". Left – aerial scene, right – raster of estimated biomass (tonnes per ha).*
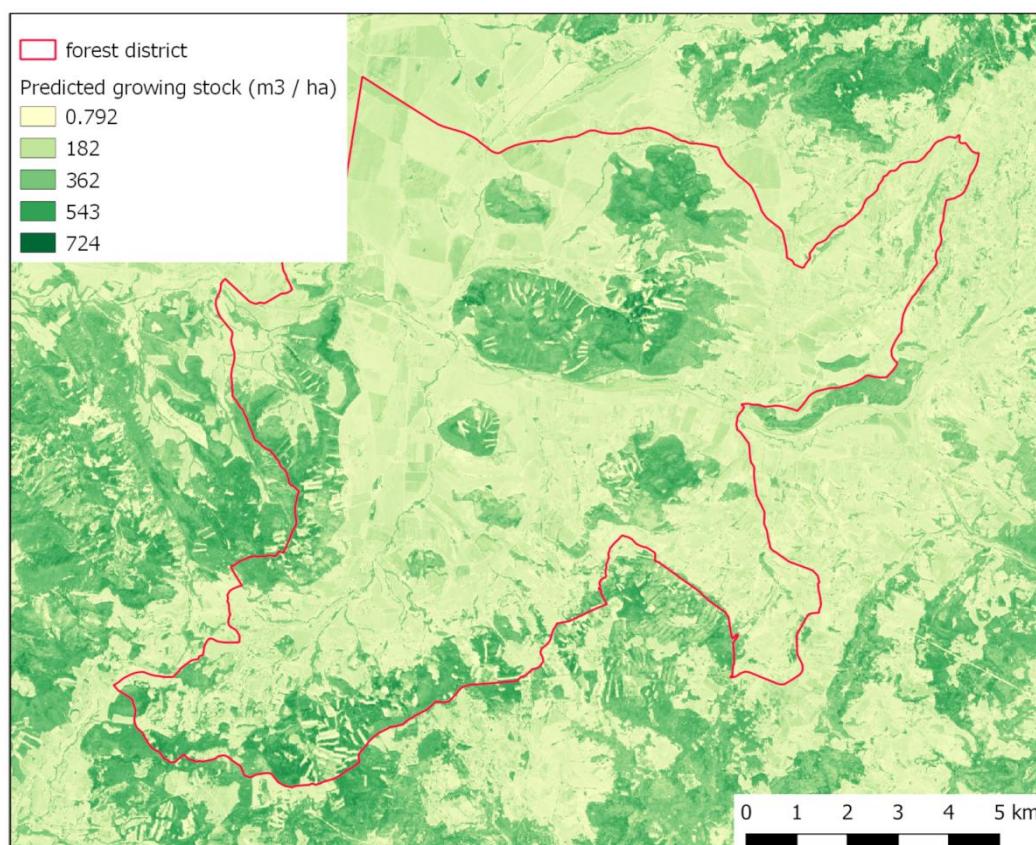
Figure 5.28. Predicted growing stock (m³/ha), Vígľaš test area, based on Random Forest algorithm.

Applications of airborne laser scanner technology in the forest management

Remote sensing activities related to the airborne laser scanning (ALS) over the years 2018-19 were solved based on research projects "Innovations in the forest inventories based on progressive technologies of remote sensing" (APVV-15-0393) and "Research and development for support of the competitiveness of Slovak forestry – New methods of forest inventory based on combination of terrestrial and aerial laser scanning" (SLOV-LES).

The main objective of all activities was an enhancement of the current inventory methods based on more precise and economically effective combination of different approaches (e.g. individual tree defection approach and area-based approach) and different remote sensing data (e.g. combination of ALS data with optical and/or radar data from terrestrial, aerial and satellite remote sensing platform; Fig. 5.29).

The proposal of algorithm is implemented in reFLex (remote Forest Land explorer) software and several studies already demonstrated that forest stand variables can be estimated with sufficient accuracy using developed algorithm. A Forest Management Unit Vígľaš covering a total area of 12,472 ha was selected for assessment of accuracy and feasibility of developed algorithm. Specifically, the differences between ground-measured and RS-estimated forest stands variables reached values of 16.4%, 12.1%, −26.8%, and −35.4% for the mean

height, mean diameter, volume per hectare, and trees per hectare, respectively (Sačkov et al. 2019a, 2019b).
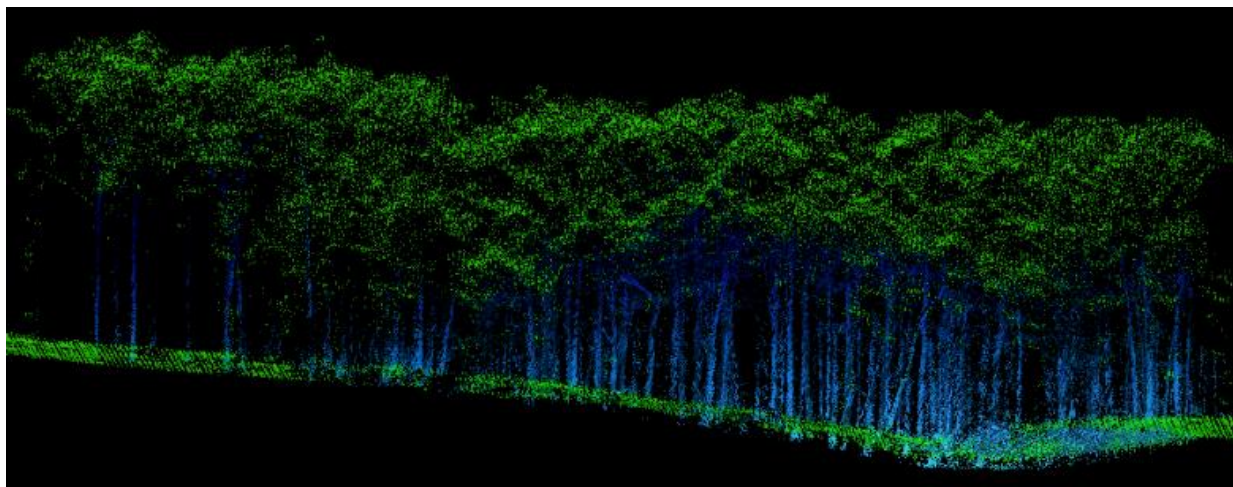
Figure 5.29. *Fusion of airborne (green colour) and terrestrial (blue colour) laser scanning data.*

Ministry of Environment of the Slovak Republic (MOE SR)

Activities of the MOE SR were concentrated on the work involved with the Copernicus programme:

Copernicus programme is the European programme for Earth Observation. The Programme entered its full operational stage in the year 2014. The work on the EU level was concentrated on cooperation with the Copernicus Committee, Copernicus Security board, Copernicus User forum and Copernicus Ground segment task force and commenting on the EU level the technical and legislative documents regarding the Programme.

Cooperation with the European Space Agency (ESA) is limited due the fact that the Slovak Republic is not full member of ESA yet. Slovakia is however actively participating in Plan for European cooperating States (PECS). Several organization and companies from Slovakia were successful in 5 open calls for PECS projects. Cooperation with the European Environment Agency (EEA) was concentrated on preparation of the next CORINE Land Cover (CLC) 2018 and High Resolution Layer (HRL) products as a part of the Copernicus Land observation service. At the national level the Slovak national Copernicus working group continued its operation with the aim to coordinate Copernicus related activities on the national level and dissemination of information related to Copernicus programme. MOE SR distributes the Sentinel satellite images for the Slovak Republic on demand. Compared to previous period user uptake and usage of the Copernicus data has growing trend but is still relatively low compared to neighbouring EU countries. Several public government organizations and private companies are actively using Copernicus spatial data. In the following years Slovakia plans to focus on user trainings in remote sensing and Programme information dissemination.

Pavol Jozef Šafárik University in Košice is member of Copernicus academy network and is actively using Copernicus programme spatial data in its courses and lectures. Private company InSAR is successfully operate as member of Copernicus Relays network, promoting the information about programme and data usage to public and professional through workshops, courses and conference. Two annual Hackathons were organised in Bratislava with successful use of the Copernicus data by the participants to develop application prototypes.

Slovak Environmental Agency (SEA) in Banská Bystrica

Activities of the SEA were concentrated on the work involved with the Copernicus programme:

Copernicus is the European programme for Earth Observation. The Programme entered its full operational stage in the year 2014. The work on the EU level was concentrated on cooperation with the Copernicus Committee, Copernicus Security board, Copernicus User forum and Copernicus Ground segment task force and commenting on the EU level the technical and legislative documents regarding the Programme. Cooperation with the European Space Agency is limited due the fact that the Slovak Republic is not full member of ESA yet. Cooperation with the European Environment Agency (ESA) was concentrated on implementation of the CORINE Land Cover (CLC) 2018 and the High Resolution Layer (HRL) products as a part of the Copernicus Land observation service. Copernicus supporting activities for the period 2017-2021:

Copernicus Land Monitoring

SEA joined the activities in project Copernicus Local Land monitoring services under Framework Contract EEA/IDM/R0/16/009/Slovakia. The contract between SEA and EEA was signed on 8 June 2017 and project tasks were implemented from autumn 2017 till end of 2018. The project flagship was CLC2018, the fifth CLC inventory in Europe. The final integrated European results are available since late 2018.

Project tasks undertaken by SEA:
- finalised in 2018-2019:
  - Verification of 2012 reference year local component products.
  - Production of CLC for the 2018 reference year.
  - Post-production verification of the HRL's for the 2015 reference year.
  - mapping national geospatial resources to EAGLE matrix

- Post 2019 tasks:
  - Post-production verification of the HRL's for the 2018 reference year.
  - Support and testing of future CLC+ (2nd generation CLC methodological improvements and developments), based on CLC2018 products.

Figure 5.30. *The screenshot of new SEA webpage.*

All of the time horizons CLC data has been published as standard OGC services and also are available through new webpage http://corine.sazp.sk (Fig. 5.30). The info day about Corine Land Cover 2018 activities and output products was also held on March, 28th, 2019 in SEA to fulfil project dissemination activities.

References:

[1] FERANEC, J., OŤAHEĽ, J., KOPECKÁ, M., NOVÁČEK, J., PAZÚR, R. (2018). *Land cover of Slovakia and its change in 1990-2012 (in Slovak), 160 pp.*, 337 pp. Veda: Bratislava.

[2] GOGA, T., FERANEC, J. BUCHA, T., RUSNÁK, M., SAČKOV, I. BARKA, I., KOPECKÁ, M., PAPČO, J., OŤAHEĽ, J., SZATMÁRI, D., PAZÚR, R., SEDLIAK, M., PAJTÍK, J., VLADOVIČ, J. (2019). A Review of the Application of Remote Sensing Data for Abandoned Agricultural Land Identification with Focus on Central and Eastern Europe. *Remote Sensing*: *Open Access Journal*, 11, 23, art. no. 2759.

[3] FERANEC, J., HOLEC, J., ŠŤASTNÝ, P., SZATMÁRI, D., KOPECKÁ, M. (2019). Visualising a comparison of simulated urban heat islands: a case study of two Slovakian cities. Ed. H. Fujita. *Advances in Cartography and GIScience of the ICA*, Vol. 1. Tokyo: International Cartographic Association, p. 1-8. Available at: https://www.adv-cartogr-giscience-int-cartogr-assoc.net/1/6/2019/

[4] GOGA, T., BOBÁĽOVÁ, H., SAČKOV, I., KOPECKÁ, M. (2019). Klasifikácia poškodenia lesa vo veľkej mierke na báze leteckých multispektrálnych snímok a lidarových dát – prípadová štúdia CHKO Dunajské Luhy (Forest damage classification in large scale based on aerial multispectral images and lidar data: a case study of Dunajské Luhy Protected Landscape Area). *Geografický časopis*, 71, 1, 51-71.

[5] KAŇUK, J., GALLAY, M., ECK, C., ZGRAGGEN, C., DVORNÝ, E. (2018). Technical Report: Unmanned Helicopter Solution for Survey-Grade Lidar and Hyperspectral Mapping. *Pure and Applied Geophysics*, 175(9), 3357-3373.

[6] KOVÁČIKOVÁ, I., KAUSITZ I. (2018). The 2018 campaign of remote-sensing control of area-based subsidies. Final report, NAFC-SSCRI Bratislava, 23 pp.

[7] KOVÁČIKOVÁ, I., SVIČEK, M., KAUSITZ, I. (2018). The 2018 campaign of remote-sensing control of area-based subsidies. Interim report, NAFC-SSCRI Bratislava, 9 pp.

[8] ONAČILLOVÁ, K., GALLAY, M. (2018). Spatio-temporal analysis of surface urban heat island based on LANDSAT ETM+ and OLI/TIRS imagery in the city of Košice, Slovakia. *Carpathian Journal of Earth and Environmental Sciences*, 13(2), 395 – 408.

[9] SAČKOV, I., KULLA, L., BUCHA, T. (2019). A Comparison of Two Tree Detection Methods for Estimation of Forest Stand and Ecological Variables from Airborne LiDAR Data in Central European Forests. *Remote Sensing,* 11, 1431.

[10] SAČKOV, I., SCHEER, L., BUCHA, T. (2019). Predicting forest stand variables from airborne LiDAR data using a tree detection method in Central European forests. *Central European Forestry Journal*, 65, 191-197.

[11] SKALSKÝ, R., FULMEKOVÁ, Z., SVIČEK, M., KUSÝ, D. (2019). Application and updating of the national agro-meteorological modelling system to estimate crop production and crop yield (SK_CGMS). Final report to solving tasks under the contract with MPRV for the year 2019. SSCRI, Bratislava, 35 pp.

[12] SKALSKÝ, R., FULMEKOVÁ, Z., SVIČEK, M., KUSÝ, D. (2019). The yield forecast of winter crops in the first decade of May 2019. *Naše pole*, 23, 8, 32- 34.

[13] SKALSKÝ, R., FULMEKOVÁ, Z., SVIČEK, M., KUSÝ, D. (2019). The yield forecast of maize, sunflower, sugar beet and potatoes on 20th September 2019. *Naše pole*, 23, 11, 43- 45.

[14] ŠAŠAK, J., GALLAY, M., KAŇUK, J., HOFIERKA, J., MINÁR, J. (2019). Combined use of terrestrial laser scanning and UAV photogrammetry in mapping alpine terrain. *Remote Sensing*, 11 (18), 2154.

[15] XIAO, H., KOPECKÁ, M., GUO, S., GUAN, Y., CAI, D., ZHANG, Ch., ZHANG, X., YAO, W. (2018) Responses of urban land surface temperature on land cover: a comparative study of Vienna and Madrid. *Sustainability*, 10, 2, art. no. 260. Available at: http://www.mdpi.com/2071-1050/10/2/260/htm

6. SPACE METEOROLOGY 2018-2019

J. Kaňák, Ľ. Okon, L. Méri, M. Jurašek

6.1. Fully automated quantitative estimation of cloud top height using stereoscopic Meteosat dual satellite observations

EUMETSAT provides perfect stereoscopic data from Meteosat 10/11 (Basic service) and Meteosat 8 (IODC service) over large areas of Central and East Europe, Middle East Asia, central and South African regions from 2016. The presented work describes proposed experimental product, which is using AMV (Atmospheric Motion Vectors algorithm) to detect mutual parallax shifts of clouds in coupled imagery. This product is based on previous investigations of manual measurements of parallax shifts, which were presented at the EUMETSAT 2017 conference in Rome. Parallax shifts we are currently calculating for 32x32 pixel boxes over 16x16 pixels grid, but are planned to be tested also for smaller/optimized boxes and grid spacing. Fully automated calculations over the big regions covered by dual satellites observations can serve as important supplement data to other methods and products like NWCSAF Cloud Top Height and Cloud Type, or shadows length based estimations of cloud top heights. Algorithm is working not only with High Resolution Visible (HRV) but also with other IR and VIS spectral bands. Considering 12 SEVIRI channels we obtained wide experimental set of dual satellite parallax shifts for different cloud types and heights. New, third generation of geostationary satellites with finer image resolution and global coverage bring us to new possibilities how to combine and use more efficiently overlapping satellite fields of view.

6.1.1. Mathematical background of automated quantitative estimation of cloud top height

Fully automated computer processing of dual satellite images is divided in SHMI operational chain into following steps:

1. Identification of cloud structures in the left and right satellite images using Atmospheric Motion Vector (AMV) algorithm
2. Coupling cloud structures using dual set of Cartesian coordinates $[x_{left}, y_{left}]$ and $[x_{right}, y_{right}]$
3. Converting Cartesian to geographical coordinates $[\lambda_{left}, \varphi_{left}]$ and $[\lambda_{right}, \varphi_{right}]$
4. Calculating parallax corrected positions of clouds in left and right image $[\lambda_{left}, \varphi_{left}]^{corr}$ and $[\lambda_{right}, \varphi_{right}]^{corr}$
5. Calculating horizontal (surface) distance d between left and right corrected positions (note that for sea level parallax correction is equal to zero):

$$d = \text{distance } \{ \ [\lambda_{\text{left}}, \varphi_{\text{left}}]^{\text{corr}}; \ [\lambda_{\text{right}}, \varphi_{\text{right}}]^{\text{corr}} \ \}$$

6. In iteration steps changing the elevation E in 100 meters steps from surface up to 20 km atmosphere layer
7. Repeating calculation steps 3, 4, 5, 6 for each elevation E to look for minimal horizontal distance d_{min}
8. Final statement of calculations: Elevation $E(d_{\text{min}})$ is corresponding to the minimum distance d_{min} is considered as the height of the cloud.

Practical realization is done by numerical iteration process – calculations of the distance d between the lines connecting the satellite and the cloud – finding the height of minimum distance (intercept-point). Graphical explanation is shown in Fig. 6.1.
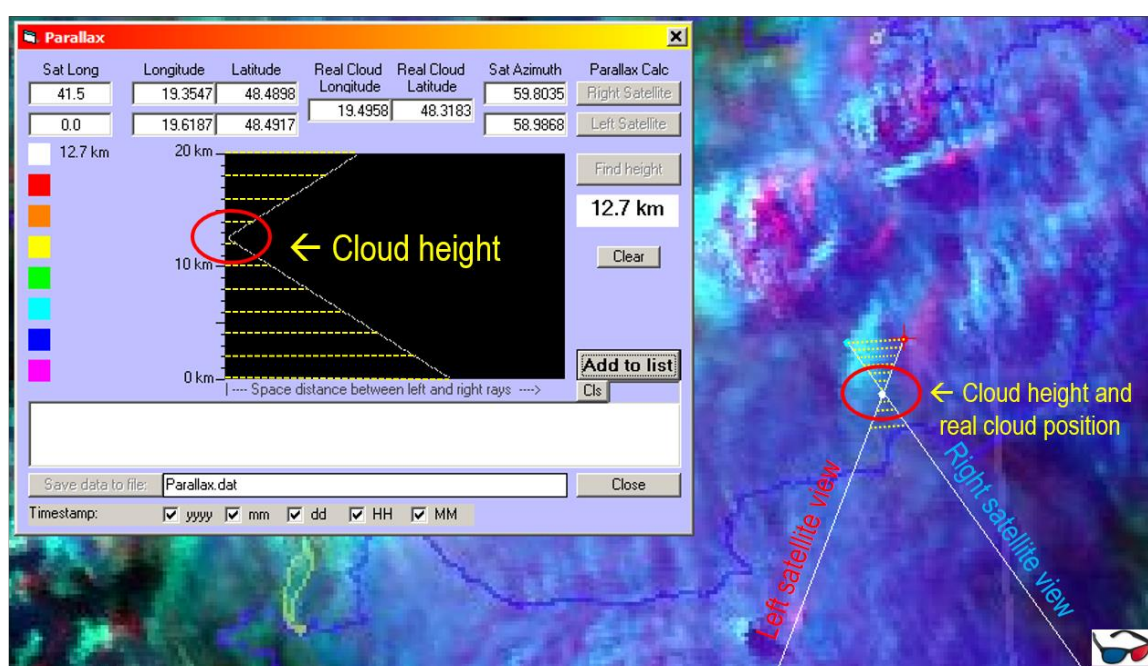
Figure 6.1. *Quantitative estimation of cloud top height using stereoscopic Meteosat dual satellite observations. Iteration process is represented by set of horizontal yellow lines. Lines are representing horizontal distance between left and right rays in different elevations. Minimum distance between lines (in optimal case d=0) is indicating the cross point of these lines – related to the cloud top height. In practice zero value of d is only limit because of various sources of errors.*

6.1.2. AMV (Atmospheric Motion Vectors) algorithm

Algorithm comes from CEI Nowcasting Project 2002-2004 in cooperation of ZAMG Austria and SHMI Slovakia. Algorithm is based on definition of limited area in the first image and look for identical image structure in the second image. Shift of structure between images corresponds to mutual parallax shift between left and right satellite cloud observations. Originally algorithm was used only for WV channels smooth structures. We made set of tests with all infrared MSG channels using standard cross-correlation technique applied to rectangular targets

71

over the image matrix with the aim of detecting optimal shift between target and matcher.

Calculations are applied to regular satellite image grid (step size is optional from maximum 10 to minimum single image pixels). Basic assumption must be fulfilled that images from left and right satellites must be re-projected from Geo-satellite view into common cartographic map. The core calculation expression is:

$$\max\left\{ r = \frac{\sum_i (x_i - \bar{x})(y_i - \bar{y})}{\sqrt{\sum_i (x_i - \bar{x})^2 \sum_i (y_i - \bar{y})^2}} \right\}$$

Software of this algorithm was originally written in Fotran-90. For the purposes of automated quantitative estimation of cloud top height algorithm was translated into C language and parametrized for optimal performance with image data of MSG SEVIRI spectral bands as follows:

Parameter:	Step 16x16	Step 8x8
Correlation window size	33	33
Span of possible displacements	36	36
X-coordinate of first column	32	32
Y-coordinate of first row	32	32
X-difference between vectors	16	8
Y-difference between vectors	16	8
Number of vectors in x-direction	122	244
Number of vectors in y-direction	91	182
Gaussian pyramid iterations	2	2
Number of smoothing cycles	3	3

6.1.3. Validation of proposed method and final product

AMV algorithm enables us to obtain quickly and automatically dual parallax cloud shifts over the big regions monitored by dual MSG satellite constellation. Output from the software is displayed in the special visualization tool, as it is shown in Fig. 6.2. This tool can be used also for validation purposes, as the length of arrows can be compared with manually measured parallax shifts and cloud top can be derived; simultaneously we can use the tool to measure the length of cloud shadows, which provide another way how to estimate cloud tops.
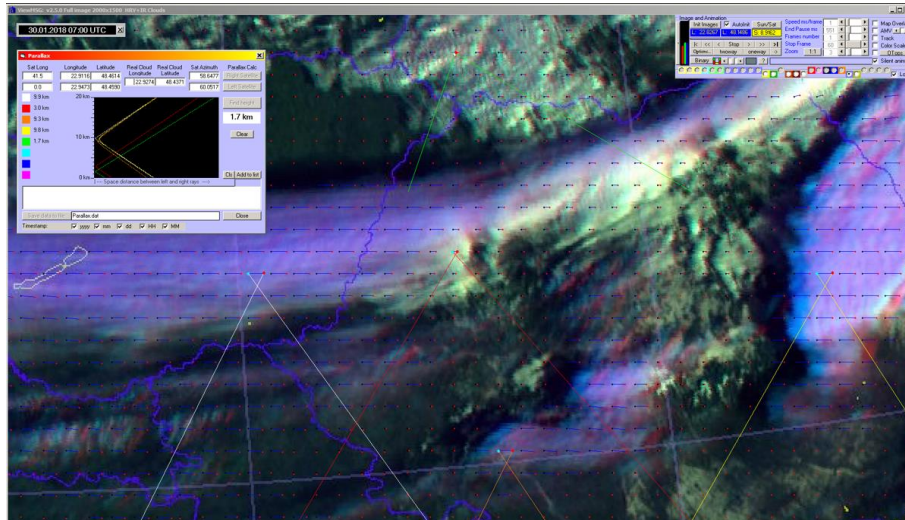
Figure 6.2. Example shows the arrows, length of which is equivalent to Cloud Top Height (CTH). Colour lines generated by validation tool represent directions to the left and right satellites. Cross points of line couples are corresponding to the real cloud top position in 3-D coordinate system.

The most common problem occurring during validation was resulting from improper or not accurate geolocation/rectification of satellite images. Precision of geolocation depends on current satellite status of its positional sensors, which provide auxiliary information for image rectification. As Meteosat-8 satellite was launched in 2002, eccentricity of satellite axis rotation is much higher and we are coupling the images from this satellite with Meteosat-10 or Meteosat-11, launched in 2012 and 2015 respectively, with high rotational stability of their movement. But using additional corrections of image rectification in case of Meteosat-8 we were able to minimize errors of mutual parallax shifts. Results after these corrections are showed in Fig. 6.3.

Final product is created using linear interpolation of gridded CTH data into the original satellite grid. Example of final product is shown in Fig. 6.4.
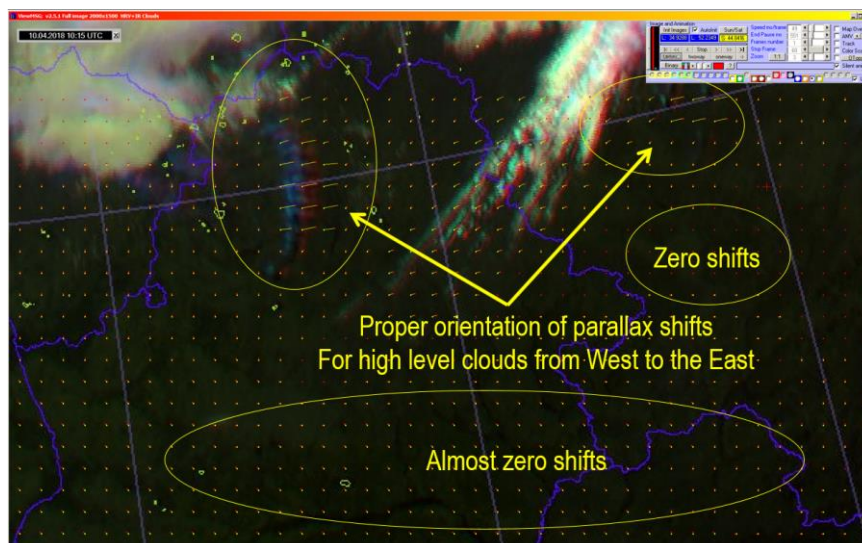
Figure 6.3. Using additional correction of image rectification for Meteosat-8 we obtained proper orientation of parallax shifts and more precise calculations of cloud tops.

73
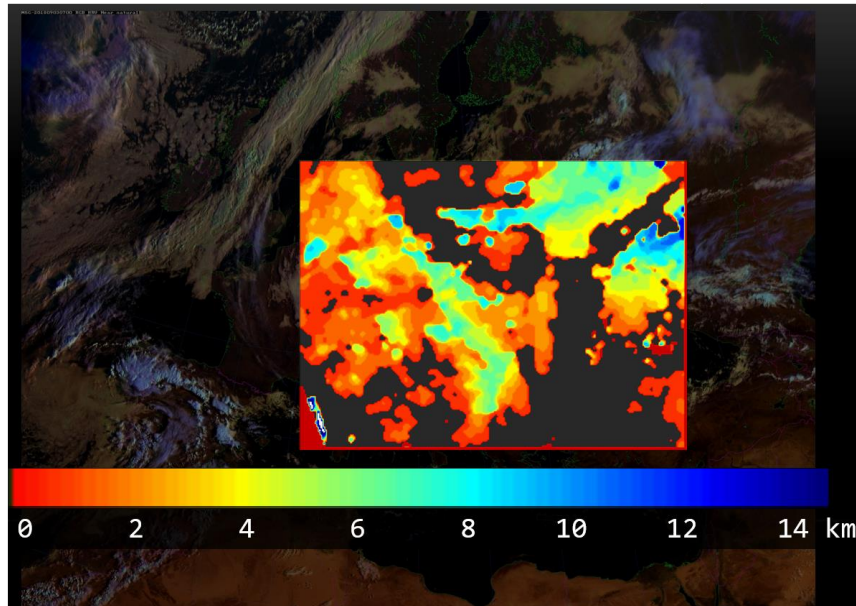
Figure 6.4. *Final Cloud Top Height product overlaid over the MSG satellite high resolution visible image. Colour scale is calibrated in kilometres. Final precision of product according validation results is 500 meters for 40% of cases and 1km for 60% of cases.*

6.2. Way from MSG to MTG satellite user's training and operational supporting tools

6.2.1. Introduction

Geostationary satellites monitor practically the whole globe except Polar Regions; therefore imagery from these satellites is very frequently used by number of users over the world for weather and climate observations, and for forecasting and nowcasting purposes. Different technical and software capabilities are available through both commercial and non-commercial opportunities for exploitation of these satellites in training and operational activities. This work presents more than 10 years of skills with SHMI MSGProc software development, distribution and communication with users who depend on solutions based on simple installation, easy maintenance and minimum hardware requirements. This kind of users was identified by EUMETSAT training division in NMHS of south-east European region countries (so called DAWBEE users), but also by our personal skills on the base of communication with users in Brazil, Africa and other countries, mainly from the universities, where our software was provided on the user's request. This, originally MSG-dedicated software, is currently renamed to "GEOProc" and enhanced to be reusable for new geostationary platforms as HIMAWARI and GOES new generation with the intention to be usable for Meteosat Third Generation (MTG) satellite imagery at the first moment of MTG operations. We recognized openness of EUMETSAT in this activity in the frame of 'MTGUP!' initiative.

74

6.2.2. Background

SHMI developed and is using operationally home-made processing software for geo satellites, starting with MSG era:

- MSGProc and new GEOProc for HIMAWARI, GOES-16, 17 data available from EUMETCast system
- New experiences thanks to close cooperation with EUMETSAT on DAWBEE project (Data Access to West Balkan and East European countries)
- The group of users was found, which requires easy to install, configure and usage software for their needs
- Opportunity to re-use current experience also for MTG satellite data

6.2.3. SHMI software solution

Some special features of SHMI solution are described and discussed in presented work, starting with data acquisition, main processing steps up to final RGB products generation and visualization. Attention is focused to effectiveness of input data processing, data calibration, and special image corrections with contribution of the Sun and satellite zenith angles, light diffusion in visible bands, and anisotropy of atmosphere in infrared spectral bands. Considering that new generation of geostationary satellites are providing much higher volumes of raw data than current MSG satellites, we are now performing online data reception tests via EUMETCast service from HIMAWARI-8, 9 and GOES-16, 17 satellites. We also perform processing of these data to RGB imagery in operational mode. First skills with the new software solution, and selected image examples of typical weather situations from already generated list of products at SHMI are shown and discussed in final part of this report.

6.2.4. Software concept and features

- Easy and quick installation
- Simple usage and maintenance
- Pre-defined RGB products are generated according well-known recipes
- New RGB products can be added easily or existing can be modified
- Effective usage of calculating resources and short processing time
- Processing of current GEO (MSG, GOES, HIMAWARI) satellite geostationary services
- C and C-shell programming without necessity of external libraries and third party software

6.2.5 Corrections of solar channels

Because of increasing number of spectral bands parallel processing and reusing of pre-calculated parameters approach was selected. Corrections of solar channels

are done for Sun height and Satellite zenith angles according functions shown in Fig. 6.5.
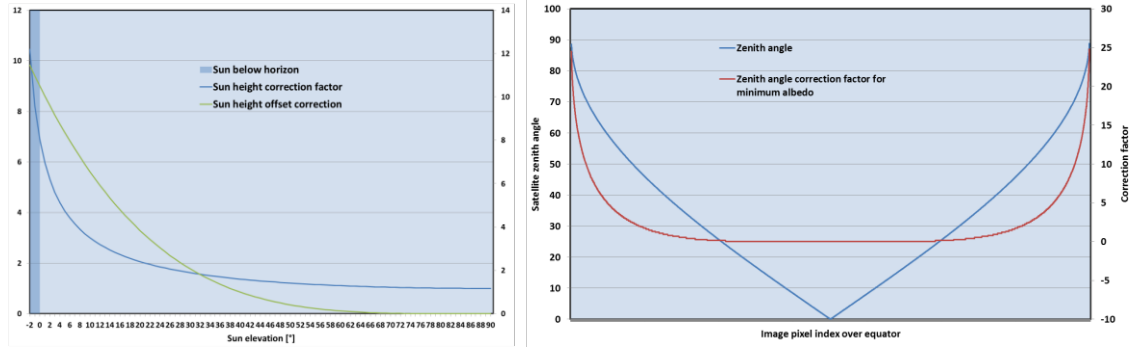
Figure 6.5. *Correction of solar albedo on Sun height (left) and on satellite zenith angle (right).*

While Sun height is determined using standard Sun coordinates – right ascension and declination, functions for corrected albedo are based on empirical equations (1).

Corr = 1./(a*sin(α)+b*sqrt(sn(α)));   where a = 0.6 b = 0.4, α is Sun zenith angle (1)
offset_sunh ≈ pow (MaxH - α, 3);   partial correction offset for Sun height
offset_satz ≈ zenith / α;   partial correction offset for Satellite zenith angle
offset = offset$_0$ - offset_sunh - offset_satz;   total correction offset

6.2.6 Airmass full Earth disk RGB enhanced
Originally set of RGB products was defined very early after the launch of the first satellite from MSG satellite series. Product parameters (colour component's minimum and maximum values) were fixed over the whole Earth disk. After the years EUMETSAT recommended to differentiate between equatorial and mid latitudes for some RGB products, mainly when convection is displayed. We suggested to use floating values instead of constants with the aim to put equatorial and mid latitudes regions into common maps. Original settings for Airmass product were:

Channel	Min	Max	Gamma
Red Diff (6.2-7.3)	-25°	0°	1
Green Diff (9.6-11.2)	-40°	5°	1
Blue WV (6.2)	208K	243K	-1

For the full disk containing also tropical regions we defined R, G, and B thresholds depending on latitude according cosine shape as follows:

Channel	Min	Max	Gamma
Red Diff (6.2-7.3)	-25+Δ/2-Δcos (φ); Δ=-8	Min+25	1
Green Diff (9.6-11.2)	-40+Δ/2-Δcos (φ); Δ=-8	Min+45	1
Blue WV (6.2)	208+Δ/2-Δcos (φ); Δ=20	Min+35	-1

Calculated new correction values for R, G and B components are shown in Fig. 6.6.
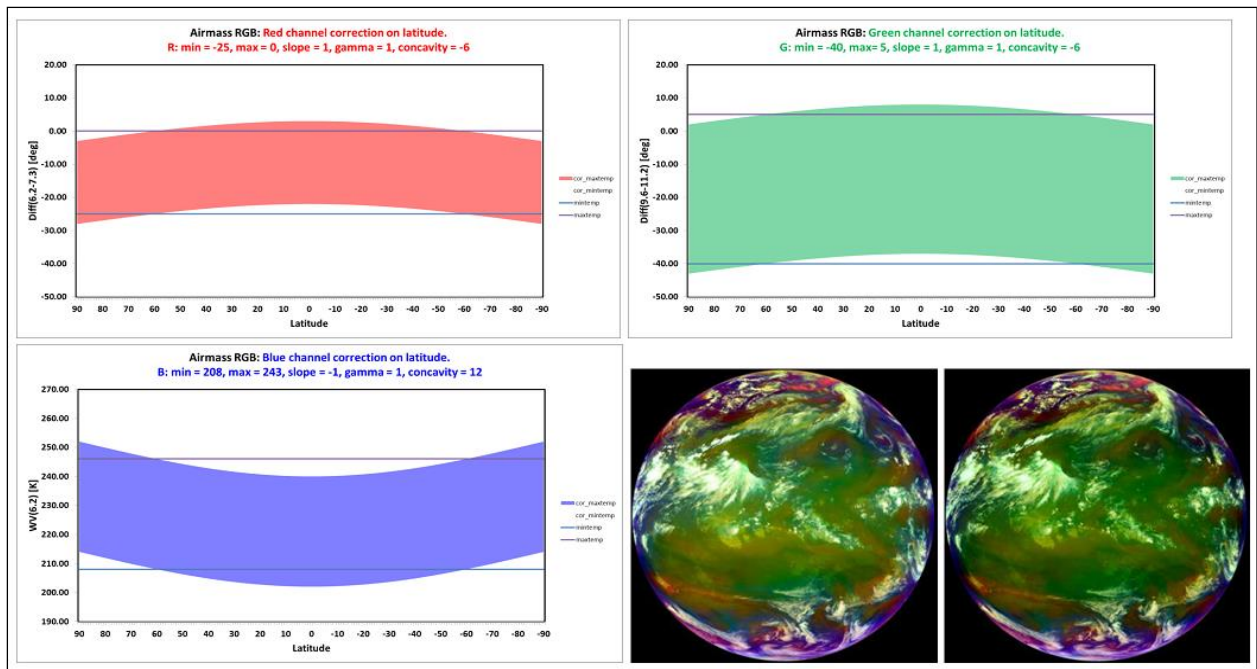
Fig. 6.6. *Latitude dependent minimum and maximum values of Airmass full Earth disk RGB product color components; red at left up, green at upper right and blue at left down plot. Processed full Earth disk image couple at right down: before (left) and after the correction (right).*

6.2.7. Selected demonstration cases and conclusions

Following list of meteorological cases was created for various scenes from GOES and HIMAWARI imagery data:

- Fire smoke and fire temp RGB products
- Raikoke eruption and rotating SO2 clouds (Airmass wholes)
- Goes-16 / MSG-4 comparison of common regions
- Twin cyclones in Australia and Pacific
- ship contrails GOES-16 2019-08-28 17:30 UTC
- Sun eclipse in South America
- Super typhoon Wutip of category 5 in western Pacific -10 minutes scan

EUMETCast Europe service of EUMETSAT is providing operationally valuable data from new GEO satellites for training purposes of SHMU staff;

Thanks to this service users have opportunity monitor and study in (near) real time weather over the globe;

Space and time of provided data is slightly reduced due to transfer capacities, but good enough to make users familiar with new RGB possibilities based on new set of 16 spectral channels (in comparison to old GEO standard 5 or 12 channels);

Users of new generation of EUMETSAT geo satellites must be aware in near future that new channels and higher space and time resolution will bring extreme requirements on data transfer and data processing; but they can await new enhanced possibilities of new physical and meteorological information for weather analyses and forecast.

6.3. Dual-frequency precipitation satellite radar and H-SAF product upscaling procedure over MSG full-disk area developed at SHMI

Slovakia (SHMI) is member of consortium in EUMETSAT H-SAF project since 2005. In cooperation with Italian Department of Civil Protection we are cooperating in validation of satellite precipitation estimations. We are using ground meteorological radar network data for standard validation of H-SAF products over European region. But for global products like Precipitation rate at ground by MW cross-track scanners (with indication of phase) it is more practical to use other similar equipment on board of satellites. We found possibility of validation using product 2ADPR – Dual-frequency Precipitation Radar (DPR) measurements on board of GPM (Global Precipitation Mission) satellites. Example of such product is shown in Fig. 6.7.
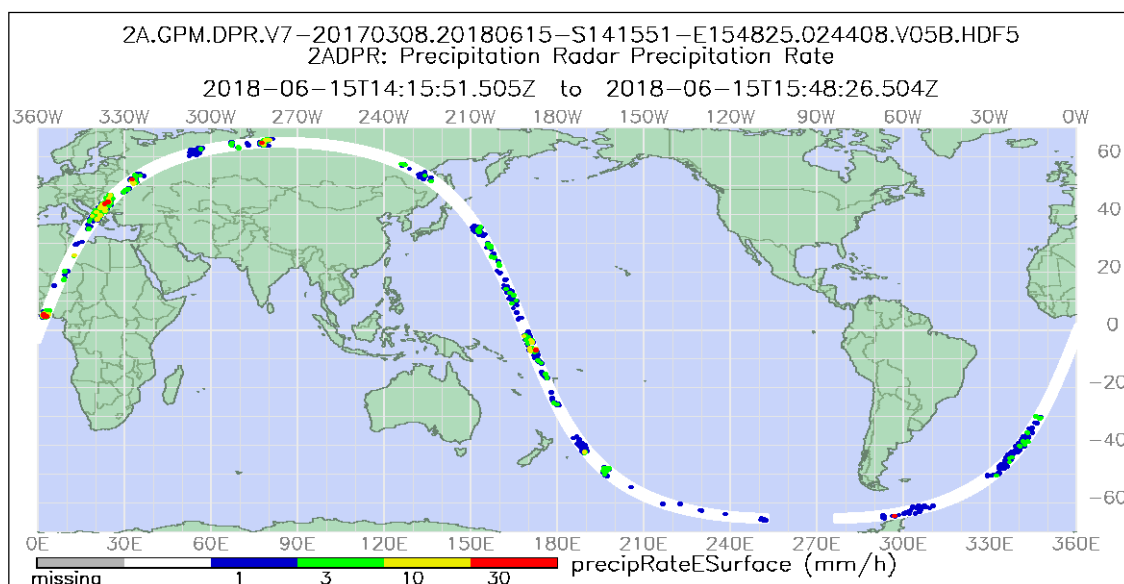

Figure 6.7. *Example of 2ADPR Precipitation Rate product based on measurements by DPR instrument on board GPM satellites.*

H-SAF product called H02B is a map of instantaneous precipitation (mm/hr) generated from MW cross-track scanning radiometers on board of satellites in sun synchronous orbit. Currently processing data are coming from AMSU-A/MHS on board European MetOp and U.S. NOAA satellites. Spatial Resolution of product corresponds to the nominal resolution of MHS, varying with the viewing scan angle from 16 x 16 km^2 (circular) at nadir to 26 x 52 km2 (ellipse) at scan edge. According to user requirements the thresholds, target and optimal accuracy of products is depending on precipitation range, as it is stated in the table:

Precipitation range	Threshold	Target	Optimal
> 10 mm/h	90	80	25
1-10 mm/h	120	105	50
< 1 mm/h	240	145	90

Example of H02B product is shown in Fig. 6.8.
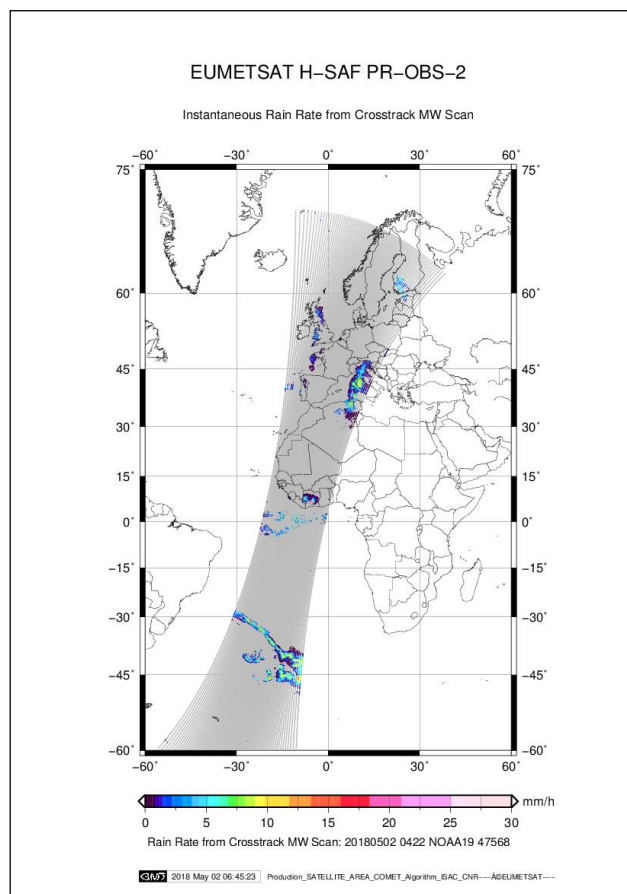
Figure 6.8. *Example of H02B product - instantaneous precipitation (mm/hr) generated from MW cross-track scanning radiometers on board of satellites in sun synchronous orbit MetOp (EUMETSAT) and NOAA.*

To validate/compare these relatively different products we elaborated special software package, which is re-mapping both products into common regular longitude-latitude grid. Complete product set contains more parameters:
- Cloud phase liquid-solid (discrete parameter)
- Rate of product confidence (discrete parameter)
- Land/Coast/Ocean flag (discrete parameter)
- Precipitation rate mm/h (continuous parameter)
- Standard deviation of precipitation rate (continuous parameter)
- Time of acquisition in Julian day (continuous parameter)

Upscaling (re-mapping) of each parameter require different approach, which depend on its characteristics. In general we split parameters to two categories – continuous and discrete. In upscaling algorithm mean value is selected for continuous and median for discrete parameters. Visualized selected parameters for H02 product are shown in Fig. 6.9, for 2DPR/GPM product in Fig. 6.10.
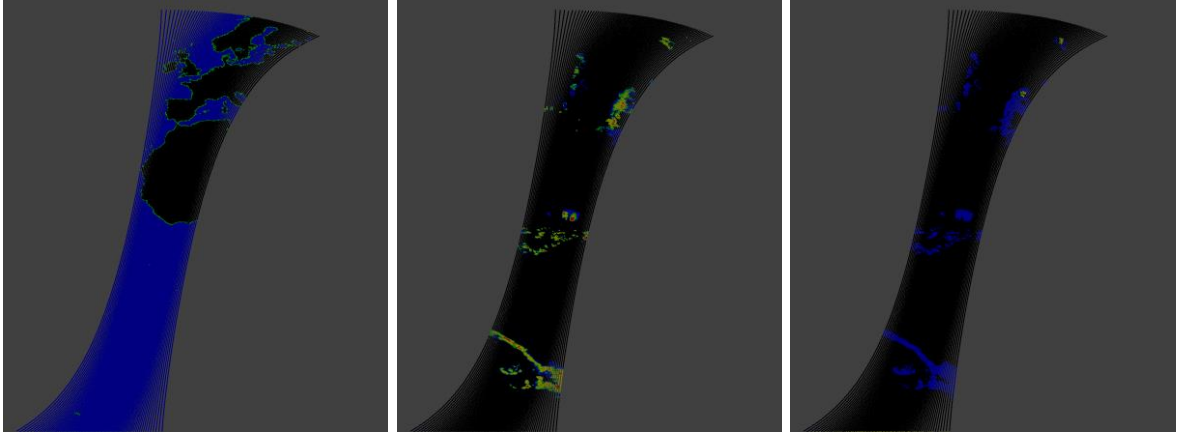
Figure 6.9. *Upscale of H02B H-SAF product parameters to regular longitude-latitude grid in resolution of 0.1x0.1 degrees. From left to the right: Land/Coast/Sea flag, Precipitation Rate, Cloud Phase.*
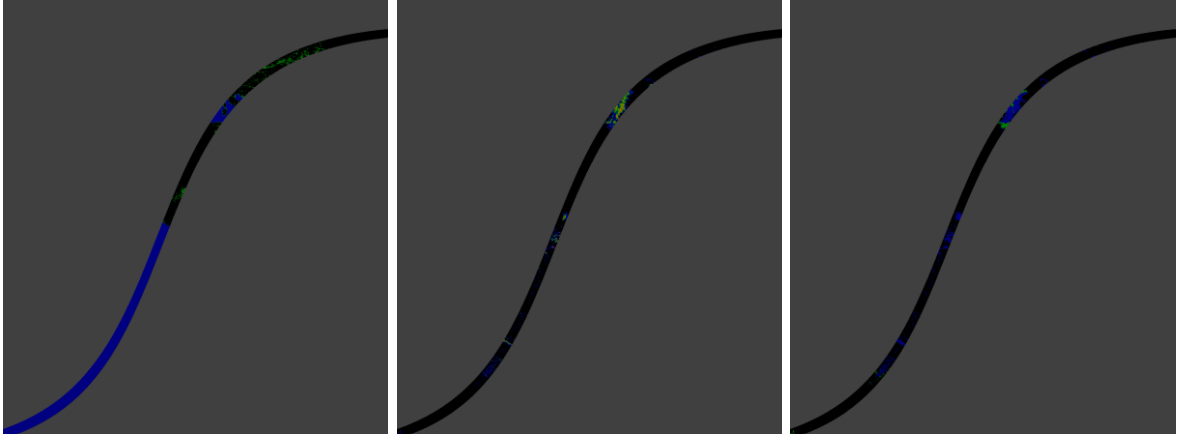
Figure 6.10. *Upscale of 2DPR/GPM product parameters to regular longitude-latitude grid in resolution of 0.1x0.1 degrees. From left to the right: Land/Coast/Sea flag, Precipitation Rate, Cloud Phase.*

H02B H-SAF product space resolution is lower, but the swath of satellite instrument is quite wide, approximately 2250 km. In opposite, space resolution of 2ADPR/GPM product is higher, but swath of dual-frequency radar is much lower, only 300 km. The advantage of 2ADPR product is that dual-frequency Doppler radar is capturing precipitation intensities and phase with high reliability and instrument data are physically better convertible to precipitation intensity than in the case of microwave measurements with MetOp and NOAA satellites.

References:

[1] KAŇÁK, J. (2018). Fully automated quantitative estimation of cloud top height using stereoscopic Meteosat satellite observations. *EUMETSAT Meteorological Satellite Conference*. Tallin, 17.-21. September 2018. https://www.eumetsat.int/website/wcm/idc/idcplg?IdcService=GET_FILE&dDocName=ZIP_CONF_2018_PRES_S3_ORAL&RevisionSelectionMethod=LatestReleased&Rendition=Web

[2] KUTIŠ, V., VALKO, P., DRŽÍK, M., SLAČKA, J., FARKAS, G., RAKÚS, M., HUBINSKÝ, P., KAŇÁK, J. (2018). *Kozmické technológie.* Bratislava: Slovenská technická univerzita.

[3] KAŇÁK, J., JURAŠEK, M., OKON, Ľ., MÉRI, L. (2019). Way from MSG to MTG satellite user's training and operational supporting tools. *Joint EUMETSAT/AMS/NOAA Conference*. Boston, 30 September – 4 October 2019. Conference paper:
https://www.researchgate.net/publication/339301631_1E2_WAY_FROM_MSG_TO_MTG_SATELLITE_USER'S_TRAINING_AND_OPERATIONAL_SUPPORTING_TOOLS
Video-record from the coference:
https://ams.confex.com/ams/JOINTSATMET/videogateway.cgi/id/504859?recordingid=504859

[4] PETRACCA, M., KAŇÁK, J., PORCU, F., IWANSKI, R., LAPETA, B., DIÓSZEGHY, M., SZENYÁN, I., BAGUIS, P., ROULIN, E., OZTOPAL, A., KRAHE, P., KUNKEL, A., ARTINIAN, E., ChERVENKOV, H., CACCIAMANI, C., TONIAZZO, A., VULPIANI, G., PUCA S. (2019). Results of comparison between precipitation estimates by MW scanner and dual-frequency precipitation satellite radar according H-SAF validation methodology over MSG full-disk area. *Joint EUMETSAT/AMS/NOAA Conference.* Boston, 30 September – 4 October 2019. Conference poster abstract link:
https://ams.confex.com/ams/JOINTSATMET/meetingapp.cgi/Paper/360562

7. INSTITUTIONS INVOLVED IN SPACE RESEARCH

Members of the National Committee of COSPAR with e-mail addresses.

The website of NC is http://nccospar.saske.sk.

Astronomical Institute (AI)
Slovak Academy of Sciences (SAS)
Stará Lesná
059 60 Tatranská Lomnica
J. Rybák (choc@astro.ta3.sk, NC member)

Faculty of Mathematics, Physics and Informatics (FMPI)
Comenius University
Mlynská dolina
842 15 Bratislava
J. Masarik (Jozef.Masarik@fmph.uniba.sk, NC member)

National Forest Centre
T.G. Masaryka 22
960 92 Zvolen
contact: T. Bucha (bucha@nlcsk.org)

Earth Science Institute (ESI)
Slovak Academy of Sciences (SAS)
Dúbravská cesta 9
840 05 Bratislava
M. Revallo (milos.revallo@savba.sk, Secretary of NC)

Institute of Animal Biochemistry and Genetics
Slovak Academy of Sciences (SAS)
Moyzesova 61
900 28 Ivanka pri Dunaji
I. Hapala (Ivan.Hapala@savba.sk, NC member)

Institute of Experimental Endocrinology (IEE), Biomedical Center
Slovak Academy of Sciences (SAS)
Dúbravská cesta 9
845 05 Bratislava

Institute of Experimental Physics (IEP)
Slovak Academy of Sciences (SAS)
Watsonova 47
040 01 Košice
P. Bobík (bobik@saske.sk, NC member)

Institute of Geography (IGG)
Slovak Academy of Sciences (SAS)
Štefánikova 49
814 73 Bratislava
J. Feranec (feranec@savba.sk, Vice-Chair of NC)

Institute of Materials and Machine Mechanics
Slovak Academy of Sciences (SAS)
Račianska 75
831 02 Bratislava 3
J. Lapin (juraj.lapin@savba.sk, NC member)

Institute of Measurement Science (IMS)
Slovak Academy of Sciences (SAS)
Dúbravská 9
842 19 Bratislava
contact: I. Frollo (frollo@savba.sk)

Institute of Normal and Pathological Physiology (INPP)
Slovak Academy of Sciences (SAS)
Sienkiewiczova 1
813 71 Bratislava
contact: F. Hlavačka (Frantisek.Hlavacka@savba.sk)

Slovak Central Observatory (SCO)
Komárňanská 137
947 01 Hurbanovo
I. Dorotovič (ivan.dorotovic@suh.sk, Chair of NC, Representative
of Slovak NC to COSPAR)

Ministry of Environment of the Slovak Republic
Tajovského 28
975 90 Banská Bystrica
contact: J. Nováček (jozef.novacek@enviro.gov.sk)

Slovak Hydrometeorological Institute
Jeséniova 17
833 15 Bratislava
contact: J. Kaňák (jan.kanak@shmu.sk, NC member)

Slovak Organization for Space Activities (SOSA)
Ilkovičova 3 (FEI STU)
812 19 Bratislava
contact: M. Musilová (michaela.musilova@stuba.sk, NC member)

National Agricultural and Food Centre
Soil Science and Conservation Research Institute
Trenčianska 55
821 09 Bratislava
contact: M. Sviček (michal.svicek@nppc.sk)